The new ITER baseline, research plan and open R&D issues

The new ITER baseline, research plan and open R&D issues

OPEN ACCESS
IOP Publishing
Plasma Physics and Controlled Fusion
Plasma Phys. Control. Fusion **67** (2025) 065023 (60pp)
https://doi.org/10.1088/1361-6587/add9c9

The new ITER baseline, research plan and open R&D issues

A Loarte[1,*], R A Pitts[1], T Wauters[1], I Nunes[1], P de Vries[1], S H Kim[1], F Köchl[1], A Polevoi[1], M Lehnen[1,27], J Artola[1], S Jachmich[1], A Pshenov[1], X Bai[1], I S Carvalho[1], M Dubrov[1,2], Y Gribov[1], M Schneider[1], L Zabeo[1], X Bonnin[1], S D Pinches[1], F Poli[1], G Suarez Lopez[1], M Merola[1], F Escourbiac[1], R Hunt[1], L Chen[1], D Boilson[1], P Veltri[1], N Casal[1], M Preynas[1], A Mukherjee[1,28], W Helou[1], F Kazarian[1], S Willms[1], I Bonnet[1], R Michling[1], L Giancarli[1], J van der Laan[1], M Walsh[1], V Udintsev[1], R Reichle[1], G Vayakis[1], A Fossen[1], M Turnyanskiy[1], A Becoulet[1], Y Kamada[1], G Zhuang[3], G Xu[4], X Gong[4], J Huang[4], M Jia[4], R Ding[4], J Qian[4], Y Sun[4], Q Yang[4], L Zhang[4], M Xu[5], L Zhang[5], S Brezinsek[6], J Stober[7], J Hobirk[7], F Rimini[8], J Garcia[9], S L Rao[10], J Ghosh[11], D Sharma[11], B Magesh[10], R P Bhattacharya[11], G Matsunaga[12], H Urano[12], T Hirose[12], K Ogawa[13], G Motojima[13], C K Sung[14], H H Lee[15], J K Park[16], M S Cheon[15], Y M Jeon[15], S Konovalov[2], S Lebedev[17], N Kirneva[2], Y Kashchuk[18], N Bakharev[17], X Chen[19], A Bortolon[20], L Casali[21], R Maingi[20], F Turco[19], K Schmid[7], Y Liu[19], J R Martín-Solís[22], C Angioni[7], I Pusztai[23], D Fajardo[7], D Mateev[6], E Lerche[24], D van Eester[24], P Vincenzi[25,26], R Futtersack[8], V Bobkov[7] and L Colas[9]

[1] ITER Organization, Route de Vinon-sur-Verdon, 13067 St Paul Lez Durance Cedex, France
[2] National Research Center Kurchatov Institute, Moscow 123182, Russia
[3] University of Science and Technology of China, 96, JinZhai Road, Hefei, Anhui, People's Republic of China
[4] Institute of Plasma Physics, Chinese Academy of Sciences, 350 Shushanhu Road, Hefei, Anhui, People's Republic of China
[5] Southwestern Institute of Physics, South section 3, 2nd Ring Road, Chengdu, Sichuan, People's Republic of China
[6] IFN-1, Forschungszentrum Jülich, 52425 Jülich, Germany
[7] Max-Planck-Institut für Plasmaphysik, Boltzmannstrasse 2, 85748 Garching b. München, Germany
[8] CCFE, Culham Science Centre, Abingdon, Oxon OX14 3DB, United Kingdom
[9] CEA, IRFM, Saint-Paul-lez-Durance 13108, France
[10] ITER-India Institute for Plasma Research, Road Koteshwar, Gandhinagar 382 424, Gujarat, India
[11] Institute For Plasma Research, Bhat Village, Near Indira Bridge, Gandhinagar 382428, Gujarat, India
[12] National Institutes for Quantum Science and Technology (QST), 801-1 Mukoyama, Naka, Ibaraki 311-0193, Japan
[13] National Institute for Fusion Science (NIFS), National Institutes of Natural Sciences, 322-6 Oroshi-cho, Toki city, Gifu 509-5292, Japan
[14] KAIST, 291 Daehak-ro, Yuseong-gu, Daejeon 34141, Republic of Korea
[15] Korea Institute of Fusion Energy, 169-148 Gwahak-ro, Yuseong-gu, Daejeon 34133, Republic of Korea
[16] Department of Nuclear Engineering, Seoul National University, Seoul, Republic of Korea
[17] Ioffe Institute, St. Petersburg 194021, Russia
[18] Institution Project Center ITER, Rosatom, Moscow 123182, Russia

[27] Deceased.
[28] Present address: ITER-India Institute for Plasma Research, Bhat-Koteshwar Road Koteshwar, Gandhinagar, 382 424, Gujarat (India).
[*] Author to whom any correspondence should be addressed.

[19] General Atomics, San Diego, CA 92121, United States of America
[20] Princeton Plasma Physics Laboratory, 100 Stellarator Road, Princeton, NJ 08543-0451, United States of America
[21] University of Tennessee, Knoxville, TN 37996, United States of America
[22] Universidad Carlos III de Madrid, Avenida de la Universidad 30, 28911 Madrid, Spain
[23] Department of Physics, Chalmers University of Technology, Göteborg SE-41296, Sweden
[24] Laboratory for Plasma Physics, EUROfusion Consortium & Trilateral Euregio Cluster Member, Renaissancelaan 30 Avenue de la Renaissance, B-1000 Brussels, Belgium
[25] Consorzio RFX, Corso Stati Uniti 4, 35127 Padova, Italy
[26] Institute for Plasma Science and Technology, National Research Council, 35127 Padova, Italy

E-mail: alberto.loarte@iter.org

Received 25 November 2024, revised 1 April 2025
Accepted for publication 16 May 2025
Published 5 June 2025

Abstract

A new baseline (NB) has been proposed by the ITER Project to ensure a robust achievement of the Projects' goals, in view of past challenges including delays incurred due to the Covid-19 pandemic, technical challenges in completing first-of-a-kind components and in nuclear licensing. The NB includes modifications to the configuration of the ITER device and its ancillaries (e.g. change from beryllium to tungsten as first wall material, modification of the heating and current drive mix, etc.) as well as additional testing of components (e.g. toroidal field coils) or phased installation (start with inertially cooled first wall before later installation of the final actively water-cooled components) to minimise operational risks. In the NB, the ITER research plan (IRP) will be divided into three main phases: (a) start of research operation, with 40 MW of ECH and 10 MW of ICH, which will focus on the demonstration of 15 MA operation in L-mode, commissioning of all required systems, including disruption mitigation, and the demonstration of H-mode plasma operation in deuterium; (b) DT-1, with 60–67 MW of ECH, 33 MW of neutral beam injection (NBI) and 10–20 MW of ICH, which will demonstrate robust operation in high confinement H-mode plasmas in DT up to $Q \geqslant 10$ and for burn durations of 300–500 s within an accumulated neutron fluence of $\sim$1% of the ITER machine's lifetime total, and; (c) DT-2, with up to 67 MW of ECH, up to 49.5 MW of NBI and up to 20 MW of ICH, with the ITER tokamak and ancillaries in their final configuration to demonstrate routine operation in DT plasmas at high Q and the $Q \geqslant 5$ long-pulse and steady-state scenarios to the final neutron fluence and to perform R&D on nuclear fusion reactor issues. The logic, physics basis, modelling and experimental evaluations carried out to support the NB and the associated IRP are described. These include the impact of the tungsten wall on plasma scenarios and associated risk mitigation measures, as well as the optimisation of the tokamak components and ancillaries to minimise Project risks. Open R&D issues related to these evaluations and mitigation measures are also described together with experimental, modelling and validation activities required to address them.

Keywords: ITER, research plan, burning plasmas, W wall, heating and current drive, open R&D issues

1. Introduction

The ITER Project has recently proposed a new baseline (NB) [Barabaschi2023, Barabaschi2025] to ensure a robust achievement of the Project's goals in view of challenges experienced in the last years. These concerned delays incurred due to the Covid-19 pandemic, technical issues in completing first of a kind components (in particular, vacuum vessel and thermal shields) and in nuclear licensing. All these factors rendered the previous 2016 baseline [Bigot2022] unviable and, together with it, the associated research plan [ITR-2024-005]. The new ITER baseline addresses the challenges found through the elaboration of a realistic plan for machine assembly commissioning and operation/scientific exploitation together with a revised licencing strategy leading to the realisation of the Project's goals through three main experimental phases of its research plan: Start of Research Operation (SRO) and two DT operational phases (DT-1 and DT-2) with specific goals,

machine configuration and intermediate steps to address and retire operational risks with minimum impact on operational time :

- SRO takes advantage of progress in the construction of ancillary systems, while repairs to vacuum vessel and thermal shields and core machine assembly take place, leading to a more complete first assembly of tokamak components and systems than foreseen for start of plasma operations in the 2016 baseline [Bigot2022]. This enables the start of ITER scientific exploitation with more ambitious and fusion relevant goals than the 2016 first plasma (FP) and engineering operation phase, namely the demonstration of operation at full magnetic energy (W_{mag} at 15 MA/5.3 T) and exploration of H-mode operation up to 7.5 MA/2.65 T. To achieve this all the required control and protection systems (including disruption mitigation) will be commissioned and demonstrated. To provide a robust and realistic path to the achievement of these goals specific configurations of systems/components are chosen for this phase (e.g. an inertially cooled first wall, 40 MW of electron cyclotron heating (ECH) and 10 MW of ion cyclotron heating (ICH)) together with operational choices. This includes, for example, the use of deuterium (DD) plasmas for robust H-mode scenarios marking the start of ITER's nuclear operation in SRO.
- DT-1 is an initial phase of DT operation with the specific goal of demonstrating $Q \geqslant 10$ operation with fusion power (P_{fus}) of 500 MW for 300–500s in a reproducible way, addressing burning plasma physics and demonstrating tritium breeding with the Test Blanket Modules (TBMs) within a restricted neutron fluence of 3.5×10^{25} DT neutrons ($\sim 1\%$ of the ultimate ITER lifetime target) which will provide the basis for the final nuclear licence. In this phase the tokamak and ancillary systems will be in near final configuration with the water cooled first wall installed as well as 60 MW (67 MW optional) of ECH, 10 MW (20 MW optional) of ICH and 33 MW of neutral beam injection (NBI). The demonstration of tritium breeding will require operation with $P_{\mathrm{fus}} \geqslant 250$ MW, 300 s burn duration at high duty (1 pulse every 30 min).
- DT-2 is the final phase of DT operation with the goals of demonstrating $Q \geqslant 10$ operation with P_{fus} of 500 MW for 300–500 s at high duty, and the ITER reference long pulse and steady-state scenarios (1000–3000 s) with $Q \geqslant 5$ up to the final neutron fluence of 3×10^{27} DT neutrons or that allowed by the licencing process based on DT-1 operational results. In addition, research targeted towards fusion reactor physics, design and operational aspects will be addressed in this phase. To achieve the goals of DT-2 a series of system upgrades may be required after DT-1 such as for the tritium plant, hot cell and radwaste processing and, chiefly, of the installed NBI power up to 49.5 MW (an additional beam injector) to demonstrate steady-state operation in ITER.

To ensure a realistic, robust and reactor relevant path to the achievement the Project's goals some modifications to the tokamak components and systems have been incorporated into the NB. These include the use of tungsten (W), instead of beryllium (Be), as first wall material and the increase of heating power and modification of the power mix favouring ECH. For SRO operation 40 MW ECH + 10 MW ICH are installed compared to either 5.8 MW of ECH for FP or 20 MW of ECH for PFPO-1 in the 2016 baseline [ITR-24-005]. For DT-1 operation 33 MW NBI, 60–67 MW ECH and 10–20 MW ICH are installed versus (33 MW NBI, 20 MW ECH, 20 MW ICH) in the 2016 baseline [ITR-24-005].

In this paper we discuss the logic and physics basis behind the tokamak configuration choices in the NB as well as the operational path chosen to demonstrate the Projects' goals in the NB ITER research plan (NB-IRP) together with the areas where further R&D is required to define the NB-IRP in detail. The paper is organised as follows: in section 2 we review the experimental basis behind the choices made for the tokamak and ancillaries configuration in the NB, specifically the change of wall material and its implications, as well as the configuration of the heating and current drive (H&CD) systems. In section 3 we describe the tokamak and ancillaries configuration, goals and operational strategy for each phase of the NB-IRP together with supporting modelling assessments for each of them, as well as the associated open R&D issues. Finally in section 4 we summarise the NB-IRP and draw conclusions.

2. Experimental basis for the use of W as first wall material in ITER and the choice of H&CD systems in the new ITER baseline

The wall material of the 2016 baseline was Beryllium (Be), the choice being justified because of the low impact of plasma contamination by wall sputtered impurities on plasma performance, due to its low atomic charge, as well as its superb oxygen gettering properties providing high quality vacuum for plasma operation. As evaluations for the 2016 baseline proceeded, some of the drawbacks of Be and their consequences became better understood. These ranged from technical assembly issues (inefficiency in machine assembly due to measures to ensure workers health due to the Be toxicity) to those associated with the high sputtering rate of Be as well as its low melting temperature and thus lower resilience to transients. The former potentially required the replacement of a significant number of eroded first panels, and/or the change of wall material to W, in the most eroded regions of the first wall, after the first three DT campaigns [Pitts2021]. The latter required a very high efficiency of disruption mitigation for operation with plasma current above $\sim$7 MA [Lehnen2015] since significant melting of Be and melt layer displacement could modify the induced current paths in the first wall and lead to its mechanical failure [Pitts2025]. This, together with an improved understanding of the implications of the use of W as first wall material for plasma operation and performance, led to the change to W for the first wall in the NB. Below we review the experimental physics basis for W wall operation in ITER, while detailed evaluations for plasma-wall interaction and related issues are described in [Pitts2025, Wauters2024].

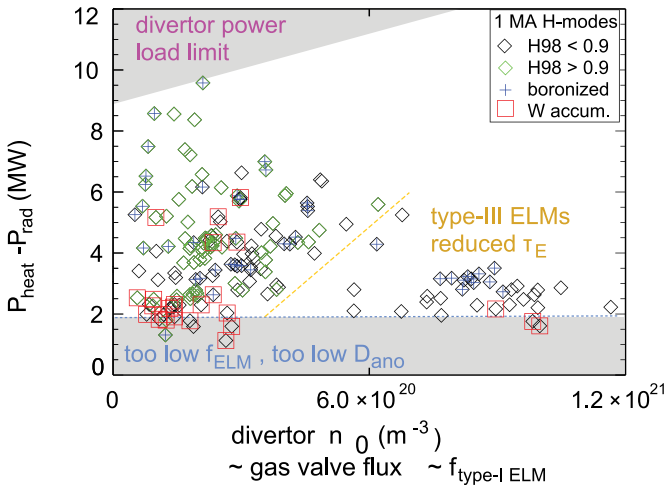

Figure 1. H-mode operational space in terms of divertor neutral density, $n_{0,\mathrm{div}}$, and target heat load, $P_{\mathrm{heat}}-P_{\mathrm{rad}}$ in ASDEX upgrade. Data points represent either steady-state flattop phases or phases leading to central W accumulation (red squares), averaging time is typically 0.5 s. Reproduced from [Kallenbach2009]. © 2009 IAEA, Vienna. The divertor neutral density is nearly proportional to the total gas valve flux. Black diamonds denote discharges with H-factors, H_{98y2} below 0.9, which are typically Type-III ELMy H-modes. The limits indicated are just sketches guided by the data points. Plasma current $I_p = 1$ MA. The typical L–H transition power for these plasma conditions is 1.5 MW [Ryter2013].

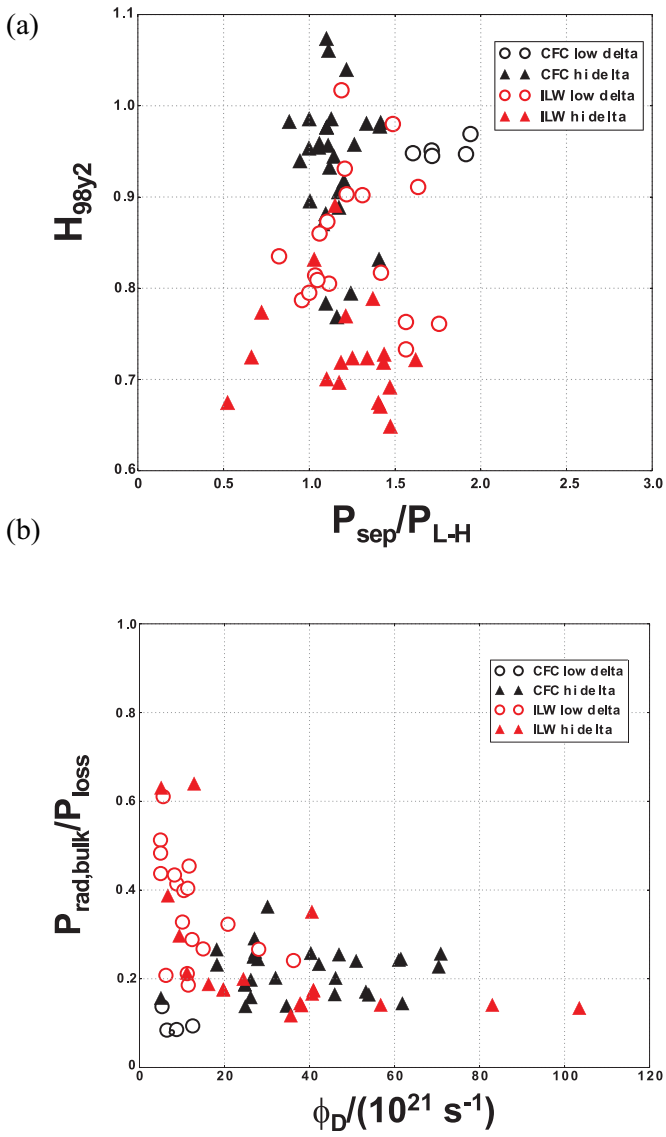

Figure 2. (a) H_{98y2} versus $P_{\mathrm{sep}}/P_{\mathrm{LH}}$ and b) $P_{\mathrm{rad}}{}^{\mathrm{core}}/P_{\mathrm{heat}}$ versus gas fuelling rates for JET initial H-mode plasmas with the ILW compared with carbon PFC operation (derived from experimental results in [Joffrin2014]).

2.1. Experimental physics basis for W wall operation in ITER

Operation with W plasma-facing components (PFCs) can cause increased core plasma radiation, which decreases the operational range of H-mode plasmas and may lead to uncontrolled W accumulation (i.e. uncontrolled rise of the core W density at constant edge density) [Kallenbach2005]. As will be discussed later in this section, the direct empirical extrapolation of the findings in present experiments to ITER is not straightforward. For some cases, the physics processes driving W transport differ between present experiments and ITER (e.g. core particle sources), or because the experimental plasma conditions showing large W core densities are not accessible in ITER (e.g. low-density plasma conditions leading to excessive divertor loads). With these caveats, guidance from experiments can be used to evaluate the impact that a W first wall may have in the expected range of operational conditions to be explored in ITER. We note that this is not a fully exhaustive review of the literature and we use, for simplicity, many examples from ASDEX Upgrade (AUG) since it has operated with full W PFCs from 2007 onwards, supplemented with recent results from EAST for specific issues [Jia2024]. The findings presented here are similar to those of other tokamak experiments operating with high Z PFCs (namely Alcator C-Mod, KSTAR, WEST and JET), or that have addressed high Z core impurity transport (e.g. DIII-D).

2.1.1. Impact of W wall on H-mode operation (including H&CD aspects). Experiments in ASDEX-Upgrade [Kallenbach2009] with boronised and unboronised W walls show that stationary H-mode conditions can be maintained for a separatrix power flux 50% higher than the H-mode threshold power ($P_{\mathrm{sep}} \geqslant 1.5\ P_{\mathrm{LH}}$), with a typical level of core plasma radiation $P_{\mathrm{rad}}{}^{\mathrm{core}} \leqslant (0.4\text{–}0.5)\ P_{\mathrm{heat}}$, as shown in figure 1. The operational space for JET with a Be wall and W divertor (ITER-like Wall or ILW) in terms of the same parameters has been re-examined for the initial ILW H-mode operation [Joffrin2014] when such scenarios were first developed and the results are shown in figure 2. In terms of maximum $P_{\mathrm{rad}}{}^{\mathrm{core}}/P_{\mathrm{aux}}$ the values are comparable to those in AUG, while in terms of the margin to the L–H threshold power, these initial JET ILW H-mode plasmas operated with $1.0 \leqslant P_{\mathrm{sep}}/P_{\mathrm{LH}} \leqslant 1.5$ and, thus, with lower margin than ASDEX-Upgrade. It should be noted, however, that in the case of JET, P_{LH} is evaluated from the 2008 scaling [Martin2008] and the real H-mode

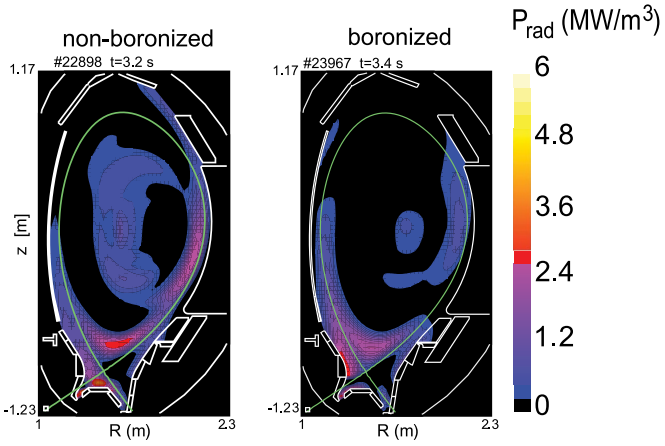

Figure 3. Comparison of the radiation distribution from bolometry of two ASDEX Upgrade discharges with identical heating power and D fuelling for non-boronised and boronised conditions. The total radiated powers are 4.5 MW for the non-boronised and 3.4 MW for the boronised discharge. Reproduced from [Kallenbach2009]. © 2009 IAEA, Vienna.

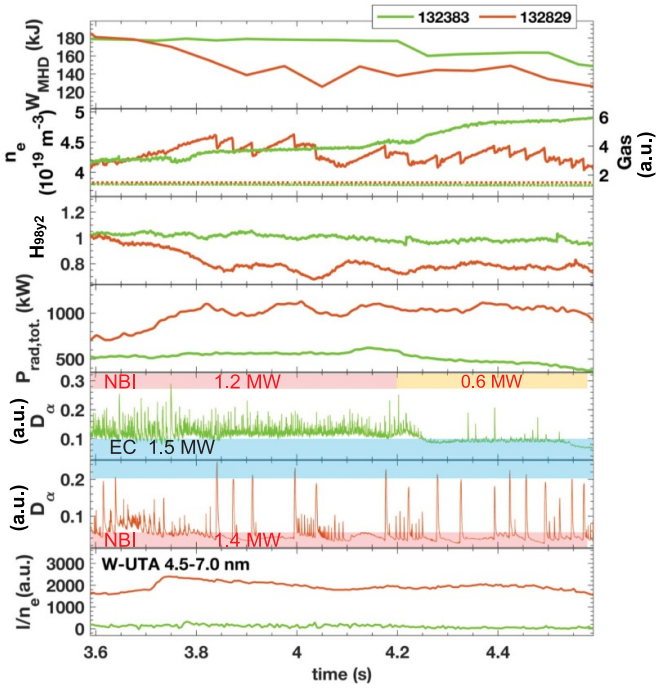

Figure 4. Impact of W limiter boron coverage on H-mode performance in EAST; Type II ELMy H-modes (132383 in green) with high B cover perform much better than Type I ELMy H-modes 132 829 in red) with low boron cover (both discharges have an 8 cm separatrix—W limiter distance, $P_{\mathrm{NBI}} = 1.2$–1.4 MW, $P_{\mathrm{ECH}} = 1.5$ MW). Reproduced from the 50$^{\mathrm{th}}$ EPS conference with permission from [Jia2024].

threshold in JET with the ILW tends to be lower than the value derived from this scaling.

A quantitative comparison of the effect of the W wall on H-mode performance in AUG can be found in [Kallenbach2009, Schweinzer2016] in which plasmas with no/low boron (B) coverage of the wall are compared with similar plasmas with large B coverage. Further details on the impact of B on wall conditions, beyond covering of W PFCs by B, are discussed in section 2.1.4. As can be seen in figure 3 the W wall increases the radiation level by ∼30% compared to a low Z wall (boronised) and increases the W concentration. This has been recently confirmed in EAST by applying boronisation with carborane and comparing discharges carried out soon after boronisation and after substantial plasma operation which removes boron from the plasma exposed W limiter. The main outcome of the EAST study was that the B coverage of the W limiter significantly reduced the core plasma W density in H-mode plasmas in EAST in a similar way to AUG. As a result (see figure 4), reference high β_{p} Type II edge localised mode (ELMy) operation (with large separatrix to W limiter separation) could be obtained with P_{ECH} ∼1.5 MW, a factor 2 lower than with no B coverage of the W limiter. In the case of low boron limiter coverage, a similar pulse with the same heating mix and plasma-limiter gap yields only a low confinement type I ELMy H-mode [Jia2024].

Despite the increased W influxes, the W concentration in H-mode plasmas can be maintained at levels of ∼few 10^{-5} with a non-boronised W wall, as required for $Q \geqslant 10$ in ITER (see section 3.4.6), by the application of ECH or ICH heating in the flattop as shown in figures 5 and 6 for AUG. An essential ingredient to achieve these acceptable concentrations under stationary operating conditions is to ensure that ELMs are maintained controlled at sufficient frequency since, in present experiments, they provide a very effective means to exhaust W from the edge plasma. This aspect has been thoroughly assessed in recent EAST experiments, specifically carried out to support the new ITER baseline, in which a range of H&CD schemes has been explored together with systematic scans of the plasma separatrix to the W limiter. The details of such experimental results can be found in [Jia2024] while here we provide a high-level summary. In the context of the new ITER baseline it is important to note that EAST is equipped with a W divertor and outer poloidal limiter, both fully actively cooled. The outer limiter intercepts most of the plasma flux to the wall, while the neutral flux also impacts the first wall which is mostly covered by Molybdenum PFCs and no boronisation was applied for these experiments. The tokamak is also equipped with an extensive set of additional heating systems (ECH, ICH, NBI and lower hybrid current drive (LHCD)). The plasma scenario selected at EAST was a near double-null (with dominant lower X-point) with $I_{\mathrm{p}} \sim 450$ kA, $B_{\mathrm{t}} \sim 2.45$ T ($q_{95} \sim 6$) which allows access to Type I and II ELMy H-modes. In all cases central heating was applied with P_{ECH} up to 3 MW. Further additional heating was also provided by NBI and by LHCD with typically up to 2 MW of coupled plasma heating power. As shown in figure 7, operation with Type II ELMs provides higher confinement and lower radiated power levels for the same plasma density. This is consistent with more efficient exhaust of W, or a lower W source being provided by

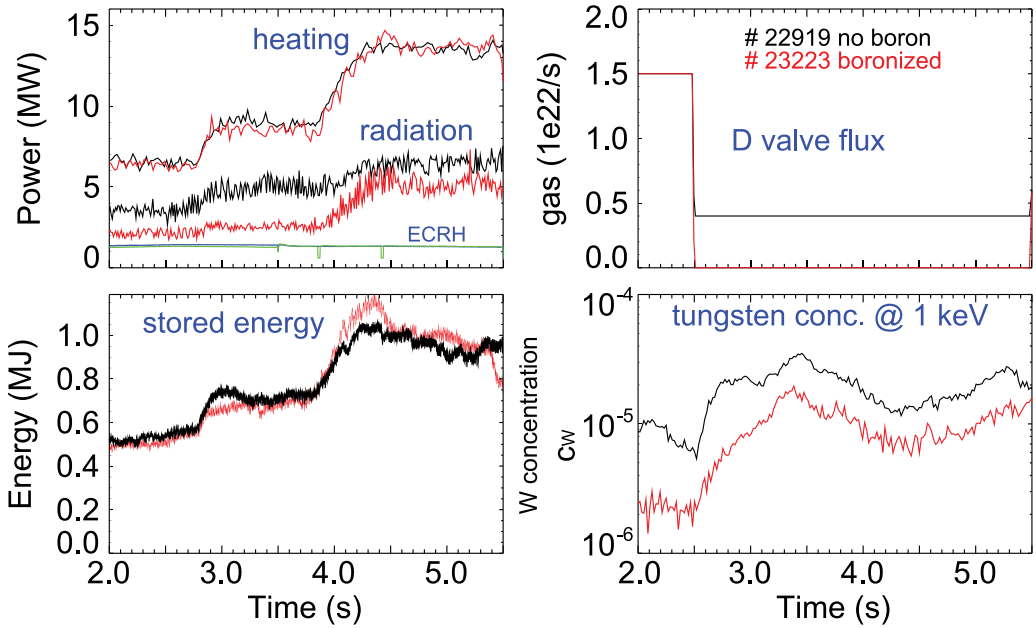

Figure 5. Comparison between high power improved H-mode discharges with identical heating schemes under non-boronised and boronised conditions in ASDEX Upgrade. Shown are the heating power (almost identical) and total radiation time traces, the gas puff, stored energy and W concentration. The H-factor $H_{98y,2}$ at $t = 4.3$ s is 1.1 for the unboronised and 1.3 for the boronised discharge without D puff. For the latter discharge, confinement is slightly decreased by moderate neoclassical tearing mode activity. $I_p = 1$ MA, $q_{95} = 4.7$. Reproduced from [Kallenbach2009]. © 2009 IAEA, Vienna.

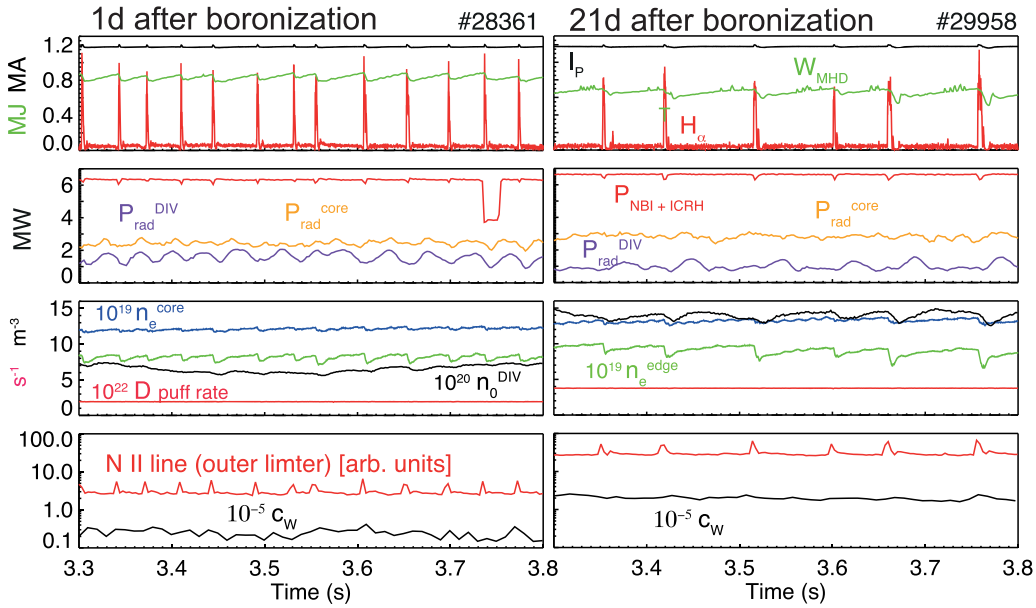

Figure 6. Comparison of ITER Baseline ASDEX Upgrade discharges heated by NBI + ICH during phases of 0.5 s duration. Discharge parameters are identical except gas puff and 'freshness' of boronisation. While the discharge on the left (#28361) was conducted 1 d after a boronisation, the one on the right (#29958) was executed 21 d after a boronisation. Different gas puff levels 1.9×10^{22} and 3.8×10^{22} atoms s^{-1} were necessary to reach stationarity for discharges #28361 and #29958, respectively, which lowers the plasma energy in discharge #29958. Reproduced from [Schweinzer2016]. © 2016 IAEA, Vienna.

type II than by type I ELMs. Similarly, the proximity of the W limiter has a larger impact for type I than for type II ELMy H-modes. This illustrates the need to maintain good ELM control, besides central ECH heating in EAST, to sustain high confinement operation in H-modes with a W wall.

While central ECH heating has been demonstrated to be effective in avoiding uncontrolled W accumulation in present experiments, as shown in figure 8(a), ICH can also provide a similar effect, as shown in figure 8(b), provided that the additional W influx generated by specific ICH-W plasma-

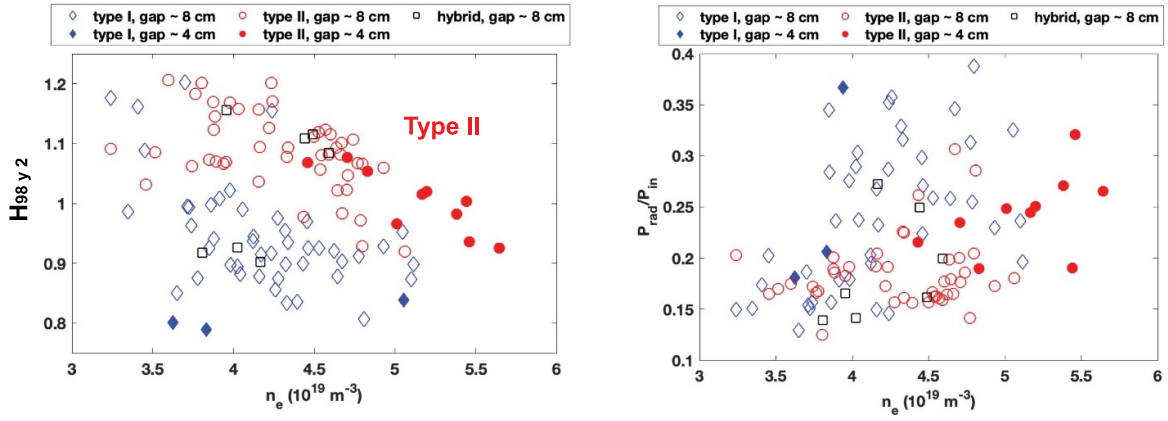

Figure 7. Plasma density dependence of: (a) H_{98y2} and (b) radiated power for EAST H-mode experiments with a W limiter/Mo-first wall for two separatrix-W limiter gaps and various ELM type H-modes (I, II and hybrid-I–II) with no impurity seeding. These results demonstrate the higher performance and lower impact of the separatrix-limiter gap and lower $f_{\rm rad}$ that can be achieved at the same density with the higher degree of W edge exhaust provided by Type II compared with Type I ELMs. Reproduced from the 50$^{\rm th}$ EPS conference with permission from [Jia2024].

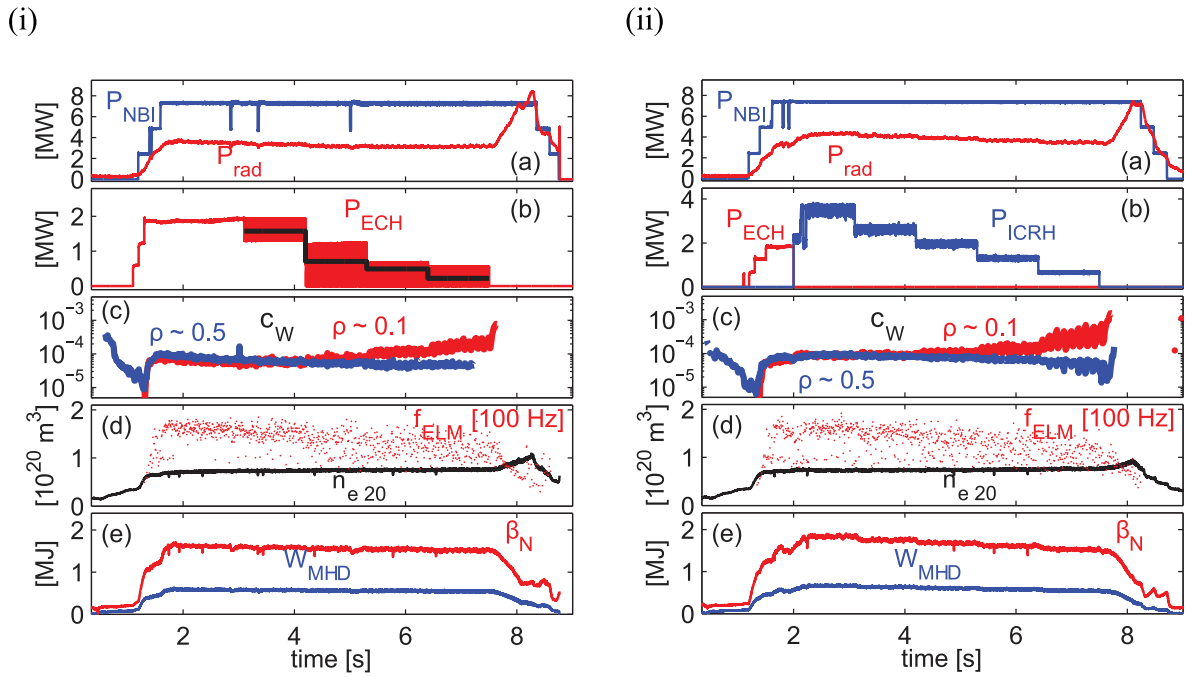

Figure 8. Time traces of ASDEX Upgrade shot (i —32 408 and ii −32404) with decreasing steps of ECH and ICH, respectively: (a) total NBI and radiated powers, (b) total ECH and ICH powers, (c) W concentration $c_{\rm W}$ at normalised minor radius ($\rho = r/a$) $\rho \sim 0.1$ and $\rho \sim 0.5$, (d) ELM frequency and line averaged density, (e) normalised β and total stored energy. Reproduced from [Angioni2017]. © 2017 IAEA, Vienna.

wall interactions remains small thanks to the antenna design [Angioni2017]. This can be achieved by the installation of low Z PFCs at the antenna sides or by covering the W side elements by boronisation; these schemes are not suitable for ITER with a full-W wall. Approaches to accomplish the same goal by antenna design that are relevant for ITER have been demonstrated in present experiments such as AUG [Bobkov2010, Bobkov2017] (see figure 9(a) for a non-optimised design and figure 9(b) for an optimised design), Alcator C-Mod [Lin2020] and JET [Chomiczewska2024], which can be made compatible with the ITER ICH antenna design. Studies of the W influxes associated with application of ICH in ITER plasmas in the NB and their optimisation can be found in [Helou2023, Colas2024, Bobkov2024]. It should be noted that the temperature anisotropy of ICH resonant species leads to direct effects on W transport and to poloidal asymmetries of the electrostatic potential [Angioni2021] which also affect W transport. The combination of such ICH-driven effects can impact core

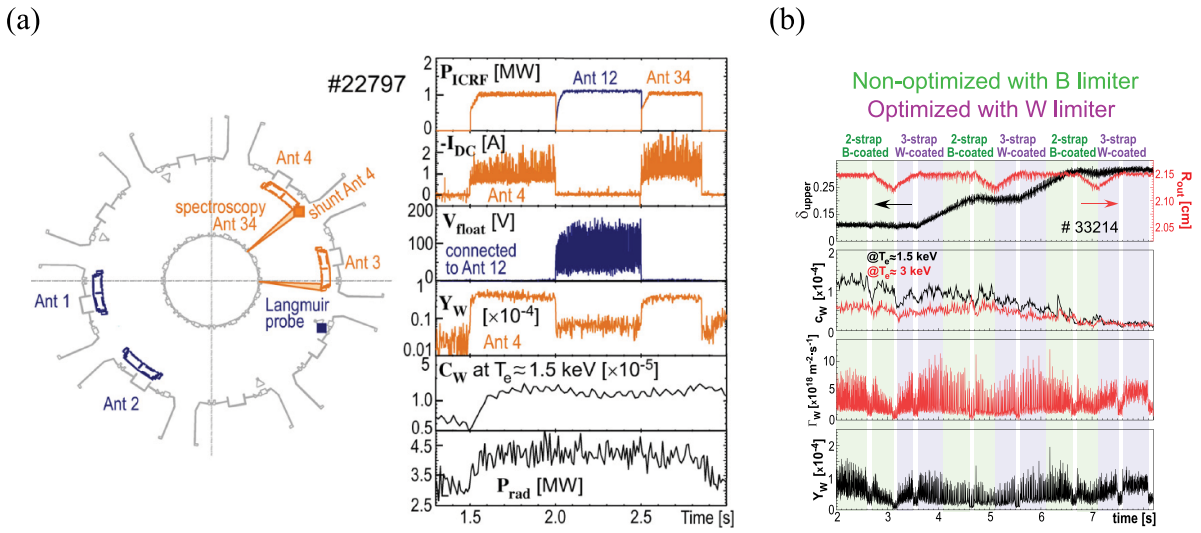

Figure 9. (a) Characterisation of the W release during ICH power input from antenna pairs 12 and 34 for shot #22797 before boronisation in ASDEX Upgrade with non-optimised (2-strap) antennas. Reproduced from [Bobkov2010]. © 2010 IAEA, Vienna. (b) Comparison of the B-coated antennas with the W-coated antennas during scans of plasma triangularity and the radial position in deuterium plasmas in ASDEX Upgrade. Every antenna pair provides $P_{ICH} = 1.5$ MW in the highlighted time windows on top of $P_{aux} = 6.3$ MW. The non-optimised (2-strap) antennas are B-coated and the optimised (3-strap) antennas are W-coated. Reproduced from [Bobkov2017]. © IOP Publishing Ltd. All rights reserved.

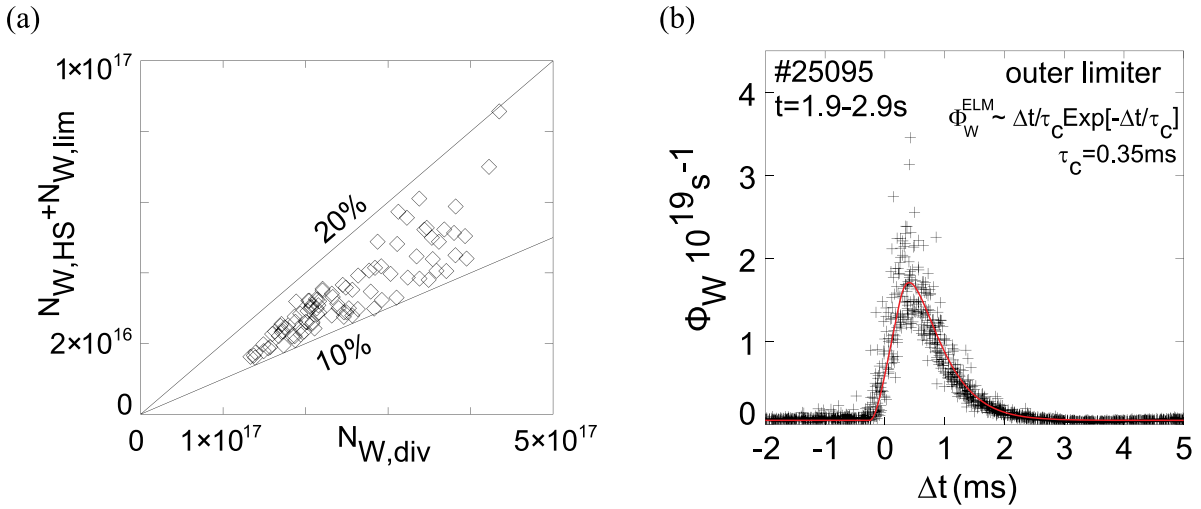

Figure 10. (a) ELM W source at the main chamber components versus the divertor W source in ASDEX upgrade. (b) Evolution of the W source rate at the outboard limiters during a type-I ELM. The temporal coordinate Δt is the time difference to the arrival time of the ELM in the outboard divertor and the data of 117 ELMs are overlaid. Reproduced from [Dux2011]. © 2011 IAEA, Vienna.

W transport positively (i.e. outwards) or negatively (inwards) depending on plasma conditions [Maget2022a].

2.1.2. W sources and transport in H-mode plasmas. Gross W sources in present experiments are dominated by the divertor; the gross wall W source is typically a factor of 5–10 lower than that from the divertor in AUG [Dux2011], as shown in figure 10(a). For ELMy H-modes, the W wall source can be dominated by the ELMs or by the inter-ELM plasma flux depending on whether the plasma-wall distance is small (inter-ELM dominated) or large (ELM dominated) compared to the characteristic distance for radial particle flux decay. An example for ELM dominated W wall influx [Dux2011] is shown in figure 10(b).

Despite the much smaller magnitude of the W wall source its effect on the core W plasma density is sizeable. This is because W prompt redeposition is smaller at the wall than at the divertor and also due to the less efficient penetration of divertor produced impurities by screening in the divertor plasma. To document this experimentally, plasma-wall distance scans at constant plasma and divertor conditions were performed in AUG; results are shown in figure 11 [Dux2009]. Increasing the gross W influx from the low field side (LFS) leads to an increase by a factor of ∼2 of the core W concentration, even if the LFS W gross influx remains about an order of

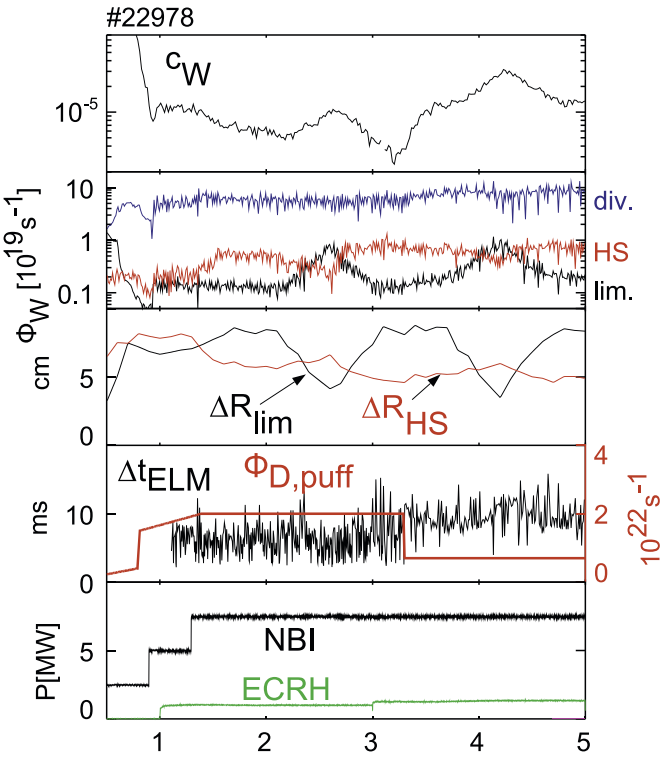

Figure 11. Time traces for an ASDEX upgrade discharge (#22978) with variations of the outer separatrix radius at two levels of gas puffing showing the increase of the W core density when the LFS (lim) W wall flux increases. From top to bottom: W concentration, gross W sources from the divertor, high field side (HFS) and LFS, distance between the separatrix and the wall at the LFS and HFS, gas puffing level and resulting ELM frequency, NBI and ECH heating waveforms. Reprinted from [Dux2009], Copyright (2009), with permission from Elsevier.

magnitude lower than that from the divertor. This implies an effective contamination efficiency for LFS wall produced W an order of magnitude larger than from the divertor. The recent experiments carried out in EAST (see figure 7) are consistent with the findings in AUG although the source of W from the limiter could not be measured and a quantitative comparison is, thus, not possible.

The W that enters the edge plasma has to be transported from the wall across the scrape off layer to the separatrix and into the pedestal of H-mode plasmas; the experimental determination of the magnitude and processes dominating this transport remain very uncertain, especially for the scrape-off layer. Experimental and modelling studies have shown that impurity transport in the H-mode pedestal between ELMs can be described by neoclassical transport. The direction and magnitude of the W transport is, thus, determined by the density and temperature gradients in the pedestal. For the usual experimental conditions achievable in today's experiments (with $|R/L_n| > |R/2L_T|$, where L_n and L_T are the density and temperature gradient scale lengths in the pedestal) this implies a negative inwards pinch and, thus, a significant increase of impurity density from the separatrix to the top of the pedestal, as shown in figure 12 [Pütterich2011]. For conditions obtained at JET in plasmas with high ion temperatures, in which $|R/L_n| < |R/2L_T|$, a decreased W density at the edge is observed as expected from neoclassical transport predictions [Garcia2022, Field2023] see figure 13.

Drawing direct conclusions on the implications of a W wall for ITER solely based on direct extrapolation of experimental results is not simple, since quantitative extrapolation is subject to large uncertainties and also because for some key specific issues it is already known that the behaviour expected in ITER is qualitatively different from that in present experiments. For such specific issues, direct extrapolation is simply incorrect. Taking this into account, the following overall implications can be considered for ITER:

- Robust H-mode operation with a W wall should be maintained in ITER up to core radiative power fractions of $P_{rad}{}^{core}/P_{aux} \leqslant 0.5$. These are typical radiated power fractions found in the development of H-modes for devices with W PFCs. When the net W impurity influxes into the plasma are optimised (e.g. by source reduction or increased outflux by ELMs), lower radiation fractions can be achieved with all-W PFCs in present experiments;
- Robust H-mode operation (in DD/DT plasma) requires that the edge power flow with some margin above the L–H power threshold be maintained. Based on experimental results, $P_{sep} \geqslant 1.5\ P_{LH}$ can be adopted as a conservative guideline for ITER;
- Sufficient capability for central ECH heating should be maintained to ensure efficient plasma heating and good core W accumulation control. This should be in addition to other control missions of the ECH system in ITER such as neoclassical tearing mode (NTM) control;
- Sufficient capability for central ICH heating is desirable for W control and for the flexibility of the experimental programme. Note that, as discussed in the next section, the ICH system is also required in ITER for Ion Cyclotron Wall Conditioning (ICWC) to provide fuel removal associated with the use of boronisation;
- Good ELM control is mandatory for operation in H-mode with all-W PFCs.

Two key aspects of W transport physics that are already known to be different from most present experimental evidence due to physics differences or integration aspects in ITER, are:

Mechanisms driving core W accumulation

In present experiments, the existence of a strong core particle source and plasma rotation (usually provided by NBI) is key to cause the uncontrolled accumulation of W by enhancing neoclassical transport over turbulent transport, as confirmed in Alcator C-Mod, AUG and WEST [Loarte2015, Manas2021, Yang2020]. A source of comparable strength is not provided by ITER NBIs because the high energy of the injected neutrals (~1 MeV) entails a very low core particle source for similar levels of injected power (~10 s of MW) [Loarte2015]. Similarly normalised plasma rotation in ITER is low, despite comparable toroidal rotation speeds to present experiments,

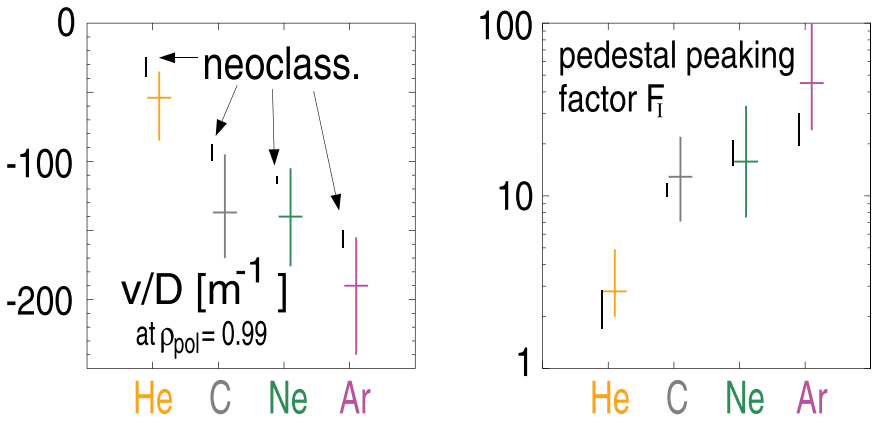

Figure 12. Measured and modelled (assuming neoclassical transport) inverse scale lengths for a range of impurities in the ASDEX upgrade pedestal and resulting pedestal peaking (namely the ratio of the impurity density at the top of the pedestal and at the separatrix). Reprinted from [Pütterich2011], Copyright (2011), with permission from Elsevier.

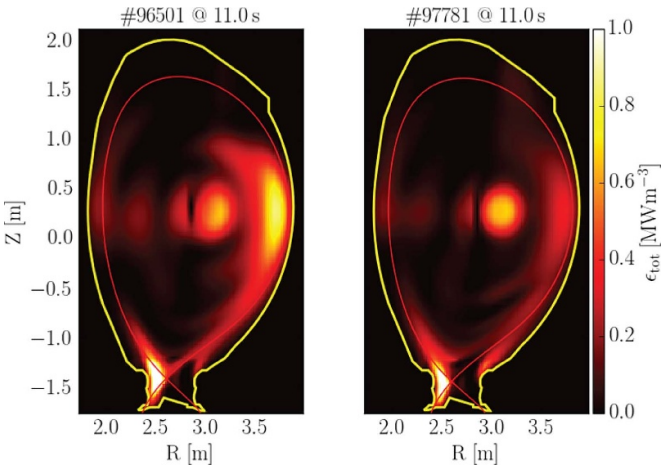

Figure 13. Comparison of the total radiated emissivity distributions, dominated by W radiation, from tomographic inversions of bolometric measurements for two hybrid JET pulses (#96501 (left) and #97781 (right) at 11 s) showing the decrease of the edge W density associated with neoclassical screening in pulse #97781. The first wall and separatrix contours are shown in yellow and red respectively. Reproduced from [Field2023]. © Crown copyright, 2022. Licensed under the terms of the Open Government Licence v3.0.

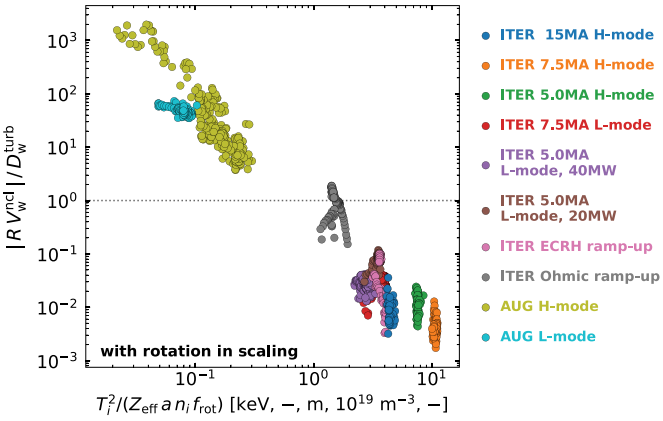

Figure 14. Ratio of core neoclassical inwards convection to turbulent diffusion in typical plasma conditions in ASDEX Upgrade (AUG) and ITER against a scaling derived on the basis of integrated transport studies. Reproduced from [Fajardo2024a]. CC BY 4.0. This scaling parameter depends on ion temperature (T_i), effective charge (Z_{eff}), minor radius (a), ion density (n_i) and a parameter (f_{rot}) that depends on plasma toroidal rotation, which impacts W transport due to neoclassical effects.

because of the high ion temperatures. Thus, rotation does not significantly enhance neoclassical W transport, unlike in present experiments [Angioni2014, Loarte2016]. As a result of this, anomalous transport is expected to dominate the core of ITER plasmas over a wide range of parameters, as shown in figure 14 [Fajardo2024 a], and the physics processes leading to W accumulation in present experiments are not expected to materialise in ITER. Indeed $Q \geqslant 10$ H-mode plasmas show rather flat W profiles [ITER-24-004, Fajardo2024b] over a wide range of concentrations so that the collapse of plasmas in these conditions is due to an edge power deficit to sustain the H-mode rather than to an uncontrolled peaking of the W density [Fajardo2024b]. We note, however, that in low power L-mode plasmas W accumulation can take place driven by neoclassical transport as well as when there is a local negative power balance (higher W radiation losses at a given plasma radius than local heat flux), as it will be shown later for limiter plasmas in ITER (section 3.4.6).

Pedestal transport and W exhaust by ELMs

Pedestal transport in ITER H-modes is expected to be regulated by neoclassical physics as in present experiments, although uncertainties remain regarding the level of accuracy to which neoclassical physics can describe W transport across the ITER pedestal [Reynolds-Barredo2020]. On this basis, the relationship between edge density and temperature gradients is key to determine the radial direction of the W flow at the edge. In most conditions in present experiments, with steep pedestal density and temperature gradients, this implies that neoclassical inwards pinch dominates and W transport is inwards.

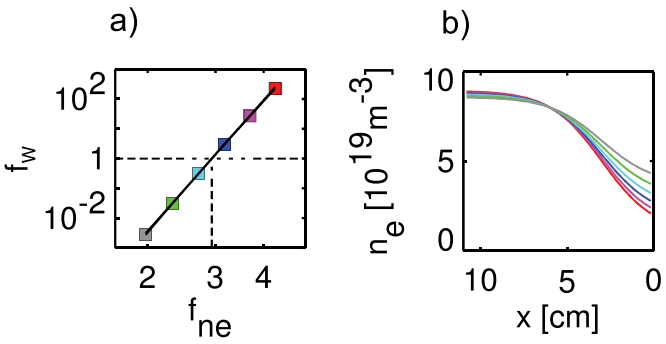

Figure 15. (a) Modelled ratio of the W density peaking f_W (W density at pedestal top divided by that at the separatrix) in the ITER pedestal for $Q \geqslant 10$ plasma conditions for a range of separatrix densities. (b) Edge density profiles considered in modelling W transport in which the separatrix density is varied at constant pedestal densities. For separatrix densities above 3×10^{19} m^{-3}, screening of the W (i.e. lower W pedestal density than at the separatrix) is expected. Reproduced from [Dux2014]. © IOP Publishing Ltd. All rights reserved. Note that for appropriate power exhaust for $Q \geqslant 10$ plasmas $n_{esep} \geqslant 4 \times 10^{19}$ m^{-3} is required [Pitts2019].

As a result, the W density at the pedestal top is much higher than at the separatrix and, thus, W accumulation in the pedestal is an almost ubiquitous finding. However, integration of ITER plasmas with acceptable divertor power loads, particularly with high levels of additional heating and for high Q operation, implies that the separatrix density has to be, typically, in the range of $n_{sep}/n_{ped} > 0.5$ [Pitts2019]. This results in much lower density gradients at the plasma edge than in present experiments, while those of the plasma temperature remain high in ITER ($T_{sep}/T_{ped} < 0.1$). Under such conditions, edge temperature screening dominates and W transport is outwards in the pedestal [Dux2014], as shown in figure 15, so that the pedestal W density is much lower than at the separatrix thanks to pedestal plasma W screening in ITER. As mentioned above, this is unlike the vast majority of experimental evidence, except the JET results quoted above [Garcia2022, Field2023], in which ITER-like pedestal edge gradients were obtained. Therefore, assuming by default that W transport at the ITER plasma edge would be inwards and drawing consequences from present experiments along these lines is incorrect for ITER.

We note, in addition, that ELMs are expected to melt the divertor monoblocks at least in some locations (e.g. toroidal gap edges) for plasma current above ∼5 MA in ITER [Gunn2017] and that they need to be strongly mitigated or suppressed for higher current levels. Therefore, even if it were effective (see below), increasing the ELM frequency cannot be considered as an edge W control scheme for plasma currents above 5 MA, since the associated ELM power fluxes would be intolerable in the divertor.

In most present experimental conditions, with W accumulation in the pedestal, ELMs are very effective to flush W out of the plasma. The ELMs cause an interchange-like perturbation of the plasma density [Huijsmans2013] leading to outwards flow from the pedestal and inwards flow from the scrape-off layer into the confined plasma. This provides effective W exhaust in present experiments since the W pedestal density is much larger than that in the SOL. Thus, increasing the ELM frequency increases W exhaust in present experiments. However, it is also incorrect to assume that ELM control through ELM frequency increase will routinely provide appropriate W density control in ITER. The efficiency of ELM control by frequency increase to provide W exhaust from the edge plasma is directly correlated with the shape of the edge W density profile. For conditions in which edge W transport is inwards and W profiles in the pedestal are peaked, as is the case in the vast majority of present experiments, ELMs provide efficient W exhaust as described above. On the contrary, for conditions in which W screening dominates (high power and/or high Q in ITER) and W density profiles in the pedestal are hollow, ELMs produce an inwards W influx and therefore increase the core W concentration rather than decrease it. This was originally identified for ITER in [van Vugt2019, Dux2017], as shown in figure 16 and confirmed in the JET experiments mentioned above [Garcia2022, Field2023]. This implies that in conditions with W screening in ITER ELM suppression or ELMs whose perturbation does not penetrate deep in the pedestal, rather than controlled Type I ELMs by active triggering, will be required for W control independently of the needs for divertor ELM power flux control (melt avoidance). We note that application of 3D fields for ELM control have direct effects on W neoclassical transport at the edge beyond those expected from their 2D averaged effect on the pedestal plasma parameters. This is due to the formation of 3D structures in the edge magnetic and electric fields that increase W outwards transport in edge plasma conditions in which neoclassical transport in 2D is inwards [Korving2024]. Those structures also decrease W outwards transport in edge plasma conditions for which W screening in 2D is expected at the pedestal. This implies that a balance between the needs for ELM control and preserving W pedestal screening will be required for the minimisation of W contamination in ITER core H-mode plasmas [Loarte2017].

2.1.3. Limiter and L-mode operation with a W limiter and wall.

Plasma start-up on limiters with W PFCs poses specific issues associated with W radiation, leading to radiative collapse of the early phase plasma [Neu2009, Maget2022b, Gong2024, Pitts2025]. In the very early phase of the start-up, temperatures at the plasma edge are sufficient for W to be released by physical sputtering due to the impact of low Z impurities present in the plasma, chiefly oxygen in the absence of boronisation. The sputtered W neutrals can reach the confined plasma much more readily than in a diverted configuration and may be ionised to high charge states. Since the W self-sputtering yields can easily exceed unity for highly charged W ions accelerated to high energy in the plasma sheath, the plasma W concentration can rise very rapidly in the initial phase of the limiter start-up once some W sputtering occurs. As discussed below, the plasma-W system is to a large extent

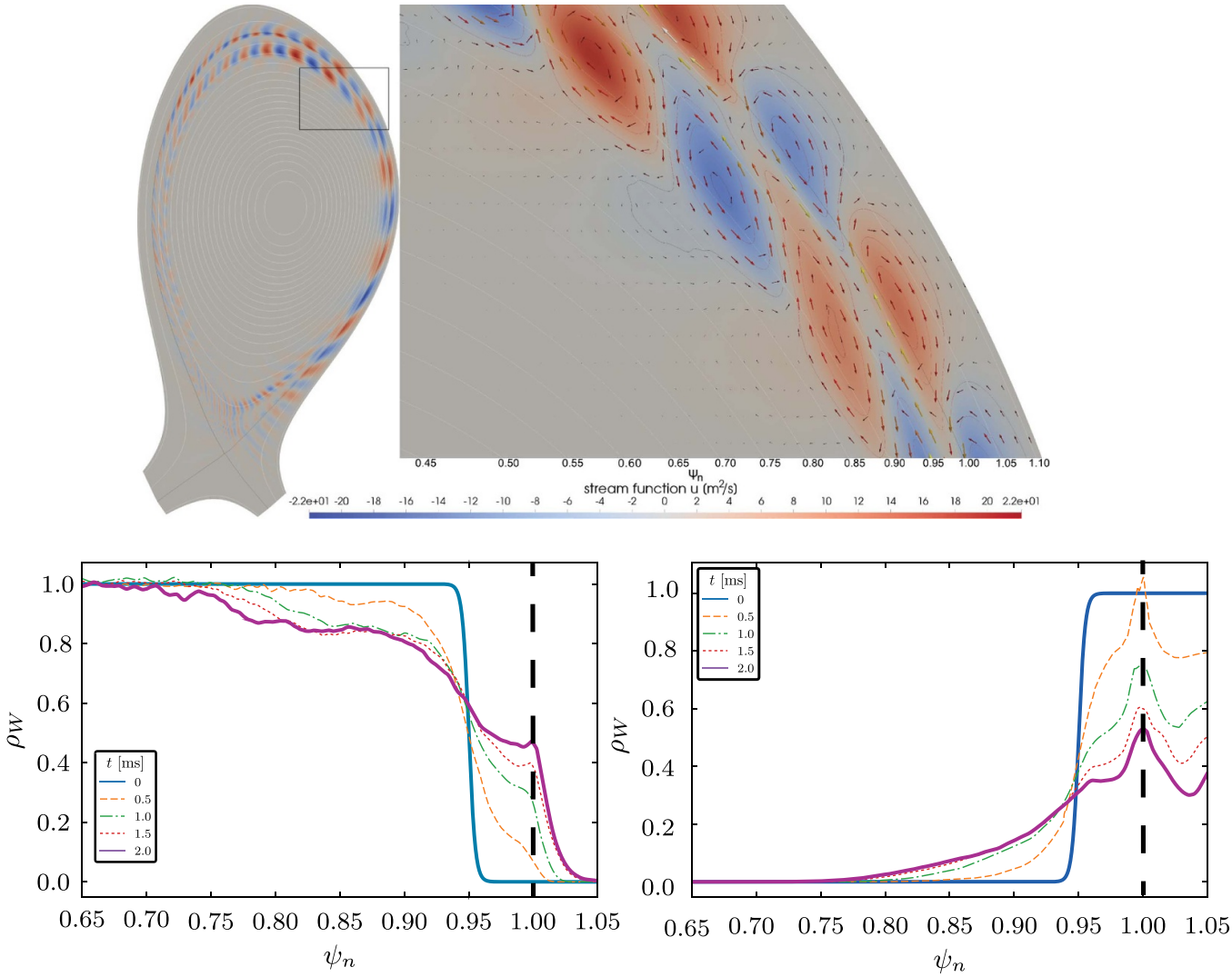

Figure 16. Upper: JOREK model fluid velocity during ELMs for ASDEX Upgrade (arrows indicate the direction of the drift, with the colour indicating the magnitude). Lower left: W impurity distribution before (blue) and after (violet) the ELM assuming inwards edge W transport between ELMs as in present experiments. Lower right: W impurity distribution before (blue) and after (violet) the ELM assuming outwards edge W transport between ELMs as expected in ITER. The dashed vertical line at $\psi_n = 1$ corresponds to the separatrix and the horizontal axis is in normalised flux units. Reprinted from [van Vugt2019], with the permission of AIP Publishing.

self-regulated since the high initial W release leads to high radiative losses, which in turn reduces the edge temperature and hence the sputtered influx. The issue is whether or not the plasma passes through this early phase to higher plasma current or collapses radiatively.

On present all-W devices, even without the use of wall coverage techniques (such as boronisation), limiter start-up has proven possible on pure W surfaces, albeit requiring some optimisation to allow adequate burn through. On AUG, careful tailoring of the density and very early ECH heating is a recipe which has been used successfully to achieve plasma start-up after a vent without boronisation as shown in figure 17 [Neu2009], although the limiter phase has a much shorter duration than in ITER.

On WEST, when operations with the full-W wall began, start-up was found to be rather problematic on the W inner bumper limiters, with early nitrogen (N) injection used as a mitigation strategy [Maget2022b]. The tiles were ultimately exchanged for boron nitride (BN) units at the end of WEST Phase 1 (Campaign C5), but have since been observed to coat with W eroded from elsewhere in the device. Meanwhile, start-up recipes have been improved so that limiter ramp-up on these quasi-W surfaces is now possible without resorting, for example, to early N seeding [Tsitrone2024]. Extensive W limiter deuterium start-up experiments have recently been performed on EAST specifically to support the new ITER baseline, albeit EAST's main wall is made of Molybdenum (Mo). The EAST W limiter plasma studies aimed to investigate the impact of varying the start-up conditions on subsequent diverted plasma evolution. The compilation in figure 18 illustrates the experimental set-up, showing the actively cooled W outer poloidal limiter, a toroidal cross-section to situate the

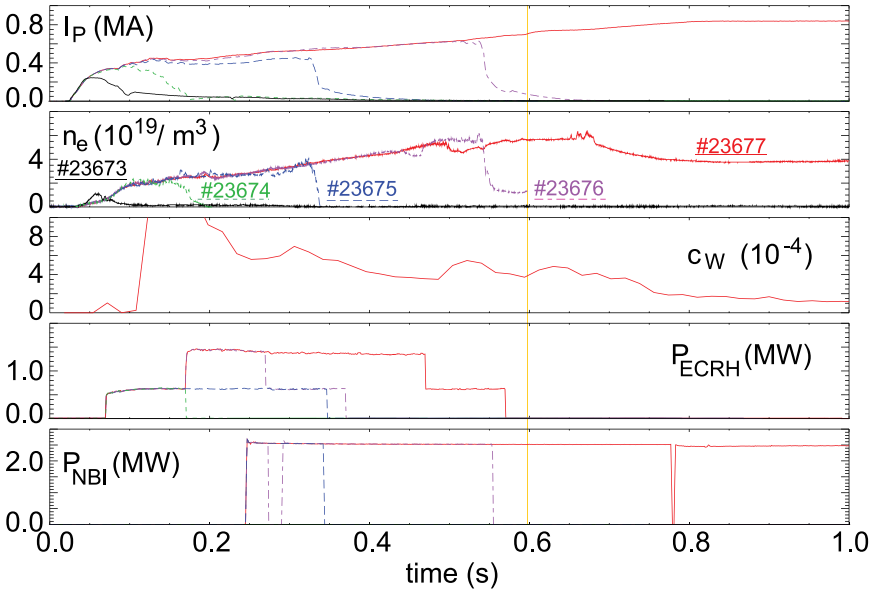

Figure 17. Time traces from restart attempts following a 2008 machine maintenance vent in the full-W ASDEX Upgrade. The deuterium plasma is ramped up on outboard W limiters, using early injection of ECH power, with NBI added from ∼0.3 s. The transition to the divertor is performed as early as possible ($t = 0.6$ s). Five discharges were required to reach the pre-programmed I_p flattop and only 4 more to achieve the first H-mode plasmas. Note that the average W concentration (c_W) is shown only for the final discharge in the sequence. Reproduced from [Neu2009]. © IOP Publishing Ltd. All rights reserved.

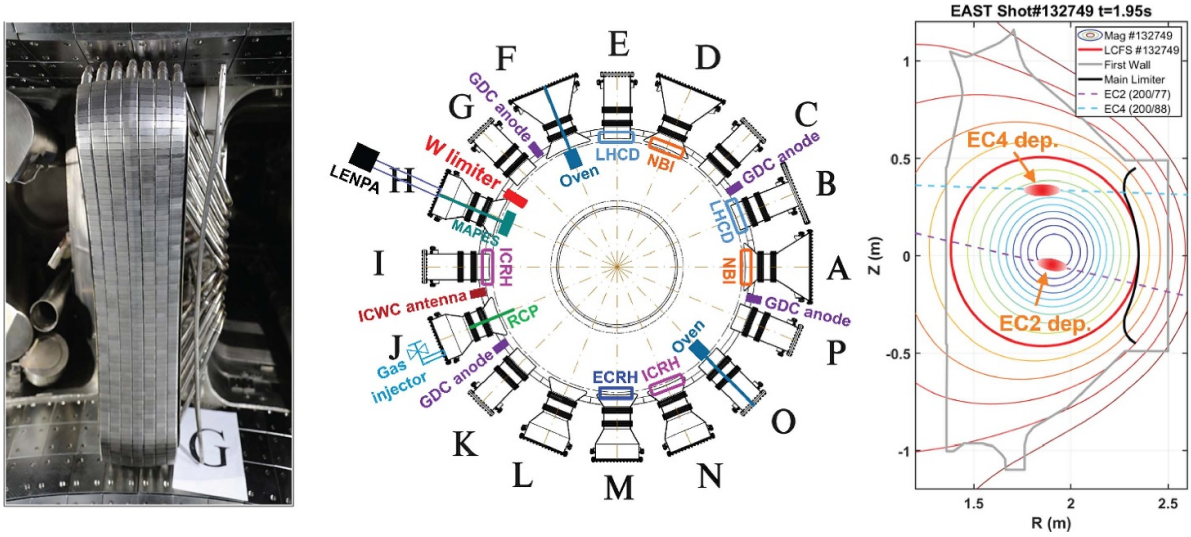

Figure 18. Left: photograph at pre-installation of the EAST actively cooled outer poloidal W limiter (based on a monoblock/plasma-facing unit design similar to the components used in the ITER divertor and the EAST upper divertor). Centre: toroidal cross-section of the EAST tokamak, indicating locations of the outer W limiter, heating systems, GDC and ICWC electrodes and selected diagnostics. Right: poloidal cross-section showing the magnetic equilibrium of the typical outer limiter circular plasma used in the EAST start-up experiments with positions of central and off-axis ECH deposition [Pitts2025, Gong2024]. Reproduced with permission from [Pitts2025]. CC BY-NC-ND 4.0.

locations of the limiter and ECH launchers, and the magnetic equilibrium reconstruction of the typical circular outboard limiter plasma used in the studies which reached $I_p = 200$ kA ($B_T = 2.5$ T) at two values of the plasma density $n_e/n_{GW} \sim 0.15$ and 0.35. A detailed description of the experimental results can be found in [Pitts2025, Gong2024]. Here we describe the main findings summarised by the measurements taken in three key plasma discharges shown in figure 19.

A typical EAST pulse had a flattop duration on the W outer limiter of ∼4 s and all pulses used a single 140 GHz gyrotron ($P_{ECH} \sim 0.65$ MW) heating centrally in second harmonic X-mode (EC2 in figure 18) from the discharge onset. This EC assist was mandatory for success of the discharges starting on W as expected because of the low ITER-like breakdown voltage in EAST. A second and most important result for future ITER operation is evident from pulse #132749 in

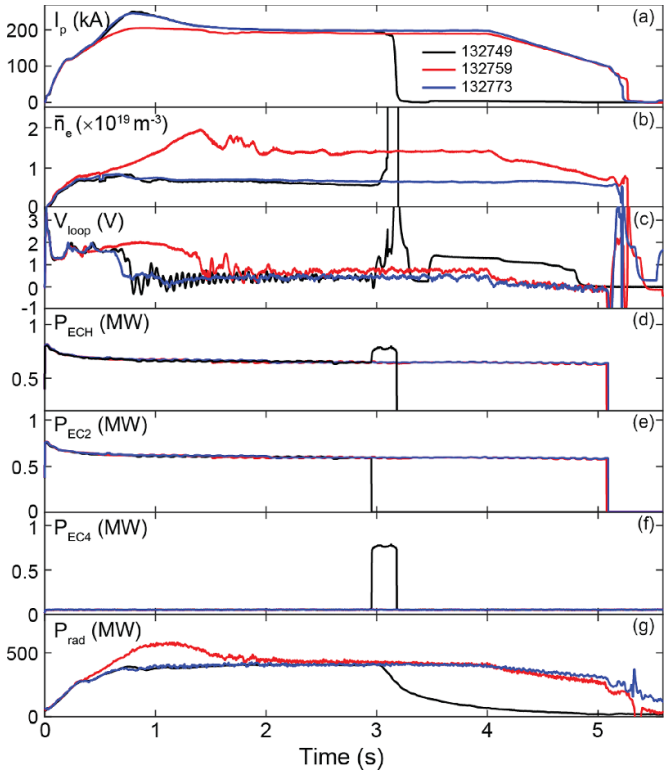

Figure 19. Summary of key time traces for a set of 3 EAST outboard deuterium W limiter plasmas. The ECH powers, P_{EC2} and P_{EC4} refer to the deposition locations shown in figure 18 (right). #132773 and #132749, lowest density with n_e/n_{GW} ~0.15 and #132759 at higher density with n_e/n_{GW} ~0.35. All have $I_p = 200$ kA. Note the low electric field ~0.12 Vm^{-1} in the early start-up phase in all cases (EAST major radius R = 1.85 m) [Pitts2025, Gong2024]. Reproduced with permission from [Pitts2025]. CC BY-NC-ND 4.0.

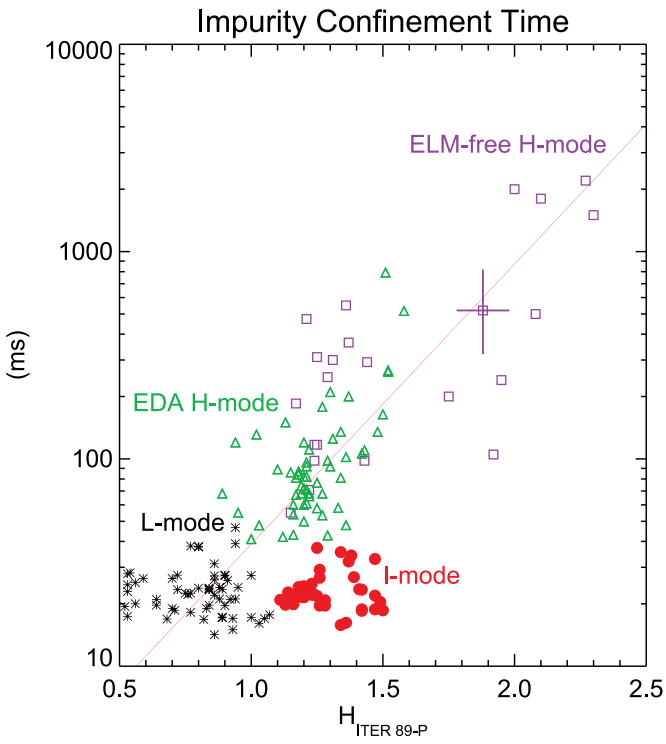

Figure 20. A log plot of the core impurity confinement time (for Calcium) as a function of energy confinement factor H_{89} for L-mode (asterisks), I-mode (dots), EDA H-mode (triangles) and ELM-free H-mode (squares) in Alcator C-Mod. The line is a fit to the L- and H-mode points. Reproduced from [Rice2015]. © YEAR IAEA, Vienna.

which, just before $t = 3$ s, the standard central heating gyrotron is switched off and replaced by a second beam (EC4) heating far off axis at r–0.6. Following this replacement, the plasma disrupts almost immediately (this is a reproducible observation). Data analysis and modelling is still required to confirm the relative contribution of W accumulation and MHD as causes of the disruption, but the need for central EC heating in avoiding issues during early ramp-up on W is clear from this EAST experiment. That central heating is required to prevent core W accumulation in the divertor phases of tokamak plasmas with W PFCs has long been known, as discussed in section 2.1.1. However, the result from EAST is a direct demonstration that the same applies in the limiter phase and, moreover, that EC power will be required in ITER not only for breakdown assist but also during the early limiter ramp-up phase on W surfaces.

In general, the impact of a W wall in L-mode plasma operation is of much less concern in present experiments due to the much lower impurity confinement time than in H-mode, as shown in figure 20 for Alcator C-Mod [Rice2015]. This is due to the higher core and edge particle transport (no edge particle transport barrier) and the lower power levels in L-mode and ensuing W sources. Nonetheless, it is essential to maintain a sufficiently low W concentration in L-mode plasmas by operating at sufficiently high density to avoid large W sources and it is important to prevent temperature collapse by local power imbalance (higher W radiation than heat flux at a given plasma radius). We note that the mechanisms for W accumulation in L-modes in ITER plasmas resemble more closely those in H-mode than those in L-mode plasmas in present experiments, in terms of the relative magnitude of neoclassical to anomalous W fluxes, as discussed in section 2.1.1. This implies that the accumulation of W, in particular for low current/low power L-modes in ITER, may be more of a concern than for high power/high Q H-modes [Fajardo2024a], despite the lower confinement times in L-mode.

2.1.4. Wall conditioning with a W wall and implications for ITER. Operation with a W wall has implications for the achievement of good vacuum conditions in ITER. Besides discharge cleaning techniques, gettering in tokamaks has been used since 1975 as a powerful tool for controlling the impurity influx into fusion plasmas [Winter1990], with specific focus on the reduction of the oxygen impurity concentration with boronisation. Since the new ITER baseline excludes the use of Be, an alternative approach for wall conditioning is necessary to minimise the influx of impurities, notably oxygen, ensuring favourable plasma conditions for effective plasma operation.

Boronisation in fusion devices involves applying a thin, amorphous B layer covering the plasma-facing surfaces through the process of plasma-enhanced chemical vapour deposition. The first boronisation was accomplished in TEXTOR through glow discharge cleaning (GDC) plasma with diluted diborane (B_2D_6) in helium [Winter1989]. Since then, and until the present day, this technique has been routinely and effectively employed in numerous fusion devices. Boronisation via pulsed ICWC plasma has been demonstrated in HT-7 and EAST with carborane as the boron source [Li1999, Gao2009]. Future application in ITER using diluted diborane requires further investigations to address key issues such as achievable deposition rate, the efficiency of deposition relative to diborane evacuation by pumps and whether ICWC may necessitate multiple ICH antennae to achieve layer uniformity, which cannot be implemented in ITER. It is presently not known (R&D is on-going) to which degree layer uniformity is required for efficient oxygen capture by boronisation. Therefore, to achieve a long-lasting oxygen gettering effect in ITER, GDC boronisation (with an as symmetric as possible anode and boron injection point configuration) remains the reference approach for ITER with ICWC being an alternative to be studied. Here we shortly summarise the experimental basis on which the ITER boronisation system is designed, a complete study can be found in [Wauters2024]. Electron cyclotron wall conditioning (ECWC) may also be used for wall conditioning in ITER, however, the plasmas that it produces are not suitable for boronisation purposes.

After completing its conversion into a full W device, the AUG tokamak operated the first experimental campaigns without boronisation [Kallenbach2009]. The relatively high impurity level in the unboronised machine led to restrictions of the H-mode operational space, since low-medium Z impurities dominated the physical sputtering of tungsten, predominantly under low or medium power conditions, as reflected in figure 1. The presence of oxygen also impacted the plasma limiter start-up. Boronisation is found to remove residual oxygen for hundreds of discharges, as shown in figure 21 for AUG [Kallenbach2009] and WEST [Bucalossi2022]. The reduction is most pronounced in the first boronisation in WEST, lasting hundreds of discharges after the third one. Boronisation in WEST improves plasma start-up by almost completely suppressing runaway electron (RE) beam formation, extending prefill ranges and reducing the edge radiation levels [Bucalossi2022].

Experimental results [Buzhinskij1997, Hong2011, Ennaceur2000] and modelling [Hagelaar2015] have been applied to define the configuration of diborane injection points and GDC electrodes to provide an as symmetric as possible boron film deposited on the ITER first wall, which is shown in figure 22, as well as to estimate the capability of the applied boron layers to absorb oxygen and their erosion lifetime. For details on these studies and evaluations the reader is referred to [Schmid2024, Wauters2024].

As boron is eroded, it is expected to migrate and deposit at the divertor [Schmid2024] and, together with it, hydrogen isotopes will be co-deposited. The phenomenology is similar

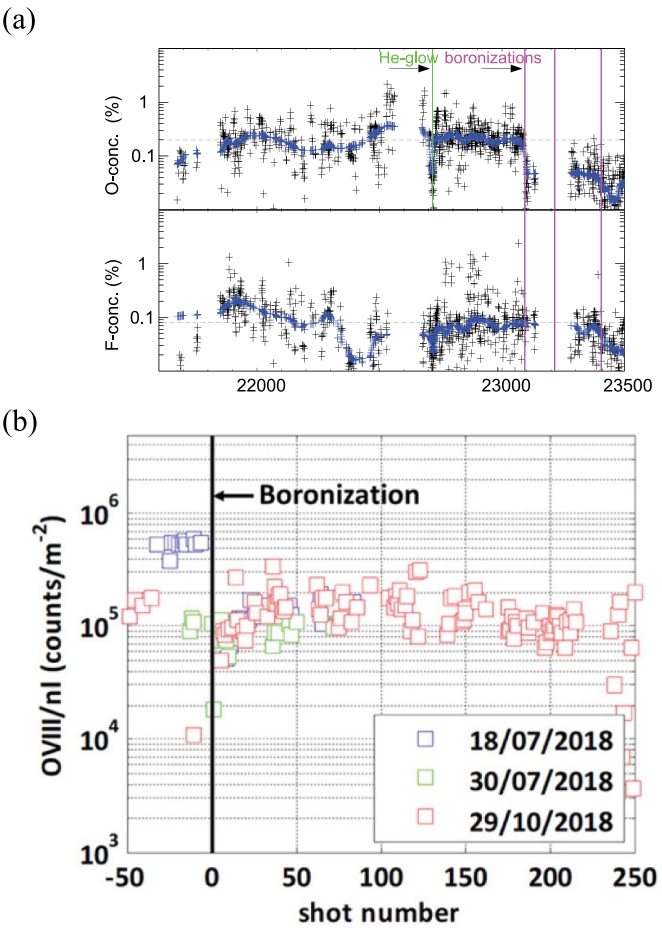

Figure 21. (a) Development of O concentrations during the unboronised, full-W ASDEX Upgrade campaign and after boronisation, from x-ray lines measured by a Bragg crystal spectrometer ($n_e > 4.5 \times 10^{19}$ m^{-3}). Reproduced from [Kallenbach2009]. © YEAR IAEA, Vienna. (b) Oxygen radiation before and after the first, second and third boronisations performed on WEST. Reproduced from [Bucalossi2022]. CC BY 4.0.

to that of Be eroded from the first wall, although it is quantitatively different for boron since the source can be quantified accurately (i.e. the boron introduced by boronisation while Be is produced by erosion of the wall). The magnitude of the co-deposition is higher for boron than for Be as well. The scheme foreseen in ITER to remove captive fuel (Tritium) in these divertor deposited layers relies on a combination of dedicated plasma operation followed by ICWC. Dedicated tokamak discharges have been developed for JET [Wauters2022] and investigated theoretically for ITER [Park2023] to recover fuel from divertor deposits. The optimum plasma scenario for fuel removal involves raising the divertor strike lines onto deposition-dominated areas, bringing plasma heat and particle flux to these locations. A concern in this approach is the possibility of re-depositing T along with B onto other PFCs during plasma operation rendering them inaccessible for subsequent cleaning through tokamak discharges. This risk can be reduced by decreasing the T content in tokamak cleaning pulses, and consequently in newly formed deposits, using

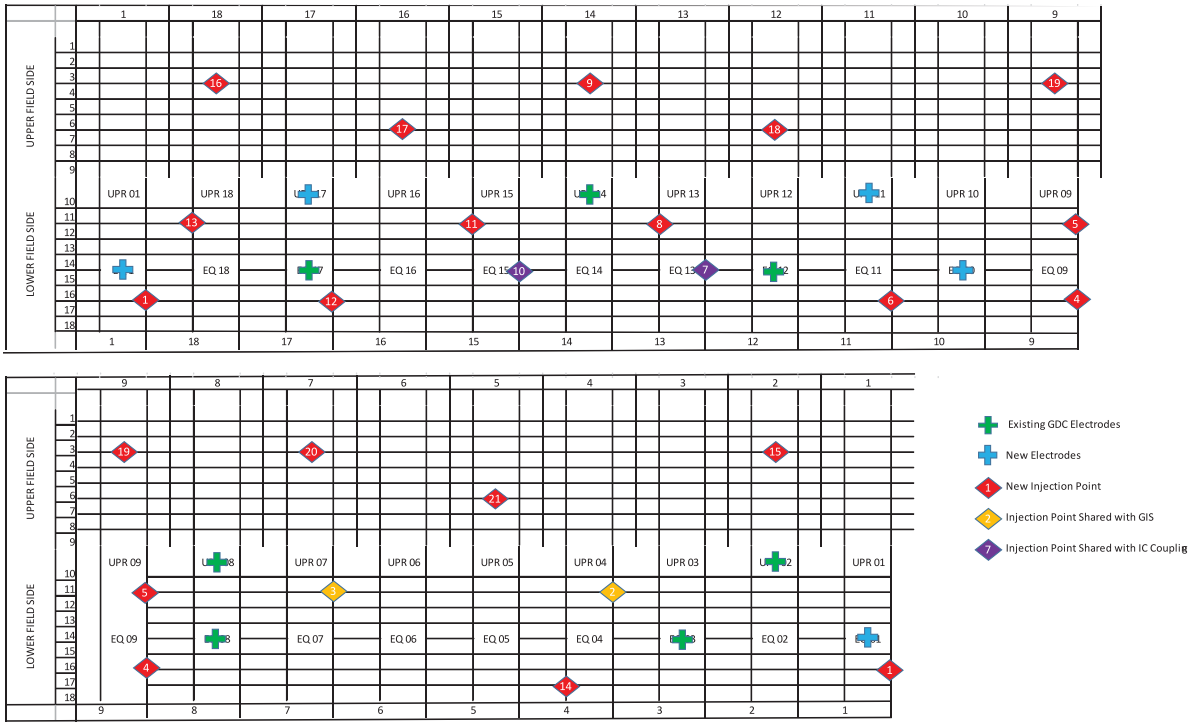

Figure 22. Simplified first wall map showing GDC Electrode and diborane injection point locations in ITER (note end columns wrap around to illustrate circular nature of the vacuum vessel).

ICWC, as demonstrated in JET [Mateev2023] since the main chamber inventory in the deposits, accumulating at lower rates on the W surfaces, can be accessed directly by ICWC. This combination of specific tokamak operation and ICWC has been thus adopted for the fuel removal strategy in ITER which will be tested, for the first time, in SRO.

2.2. Considerations on H&CD for the new ITER baseline

To guide the reconsideration of the heating level and mix for ITER operation with a W wall in the NB not only do the issues related to the wall material need to be considered, but also the objectives, experimental strategy and constraints of the SRO and DT-1 phases of the NB-IRP. These have been already summarised in the introduction and are repeated below:

For SRO the key objectives are:

- To commission control and protection systems with plasma up to 15 MA/5.3 T;
- To demonstrate disruption mitigation up to up to 15 MA/5.3 T;
- To develop plasma scenarios up to 15 MA/5.3 T in L-mode;
- To develop plasma scenarios up to 7.5 MA/2.65 T in H-mode with deuterium (DD) plasmas.

For DT-1 the key objectives are:

- To commission control and protection systems with plasma up to $Q \geqslant 10$;
- To demonstrate disruption mitigation up to $Q \geqslant 10$;
- To develop plasma scenarios in DT up to 15 MA/5.3 T in H-mode with $Q \geqslant 10$, $P_{\mathrm{fusion}} = 500$ MW over 300s (or lower plasma current if $Q \geqslant 10$ can be demonstrated at those levels);
- To study the physics of burning plasmas and their integration with an all-W PFC configuration;

For DT-2 the objectives concern the demonstration of long pulse scenarios with $Q \geqslant 5$ for 1000 s (partly inductive) and 3000 s (steady-state). The latter requires specific H&CD upgrades such as the 3$^{\mathrm{rd}}$ NBI injector [Polevoi2020, Kim2021].

The DT-1 programme needs to be implemented within a total neutron fluence of $\sim 3.5 \times 10^{25}$ DT neutrons, which is $\sim$1% of the Project Specification goal and equivalent to the fluence produced in $\sim$550 pulses with 500 MW at $Q \geqslant 10$ and 300s burn duration. As will be discussed in section 3.4, the achievement of the DT-1 goals within this fluence requires the interleaving of DD and DT H-mode scenario development as the plasma current/toroidal field levels increase towards 15 MA/5.3 T.

Thus, the additional heating power levels in the NB SRO and DT-1 phases have been defined on the basis of the requirements to sustain H-mode operation in ITER and demonstrate the SRO and DT-1 goals. The H&CD mix is, on the other hand, defined by the system and port availability in ITER together with integration issues with a W wall that favours ECH over ICH, given the potential issues of the latter related to increase W wall impurity sources. The ITER power level requirements, as described in section 2.1, are based on the following assumptions: (a) to sustain H-mode plasmas a sufficient edge power

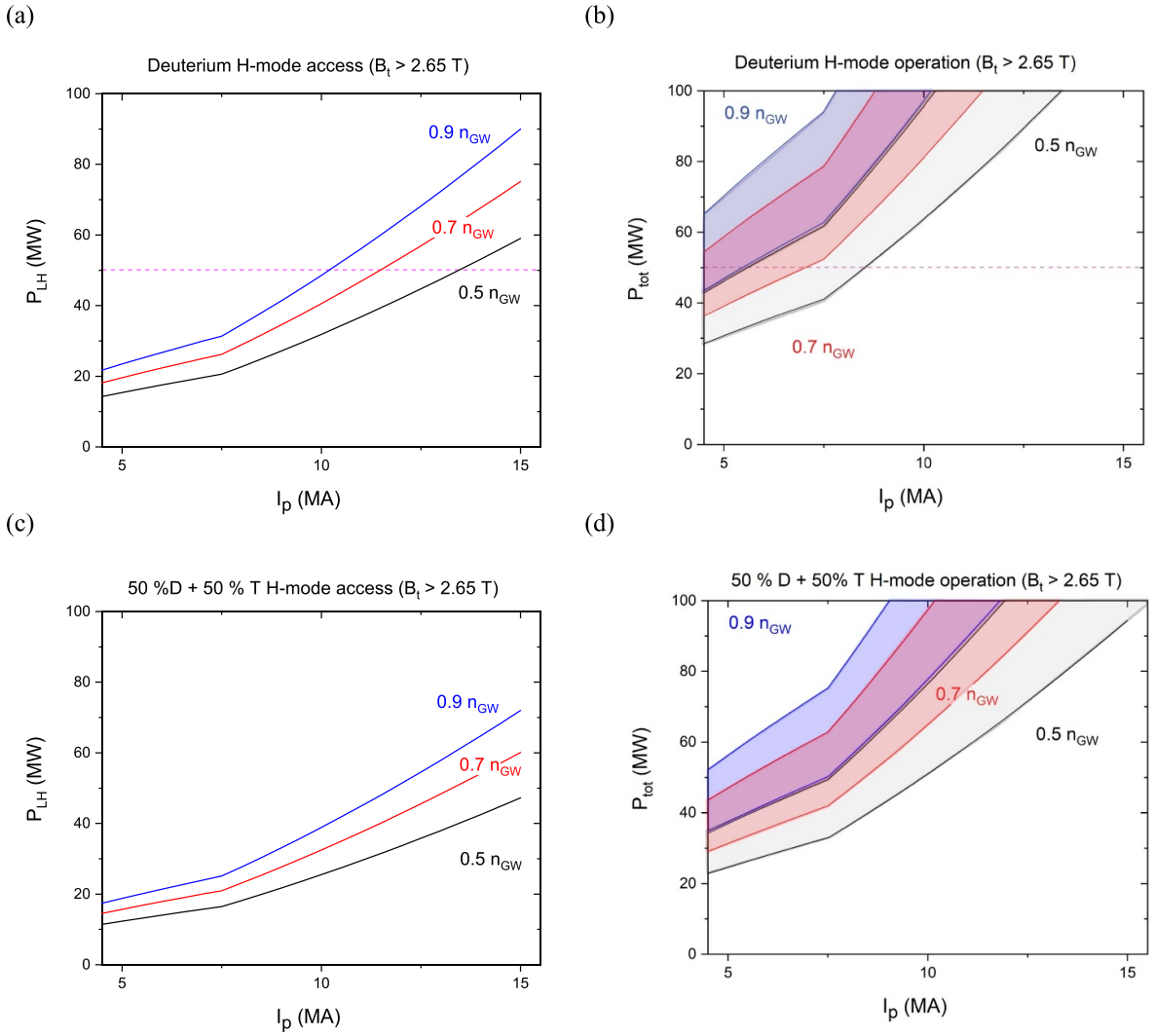

Figure 23. Power required to access H-mode (a), (c) and H-mode operational range (b), (d) for DD and 50% D—50% T plasmas and a range of operational densities. Note that for plasmas with D and T, the total power includes additional heating as well as alpha heating. The horizontal dashed line in (a), (b) corresponds to the maximum coupled additional heating power in SRO (50 MW). We note that for DT-1 the maximum additional heating coupled power (without upgrades) is 103 MW and thus close to the maximum value of the ordinate in (a)–(d).

level is required ($P_{sep} \geqslant 1.5\ P_{LH}$), and (b) the expected level of radiated core power with a W wall will be in the range from $0.25 \leqslant P_{rad}{}^{core}/P_{aux} \leqslant 0.5$. The resulting operational spaces for H-mode plasmas in SRO (DD) and DT-1 (DD and DT) are illustrated in figure 23 for a plasma density range that is expected to be above the minimum density for H-mode access in ITER [Loarte2021]. We note that we use the scaling for the L–H transition power evaluation in [Martin2008] and that we include the isotopic effect of T on the L–H transition. For the latter it is assumed that for 50–50 DT plasmas, $P_{LH,DT}/P_{LH,DD} = 0.8$ [Righi1999]; an inverse scaling of the H-mode threshold from D to T has been confirmed in the recent DTE-2 experiments at JET with the ILW [Solano2023].

From these guidelines we can conclude that an additional heating power level of 50 MW allows the demonstration of robust H-mode operation ($P_{sep} \geqslant 1.5\ P_{LH}$) in DD at 5–7.5 MA/2.65 T in a wide range of plasma density/core plasma radiation levels. On the other hand, the extension of the H-mode operational range to $I_p \geqslant 10$ MA in DD, as foreseen in DT-1, requires additional heating power levels of, at least, 100 MW. These evaluations, together with considerations of system availability and port allocation provided the basis for the additional heating systems considered for SRO ($P_{ECH} = 40$ MW and $P_{ICH} = 10$ MW) and DT-1 ($P_{ECH} = 60$–67 MW, $P_{ICH} = 10$–20 MW, $P_{NBI} = 33$ MW). For DT-2 the major driver is the increase of the H&CD capabilities to the maximum in ITER and, in particular, of the current drive with NBI ($P_{NBI} = 49.5$ MW) to enable steady-state operation [Polevoi2020, Kim2021]. Details on the H&CD systems adopted for the NB are described in [Barabaschi2024] and are summarised here for completeness:

- SRO: 20 MW from one equatorial ECH launcher, 20 MW from three upper ECH launchers (for details see [Henderson2015]) and 10 MW from one ICH antenna.

- DT-1: 40 MW from two equatorial ECH launchers, 20–27 MW from three or four upper ECH launchers, 10–20 MW from one ICH antenna and 33 MW from two NBI injectors. Note that the new equatorial ECH launcher is under design and details of its power deposition/current drive capabilities are under evaluation. Despite this, it is most likely that all injected power will provide co-current drive and central heating (typically to $\rho < 0.5$).
- DT-2: 40 MW from two equatorial ECH launchers, 20–27 MW from three or four upper ECH launchers, 10–20 MW from one ICH antenna and 49.5 MW from three NBI injectors.

An important ingredient in the above evaluations is the choice of $n_e = 0.5\ n_{GW}$ as the minimum density for sustained H-mode operation in ITER, since the required power to sustain H-mode plasmas scales as $\sim <n_e>^{0.72}$ [Martin2008]. This choice is based on the finding that the edge ion heat flux is a key physics parameter to trigger the H-mode transition [Ryter2013] for plasmas with dominant electron heating and low rotation, as expected in ITER. Applied to ITER plasmas leads to $n_e = 0.5\ n_{GW}$ being an appropriate level for the lowest density to plan H-mode operation in SRO and DT-1 taking into account that most H-mode scenarios cover a range of $q_{95} = 3$–6 [Loarte2021, Vincenzi2024a]. Since ITER plasmas are dominantly electron heated, a sufficient density is required for enough equipartition and edge ion heat flux. The criterion $n_e = 0.5\ n_{GW}$ provides the optimum compromise between sufficient edge ion heat flux and overall power level required for H-mode operation (because the required ion power increases with plasma density). The validity of such assumption has been verified in dedicated studies on the access to H-mode in D 5 MA/2.65 T ECH heated plasmas modelled by ASTRA with the TGLF-SAT2 transport model and using a scaling for H-mode access based on the ion heat flux value [Schmidtmayr2018]. This analysis shows that, in terms of the margin above the required ion heat flux for H-mode access for operation with $P_{ECH} = 40$ MW, the optimum density is $\sim 1.8 \times 10^{19}$ m^{-3} which corresponds to 45% of n_{GW}, as shown in figure 24 [Angioni2023]. At this density, the resulting edge ion heat flux exceeds by 6–8 MW that required for H-mode access. In the context of the ITER W wall, we note that the presence of W in these plasmas even to significant concentrations ($\sim 10^{-4}$) is not detrimental for H-mode, even given the much higher atomic number and radiation efficiency of W compared with Be. This is due to the fact that, although larger W radiation reduces the total edge heat flux, the resulting lower electron temperature leads to a higher equipartition and increased ion heat flux, which compensates the lower total power heating the plasma. In addition, the lower impurity content with W compared to Be leads to a smaller effect of impurity dilution on turbulence in the SAT2 model, which increases ion conductivity and, thus, edge ion heat flux.

We note that, because of the need for high levels of additional heating in DD H-mode plasmas at high I_p, the H-mode development programme in the 2016 IRP switched to DT already at 7.5 MA/2.65 T [ITR-24-005]. This strategy was

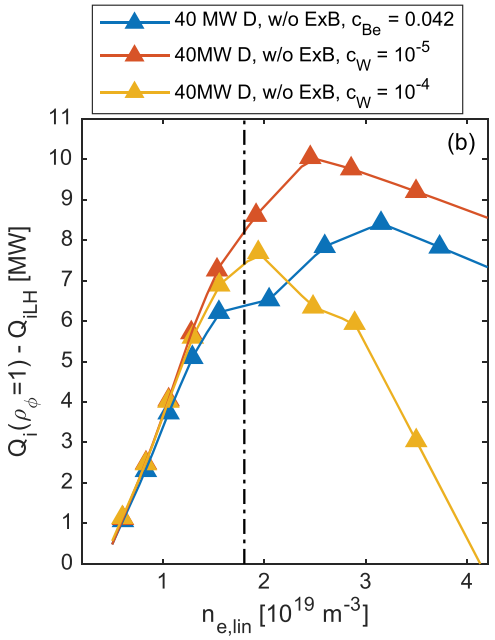

Figure 24. Ion heat fluxes in MW at $\rho = 1.0$ minus the L–H transition ion heat flux scaling [Schmidtmayr2018] for simulations with $n_{ne} \simeq n_{e,lin}/2.5$ and $T_{i,sep} = T_{e,sep} = 120$ eV, without the inclusion of the impact of the $E \times B$ shearing rate in TGLF–SAT2, for different impurity species, with Be concentration of 0.042 and with W in concentration of 10^{-4}. The vertical dash–dotted line identifies the minimum density according to [Ryter2013, Loarte2021]. Reproduced from [Angioni2023]. CC BY 4.0.

conceived to take advantage both of the lower power requirements for H-mode operation in DT plasmas, due to the lower H-mode threshold, and of the contribution of the alpha heating to sustain the H-mode scenario with increasing I_p. In the context of DT-1 in the NB, such a strategy has two major disadvantages:

- Maximises the neutron fluence, since increasing levels of alpha heating (and thus neutron production) are intrinsically required for the expansion of the H-mode operational space;
- Optimisation of alpha heating becomes an important aspect of scenario development, beyond a topic of research, towards high I_p even at moderate Q. This is because alpha heating becomes a sizeable (even if not dominant) contributor to the total heating required to maintain the plasma in H-mode (e.g. $P_\alpha/P_{add} = 0.4$ for $Q = 2$). The need for sufficient alpha heating to sustain H-mode scenarios in DT, even at moderate Q, restricts the range of D/T ratios that can be explored at a given current level and has the potential to slow down the development to $Q \geqslant 10$ (resulting in increased neutron fluence).

The availability of additional heating power in DT-1 at a level of $\sim$100 MW opens the operational space for H-modes in DD or with D + low percentage of T to high I_p, as shown in figure 23. This allows the development of scenarios towards high Q starting from DD without the need to optimise alpha heating at each single step. With the flexibility

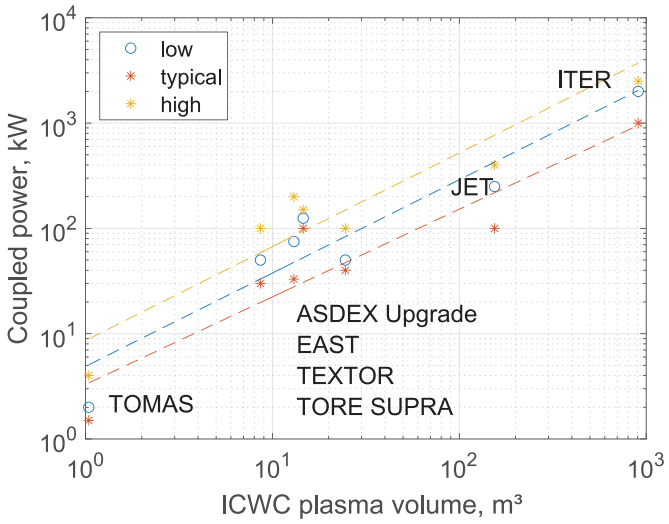

Figure 25. Plasma absorbed power for effective ICWC in present experiments showing its scaling with volume.

provided by this high level of additional heating it is possible to implement a scenario development strategy in the NB similar to that already successfully implemented in present DT tokamak experiments such as JET [Garcia2023, Maggi2024, Rimini2024] and TFTR [Strachan1997], as discussed in detail in section 3.4. Optimisation of alpha heating will, of course, still be required at the largest values of I_p to enable the achievement of $Q \geqslant 5$ in ITER.

We note that the ICH antenna will also provide the required capability for fuel removal and wall conditioning tests in SRO (to be used routinely later in DT-1), as discussed in section 2.1.4, using ICWC. Scaling from present ICWC experiments results in a coupled power to the plasma of 2 MW being required for effective ICWC application in ITER, as shown in figure 25. This implies a 5 MW ICWC power system since the absorbed power by the plasma for ICWC is typically 40% of the injected power [Kovtun2023]. The SRO system with 10 MW of ICH installed can, thus, fully fulfil this requirement.

3. The NB IRP

The strategy of the NB-IRP is based on the scientific and technical knowledge developed in the ITER Members' fusion research communities over many years. The NB-IRP defines the research and development to be executed up to the achievement of the Project's fusion power goals, including the testing program of the TBMs, provided by several ITER Members for tritium breeding and operated under the responsibility of the ITER Organisation, as well as the demonstration of ITER operation as a fully integrated fusion engineering system with the achievement of key technological goals for the demonstration of nuclear fusion as an energy source for mankind. These fusion power demonstration goals are specifically: the demonstration of 500 MW of fusion power with fusion power multiplication factor (Q) $\geqslant$ 10 for lengths of 300–500 s and of long pulse and steady-state non-inductive scenarios with $Q \geqslant 5$ and burn lengths of 1000 s and 3000 s respectively. The NB-IRP strategy has been developed consistent with the successive installation of tokamak components and ancillary systems up to the completion of the new ITER baseline configuration, with a stepwise approach to nuclear safety demonstration, including the progressive acquisition of knowledge and lessons learnt in each phase to prepare the next one.

The NB-IRP is divided into five major phases:

- **Integrated commissioning I (IC-I)**: This phase concerns the integrated commissioning of all ITER tokamak and plant components/systems installed in the Pre-SRO assembly phase up to the demonstration of the capabilities required to produce a tokamak plasma, including the achievement of nominal currents in the superconducting coils, i.e. the demonstration of full magnetic field operation. The IC-I phase is foreseen to last 18 months.
- **Start or research operation (SRO):** This phase starts with the demonstration of the first tokamak plasma and concludes with the demonstration of tokamak operation up to the nominal design parameters of 15 MA/5.3 T in a diverted plasma configuration, including the use of the electron cyclotron (40 MW ECH) and ion cyclotron (10 MW ICH) H&CD systems up to their nominal coupled power levels into the plasma and for durations of up to 50 s. Within the SRO phase an experimental campaign with deuterium plasmas at reduced current up to 7.5 MA and toroidal field (2.65 T) will take place to explore the operational space and control of H-mode plasmas in ITER. This will mark the start of nuclear operation (SNO) in ITER; the neutron fluence in the deuterium experimental campaign will be limited to enable the installation of in-vessel components foreseen in the Post-SRO assembly phase, while respecting shutdown dose rate requirements for workers involved in these activities. The SRO phase is foreseen to last 27 months, including the demonstration of the first tokamak plasma in ITER. In this phase, the engineering evaluation of the ITER tokamak as an integrated system with as-built and as-assembled components/systems will be performed.
- **Integrated commissioning II (IC-II)**: This phase concerns the integrated commissioning of all ITER tokamak and plant components/systems installed in the Post-SRO assembly phase and re-commissioning of those installed in Pre-SRO assembly up to the demonstration of the capabilities required to produce deuterium–tritium tokamak plasmas. The IC-II phase is foreseen to last 10 months.
- **First deuterium–tritium phase (DT-1):** In this phase, deuterium (D)—tritium (T) plasma scenarios will be developed to demonstrate the Project's goal of 500 MW of fusion power with multiplication factor (Q) $\geqslant$ 10 for lengths of, at least, 300 s and to demonstrate high-duty operation (1 pulse every 30 min) with fusion power levels of 250 MW for, at least, 300 s. Operations in this phase are divided into 2 yr cycles with 16 months of plasma operations, followed by 8 months of long-term maintenance, which include integrated commissioning activities before each campaign.

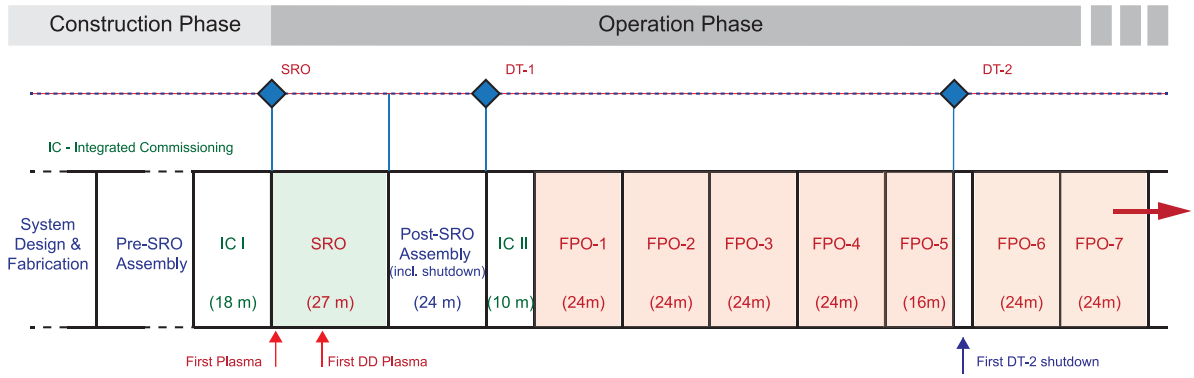

Figure 26. Schematic of the timeline for the new baseline ITER research plan.

Research in this phase will address, among others, a wide range of burning plasma physics and scenario integration issues and will provide demonstrations of key technologies required for demonstration fusion reactors such as those related to heat flux handling components at an average neutron flux $\geqslant$0.5 MW m^{-2}. The neutron fluence in this phase will be limited to enable the performance of maintenance activities in the corresponding long-term maintenance periods, while respecting shutdown dose rate requirements for workers; this fluence is evaluated to be 3.5 10^{25}, which is of the order of $\sim$1% of the ultimate Project fluence goal. This phase will also provide key reference data to perform safety-related evaluations for D–T operation in ITER (e.g. radiation maps, T retention and removal, dust production, etc.), which will be used to refine the licencing requirements details in the second deuterium–tritium phase that will follow DT-1. The DT-1 phase is foreseen to last up to 10 yrs, i.e. it includes 5 experimental campaigns.

- **Second deuterium–tritium phase (DT-2):** In this phase, D–T plasma scenarios will be developed to demonstrate all the Project's fusion power production goals. These goals are specifically: the demonstration of 500 MW of fusion power with fusion power multiplication factor (Q) $\geqslant$ 10 for lengths of 300–500 s in high duty operation and of long pulse and steady-state scenarios with and $Q \geqslant 5$ burn lengths of 1000 s and 3000 s respectively, which support the physics basis of scenarios considered for demonstration fusion reactors. In addition, research will be carried out to support the ITER Members' demonstration fusion reactor programmes including both scenario development issues (e.g. heat flux exhaust), design/operational issues (e.g. optimum H&CD mix) and their TBM programmes, in principle, up to neutron fluences of at least 0.3 MW yr^{-1} m^2 (or 3 10^{27} neutrons). The activities to be performed in this phase will be defined in detail during DT-1 once high fusion power production in D–T plasmas has been produced in ITER and the licencing requirements for DT-2 have been defined. Operations in this phase are divided into 2 yr cycles with 16 months of plasma operations, followed by 8 months of long-term maintenance, which include integrated commissioning activities before each campaign. Before the start of DT-2 specific integrated commissioning of the newly available or upgraded components or systems and recommissioning of the existing ones will take place. The DT-2 phase is foreseen to last up to 10 yrs, i.e. it includes 5 experimental campaigns.

Diagnostics play a key role in the operation and scientific exploitation of the ITER device. To achieve the objectives of the IRP, many measurements are needed, including plasma shape, position and other critical parameters. The diagnostic set in the NB has been optimised to the specific needs of each experimental phase and, for SRO, with the objective to also simplify first assembly of the tokamak. In SRO about 60% of the final set of diagnostics from the 2016 baseline [ITR-24-005] are available, including 100% of in-vessel diagnostics. Emphasis of the diagnostic set in SRO is given to those that are required for basic tokamak operation and to characterise the plasmas to be explored in SRO, as well as to acquire measurements to substantiate the DT-1 safety case, including redundancies to mitigate the risk of failure of key measurements (details provided in [Barabaschi2024]). For DT-1 operation the full 2016 baseline set will be virtually complete with the addition of the remaining diagnostics in the post-SRO shutdown. These include an extensive set of neutron, fast particle and fusion products diagnostics [Walsh2011] required to support DT operation in ITER.

The timeline of the NB-IRP is summarised in figure 26 and in more detail, together with other key activities, in figure 27. Note that assembly phases in the timeline of figures 26 and 27 are shown for information only since they are not part of the research plan. Table 1 summarises key tokamak components and systems that will be available to execute the programme in each of the phases. We now describe in more detail the operational strategy and the research to be carried out in each of the phases together with associated supporting modelling studies, as well as the open R&D issues for each phase.

3.1. Integrated commissioning I

The objective of this phase is to prepare the tokamak for plasma operation and to demonstrate that the integrated operation of the tokamak and ancillary systems, as installed in the Pre-SRO assembly phase, meet the performance requirements for plasma operation. This demonstration is required

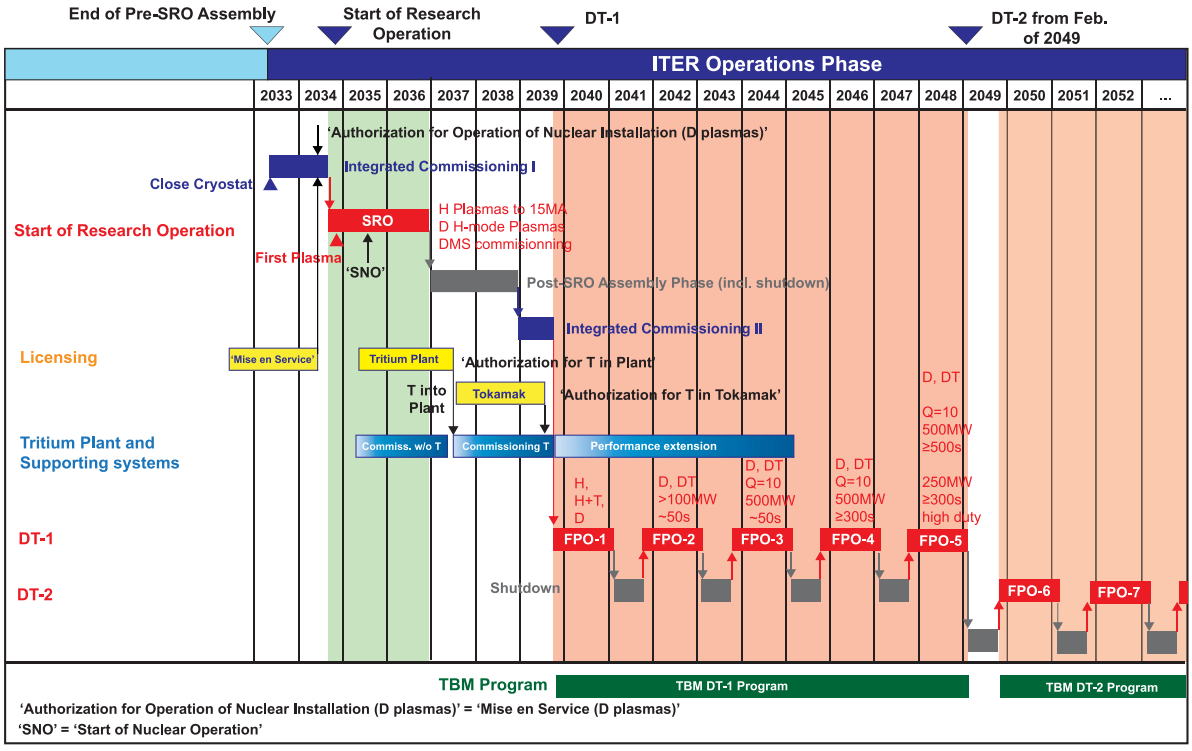

Figure 27. Operational plan for the execution of the new baseline ITER research plan to the demonstration of the $Q \geqslant 10$ 500 MW fusion power goal in the 1st deuterium–tritium phase and the initial campaigns of the 2nd deuterium–tritium phase.

before plasma operation can be attempted. The IC-I phase starts with the closure of the cryostat. The activities in this phase involve commissioning of the core tokamak components (cryostat, vacuum vessel, superconducting coils, in-vessel coils, divertor, …), conditioning of in-vessel components, and commissioning of ancillary systems such as ICH, DMS, GDC, controls, safety and interlock systems for plasma operation (plasma control system (PCS), advanced protection system (APS), central interlock system (CIS)), etc. This phase concludes with the commissioning of the superconducting magnets to full current demonstrating that they can support operation at 15 MA/5.3 T. The successful completion of this commissioning marks the culmination of IC-I and opens the way to the SRO phase. A high-level description of the IC-I activities is shown in figure 28.

The licensing process for ITER to start nuclear operation (Authorisation for operation of nuclear installation for deuterium plasmas or 'Mise en Service' for deuterium plasmas), following the delivery of the required *in-situ* qualification and commissioning test results to the nuclear regulator, shall be completed during the integrated commissioning phase in advance of SRO operations. The IC-I phase is planned to last 18 months and proceeds directly to the SRO phase.

Key outcomes of the activities planned for IC-I include:

- Superconducting coil operation at nominal current levels and ramp rates, as required for the nominal 15 MA/5.3 T scenario;
- Demonstration of high quality vacuum required for tokamak plasma operation;
- Commissioning of the controls, safety and interlock systems required for plasma operation;
- Authorisation for operation of nuclear installation for deuterium plasmas ('Mise en Service' for deuterium plasmas).

3.2. SRO

The objective of this phase is to develop the operational basis for the plasma scenarios to be later employed for fusion power production in DT-1 and to commission with plasma key systems required to support them (e.g. PCS, APS, CIS, DMS, etc.). This phase starts with the demonstration of the first tokamak plasma, which requires all tokamak, plant, and auxiliary systems to operate in an integrated way under the PCS satisfying their respective requirements for plasma operation. In the following part of the SRO phase, tokamak operation up to the nominal plasma current and field of 15 MA/5.3 T will be demonstrated in low confinement mode (L-mode). High confinement mode (H-mode) scenarios will be explored up to 7.5 MA at 2.65 T, both in diverted plasma configurations [Vincenzi2024 a]. This requires commissioning of the available H&CD systems (ECH and ICH) up to their nominal plasma coupled power levels for durations of up to 50 s. Most plasmas will be performed in hydrogen (H, with helium-3 (^{3}He) as minority species for ICH) with a specific set of experiments carried out in deuterium plasmas (DD, with H as minority species for ICH) to address the exploration of H-mode scenarios, which will mark the SNOs in ITER. The use of H and DD plasmas allows the execution of the experimental programme with low production of neutrons and tritium by

Table 1. Key tokamak and ancillary systems available for operation in the various phases of the NB IRP.

System/ancillary available	Start of research operation	DT-1	DT-2
Vacuum vessel, thermal shield and cryostat	Final configuration	Final configuration	Final configuration
Toroidal field, poloidal field, central solenoid and error field correction superconducting magnets and power supplies	Final configuration	Final configuration	Final configuration
In-vessel vertical stability and elm control coils and power supplies	Final configuration	Final configuration	Final configuration
Cryostat and torus cryopumps	Final configuration	Final configuration	Final configuration
Blanket shield modules and first wall	Temporary configuration (inertially cooled)	Final configuration	Final configuration
Divertor	Final configuration	Final configuration	Final configuration
Glow discharge system	Partial configuration	Final configuration	Final configuration
Boronisation gas distribution (B_2D_6)	Final configuration	Final configuration	Final configuration
Gas and pellet injection systems	Partial configuration	Final configuration	Final configuration
Disruption mitigation system	Final configuration	Final configuration	Final configuration
Electron cyclotron heating	Upper launchers installed (3 operational) 1 equatorial launcher (40 MW)	3 or 4 upper launchers operational 2 equatorial launchers (60–67 MW)	3 or 4 upper launchers operational 2 equatorial launchers (60–67 MW)
Ion cyclotron heating	1 antenna (10 MW)	1 antenna (10–20 MW)	1 antenna (10–20 MW)
Neutral beam heating		2 injectors (33 MW)	2 or 3 injectors (33–49.5 MW)
Diagnostic neutral beam		Final configuration	Final configuration
Diagnostics	Basic set for SRO phase (incl. for the safety-related knowledge acquisition programme)	Near complete set, including DT fusion products	Complete set
Hot cell facility	Partial configuration for operation on TFA liquid radwaste, independently of hot cell building	Operational for DT-1	Operational with expanded capabilities for DT-2
Test blanket modules and their ancillary systems		DT-1 TBMs	DT-2 TBMs
Tritium plant	Limited Configuration	Operational	Operational with expanded capabilities for DT-2

fusion reactions. The neutron fluence in the DD experimental campaign will be limited to $\sim$1.5 10^{20} to enable the installation of in-vessel components foreseen in the post-SRO assembly phase, while respecting shutdown dose rate requirements for workers involved in these activities.

The overall plan for the SRO phase is shown in figure 29 and the plasma scenarios to be covered in SRO are summarised in figure 30; the logic and strategy behind the experimental plan and the physics evaluation that support them will be described below. The SRO phase is planned for 27 months of plasma operations including the demonstration of FP. By the start of SRO many systems are in their baseline configuration while others are in a partial or temporary configuration to facilitate the achievement of the SRO objectives with minimum operational risks, such as those associated with disruption loads and their mitigation (see table 1). Of particular importance here is the use of an inertially cooled W wall in SRO since this minimises the risk that issues related to the application of plasma control schemes, which will be tested with plasma operation in SRO for the first time, as well as to the development of disruption mitigation can severely impact operation. While superficial damage of wall PFCs may not be avoided, no leak of water in the vacuum vessel will occur since the PFCs are inertially cooled and, consequently, long downtimes to recover from water leaks resulting from wall PFC damage are avoided in the SRO phase. This is the first phase of operation and will, thus, provide first evidence for the validation of many of the physics models and assumptions that have been used for the design of ITER as well to plan its operation. These, to cite a few, include verification of plasma

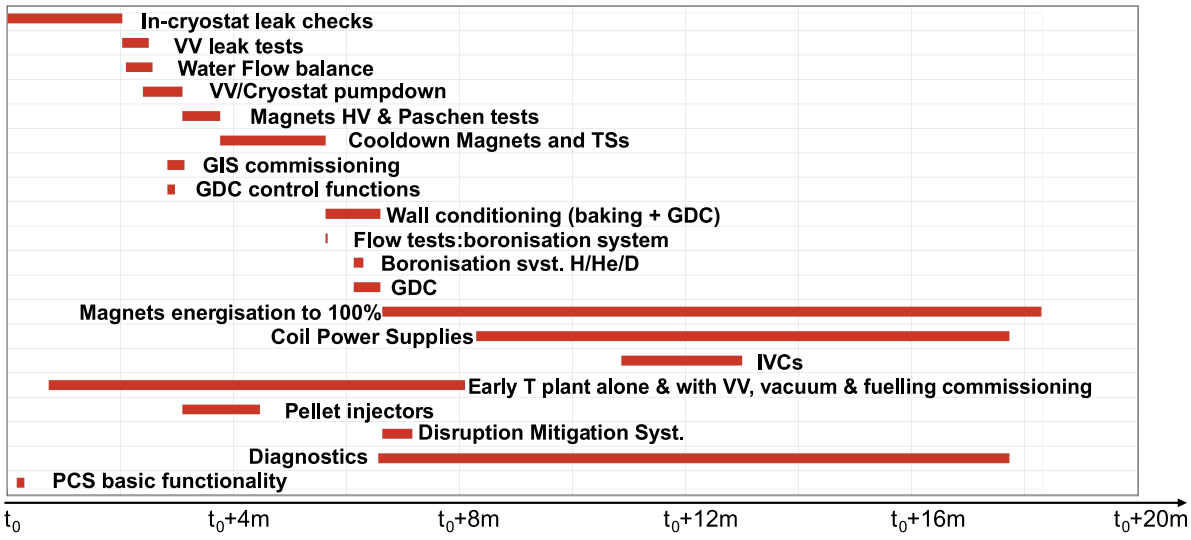

Figure 28. Overall schedule and main activities for integrated commissioning I.

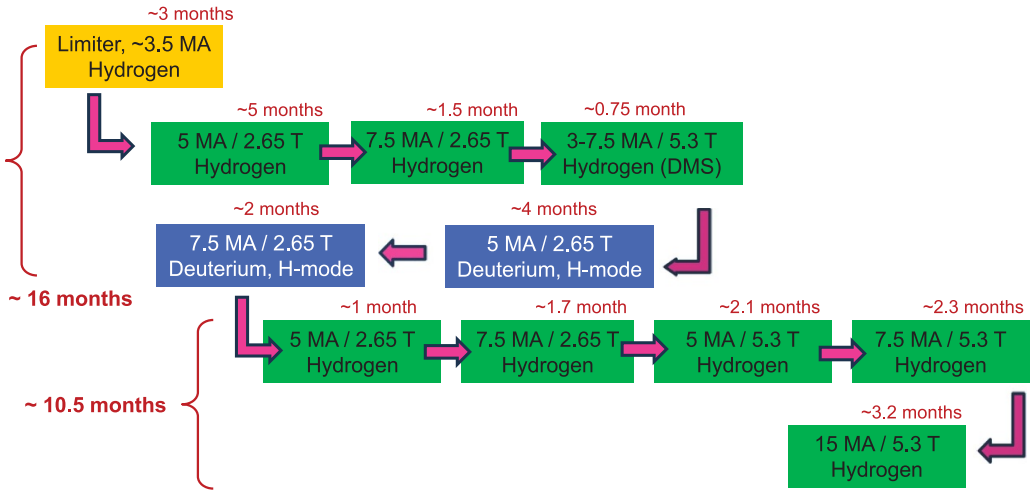

Figure 29. Sequence of main experimental research activities and foreseen time allocation for SRO.

confinement properties, SOL power width scaling, efficiency of gas fuelling versus pellet fuelling (note that gas fuelling is expected to have very low efficiency over a wide range of ITER plasma scenarios [Polevoi2018, Garzotti2019]), etc. More details on the expected outcome of SRO in terms of scenario development, engineering demonstration and physics validation are given in section 3.2.2.

The logic for the strategy behind the proposed steps in the SRO research plan is as follows:

L-mode scenario development to 7.5 MA/2.65 T in H plasmas (q_{95} = 3–6).

In this first part of SRO the basic blocks of a tokamak pulse in ITER will be developed to half of the nominal values of I_p/B_t. This will start from the production of a tokamak plasma (ECH assisted plasma initiation in second harmonic X-mode) in limiter configuration up to ~3 MA/2.65 T and then the expansion of the operational space to diverted plasmas with up to 7.5 MA/2.65 T in L-mode including the identification and correction of error fields. The need for boronisation to start plasma operation will be assessed in this initial phase by attempting plasma operation without boronisation first. If not successful, or once 3.5 MA/2.65 T divertor operation is demonstrated, boronisation will be applied and the benefits and drawbacks of boronisation, specifically on plasma initiation and on the limiter phase will be assessed. If proven necessary, the frequency of boronisation for reliable plasma operation will be assessed. It should be noted that in ITER boronisation will be applied to control oxygen levels and not with the purpose to coat the W wall surfaces. Thus, the need for boronisation depends strongly on the outgassing of PFCs and leak rates that will be finally achieved in ITER (see [Wauters2024] for more details).

In synchrony with the development of plasma scenarios and the evaluation of the associated disruption loads a large number of systems will be commissioned with plasma (plasma control/protection, ECH, diagnostics, DMS, …). This first part will provide the characterisation of L-mode plasmas in ITER

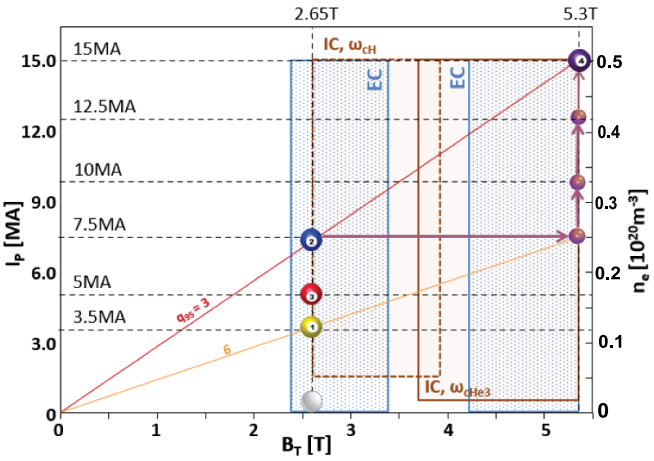

Figure 30. Sequence of plasma scenarios to be explored in SRO in terms of plasma current, toroidal field and electron density (for L-mode scenarios), assuming a typical value of ∼42% of the Greenwald limit.

and will conclude with a first attempt to H-mode plasma operation in hydrogen plasmas. Given the H-mode power threshold in ITER, H-mode operation with $P_{\mathrm{ECH}} \leqslant 40$ MW is expected to be very marginal in H [Vincenzi2024a] and the main outcome of this initial attempt is to confirm the H-mode power threshold expectations rather than a systematic exploration of H H-mode plasmas in ITER. Note that there is no ICH scheme with efficient absorption in H plasmas at 2.65 T.

L-mode scenario development to 7.5 MA/5.3 T in H plasmas ($q_{95} = 6$–9)
This second part is specifically focused at understanding the impact of high field operation on disruption loads and mitigation. It is carried out before DD operation because human access to the vacuum vessel immediately following DD operation will not be possible. The logic is, thus, that the increase of the toroidal field will allow testing of in-vessel components to 50% of the maximum electromagnetic loads that they will experience in ITER at 15 MA/5.3 T allowing the identification of infant failures and easier repair/replacement by human intervention before DD operation takes place. Operation at 5.3 T will require commissioning with plasma of systems whose performance depends on the magnetic field as well as the development of high q_{95} diverted scenarios, including plasma start-up. The impact of high q_{95} on disruption loads and mitigation will be assessed as well as on the L-mode plasma parameters and scenarios.

H-mode scenario development to 7.5 MA/2.65 T in DD plasmas ($q_{95} = 3$–6).
In this third part the first robust H-mode plasmas will be achieved in ITER. The timing and total neutron fluence produced in this phase is determined by the need to allow in-vessel radiation levels to decay before the post-SRO shutdown starts, so that human entry and extended work periods are possible. To ensure this goal the neutron fluence of the DD campaign is limited to 1.5 10^{20} and the campaign is set to end, at latest, more than 10 months before the end of SRO. SRO experiments after DD will be performed in H plasmas and thus with very low neutron production. The main objective of the SRO DD experiments is to develop H-mode plasma scenarios up to 7.5 MA/2.65 T and up to the highest levels of additional heating ($P_{\mathrm{aux}} = 50$ MW) including all the required control schemes (e.g. ELM control, W source control, etc.). This will require the testing and demonstration of ICH heating with H-minority as well as with second harmonic majority D and the determination of the ICH-specific W wall sources. The impact of H-mode plasmas on disruption loads and mitigation will also be assessed.

To end the DD campaign a change-over to H plasmas will take place. This will be used to determine the capabilities of fuel removal foreseen to be applied in the DT-1 campaign. The strategy to be applied in DT-1 and to be demonstrated in SRO consists of plasma operation with specific magnetic configurations, where the strike point reaches the areas where boron is expected to accumulate. This will release the retained fuel at the divertor and will be combined with ICWC plasmas to recover fuel from the first wall surfaces. This strategy is similar to that applied in the JET DTE-2 campaign, for further details the reader is referred to [Mateev2023].

Completion of L-mode scenario development to 7.5 MA/2.65 T in H plasmas ($q_{95} = 3$–6).
In this fourth part the development of scenarios and the commissioning with plasma of systems and control schemes, and physics assessments that could not be completed in the first part will be completed. This may include specific studies for DMS, the commissioning of NTM control, further optimisation of error field control by application of error field correction coils and ELM control coils (with $n = 2$ symmetry), etc.

Expansion of the L-mode scenario operational space to 15 MA/5.3 T in H plasmas ($q_{95} = 3$–6).
This fifth part will start with the L-mode plasma scenarios at 7.5 MA/5.3 T already demonstrated in the second part of SRO and proceed with progressive steps in plasma current from 7.5 MA to 15 MA. The steps are presently foreseen to be of 2.5 MA so that the intermediate L-mode scenarios have $q_{95} = 4.5$ and 3.6. At each I_{p} step control schemes will be retuned to account for the increasing plasma current and lower q_{95} since this is expected to affect MHD stability as well as other integration issues (e.g. reduction of power e-folding length). DMS will also be tested and retuned at every step since plasma thermal energy (W_{th}), magnetic energy (W_{mag}) and secondary RE amplification are expected to increase with I_{p}. Disruption loads in unmitigated disruptions will also be characterised potentially up to 15 MA/5.3 T if loads on the vacuum vessel and damage to in-vessel inertially cooled PFCs allow. ICH will be commissioned and applied at 5.3 T which will require the use of He^3 as minority and the assessment of ICH-specific W wall sources. The outcome of this assessment, together with that done in DD plasmas at 2.65 T above, will determine whether an upgrade of the ICH system to couple

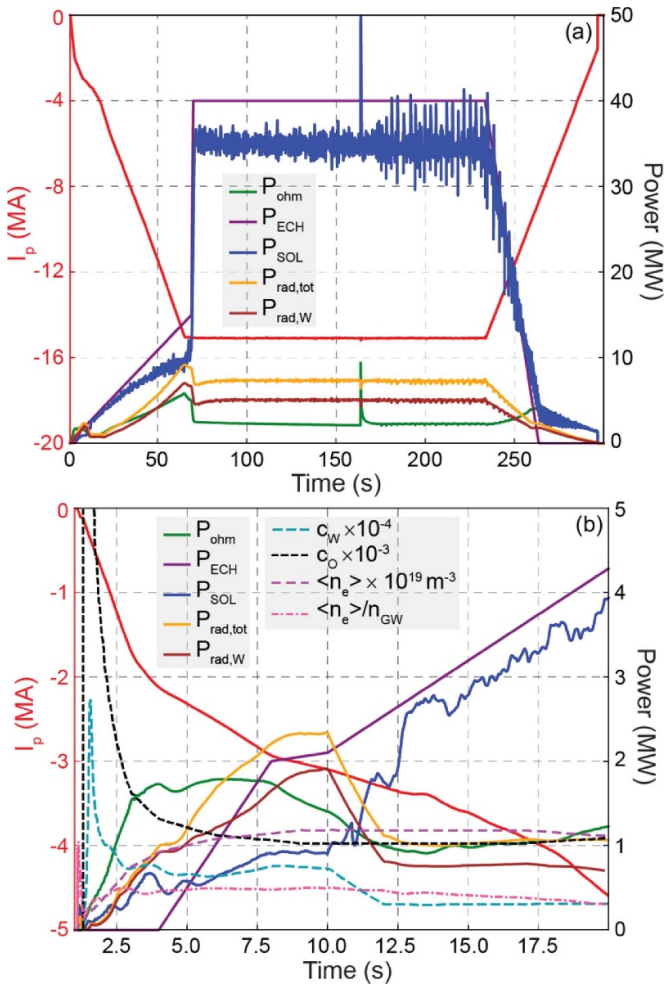

Figure 31. End-to-end DINA scenario (IMAS SIMDB: c5f61880-00ff-11f0-a7f3-9440c9e76fd0) for a hydrogen L-mode to 15 MA at 5.3 T computed using the boundary derived from the SOLPS-ITER limiter simulation database and with an assumed constant volume averaged O density,$< n_O > = 1.2 \times 10^{16}$ m^{-3} during the limiter phase: (a) main components of the power balance with the I_p waveform—the oscillations on P_{SOL} from t–164 s are due to sawteeth. Note that the first large spike corresponds to the first saw tooth which, in the simulation, produces strong variation of the plasma current profile during a single time step of the simulation (10 ms) and in turn provokes a high, and unphysical spike in P_{ohm}; (b) expanded region covering start-up, early current rise in limiter configuration with X-point transition at $t = 10$ s, including W and O impurity concentrations and plasma density waveforms. Reproduced with permission from [Pitts2025]. CC BY-NC-ND 4.0.

20 MW into the plasma to support DT-1 operation is launched at this stage or not. This part will conclude the SRO research programme with the demonstration that the ITER tokamak and ancillary systems can operate plasmas with the highest W_{mag} to be explored in ITER and with the required control systems, load mitigation (specially disruption thermal, electromagnetic and runaway loads) and all other required systems to support it. This is an essential step to proceed to DT operation in DT-1. Modelling results for a typical 15 MA/5.3 T plasma scenario to be explored in SRO are shown in figure 31.

3.2.1. Physics evaluations supporting the SRO research plan and open R&D issues. To define the steps in the development of the ITER operational scenarios in SRO, as well as the strategy for most effective mitigation/retirement of operational risks, a series of modelling studies has been carried out. In this section we summarise the main outcomes of these studies as well as the associated R&D issues.

Limiter plasmas with a W wall in ITER

Extensive modelling studies have been carried out for the limiter phase of ITER plasmas both with high fidelity edge plasma modelling codes (SOLPS-ITER) and integrated modelling codes (JINTRAC) for specific time slices in the limiter phase as well as with the DINA code for the whole 15 MA/5.3 T plasma scenario from break-down to discharge termination, including the limiter phase. The detailed description of these modelling studies can be found in [Pitts2025], here we report on the main conclusions and open issues.

The studies carried out for ITER show that the plasma conditions in the limiter phase are in a strongly self-regulated regime. The core plasma radiation determines the edge power flow and thus the W sputtering source. Since W is poorly screened from the core plasma in the limiter phase, the W sputtering source determines, in turn, the core plasma radiation. The modelling studies show that the plasma interacting with the limiter system self-regulates so that most of the power into the core plasma is radiated away by W produced by the limiter, while a small fraction is conducted to the limiter itself and provides the W source to support the plasma radiated power. Integrated modelling studies further show that the plasma-W limiter system can be thermally stable provided that central W accumulation is avoided. For this purpose, the application of central ECH heating is essential, as shown in figure 32. We note that, in agreement, with studies for core W transport in ITER discussed in section 2.1.2, in the limiter phase of ITER plasmas anomalous and neoclassical W fluxes can be comparable, unlike in fully developed H-modes.

The overall picture provided by these modelling studies for ITER resembles very strongly the results from W limiter plasmas in present experiments discussed in section 2.1.3, in particular the recent results from EAST, which provide a strong basis for these ITER predictions. The open issues in this area concern the accuracy to which the models applied for ITER can reproduce present experiments. Addressing these open issues requires a focused effort to validate the models against present experiments, which is being presently undertaken for the EAST experiments. In this respect it is essential that sufficient data is obtained in the experiments to allow this quantitative model validation to be conclusive.

We note that given the high risk that ITER plasmas in the limiter phase will thermally collapse by the associated W radiation, the NB-IRP has restricted the values of the toroidal fields at which scenarios will be developed to those for which central ECH heating is ensured. These values are namely $B_t = 2.65$ and 5.3 T since the ECH gyrotron frequency in ITER is 170 GHz. This leads to scenario development paths with decreasing q_{95} as I_p increases, unlike in the 2016 IRP for

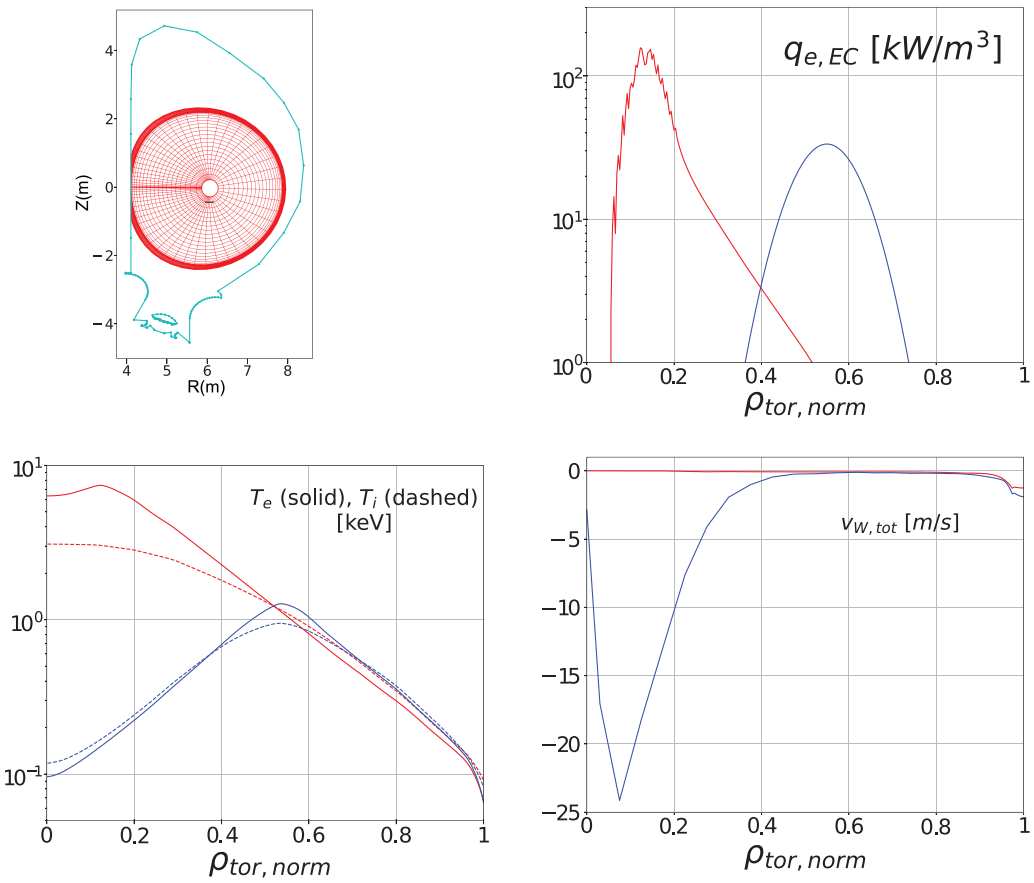

Figure 32. Modelling of an ITER plasma in the limiter phase in contact with the W first wall at the high field side for two ECH power deposition profiles (on-axis and off-axis). Top: plasma equilibrium and grid for the plasma modelled by JINTRAC and ECH power deposition profiles (red-on axis, blue-off axis). Bottom: electron and ion temperature profiles and resulting W pinch velocity (negative values for inwards W fluxes) versus square root normalised toroidal flux for the two ECH power deposition profiles. Simulation with on-axis EC deposition (IMAS SIMBD: 57ade51b-ff5f-11ef-bb6d-9440c9e76fd00 and with off-axis (IMAS SIMBD: b8cce779-ff60-11ef-8dc5-9440c9e76fd0). Reproduced with permission from [Pitts2025]. CC BY-NC-ND 4.0.

which an approximately constant q_{95} ($q_{95} = 3$–4) with increasing I_p and B_t was chosen [ITR-2024-005]. For the 2016 IRP it was considered that the risks of W accumulation due to off-axis ECH deposition were low since W was only present at the divertor (Be first wall) and W was thus well screened from the core plasma. The issues and opportunities associated with the decreasing q_{95} scenario development path adopted for the NB, in particular for DT H-mode plasmas, are discussed in section 3.4 below.

Disruption loads and mitigation in SRO

Since the characterisation of disruption loads and the demonstration of load mitigation is a key objective of SRO, specific assessments and modelling studies have been carried out to determine the operational range over which disruption loads can be characterised with acceptable risks to the integrity of SRO PFCs, as well as to the achievable demonstration of disruption load mitigation compared to the required targets for $Q \geqslant 10$ operation.

In first place, we note that the use of W as first wall material in SRO decreases the risk of surface melting of first wall PFCs compared to Be due to its higher melting point. The results of a quantitative evaluation of the decrease of this risk when replacing Be by W for the current quench phase of plasma disruptions is shown in figure 33 indicating that melting of the first wall by disruptions current quenches will take place only for I_p above 10 MA compared to ~7 MA for Be (note that W_{mag} increases as I_p^2). These evaluations use the same assumptions based on 2D disruption modelling as previous studies carried out for Be [Coburn2022] to ensure a one-to-one comparison [Chen2022]. More recent studies based on unmitigated disruption modelling with 3D non-linear MHD codes in [Artola2024] show that, even for 15 MA unmitigated current quenches, melting of the W wall only occurs in very localised areas. This reduces large scale melt layer displacement and short circuiting of first wall elements occurring in the new ITER baseline, which was identified as an important issue for first Be wall integrity in the 2016 baseline [Pitts2025].

The fact that the first wall W panels are inertially cooled in SRO can be used to eliminate the risk that loads by disruptions (including runaways) can cause water leaks either in unmitigated events or when the disruption mitigation system is commissioned with plasma. To this end, it is essential that the plasma energy during disruptions and VDEs, specially during the current quench and when RE are formed, is deposited on the first wall and not the divertor since the latter is water

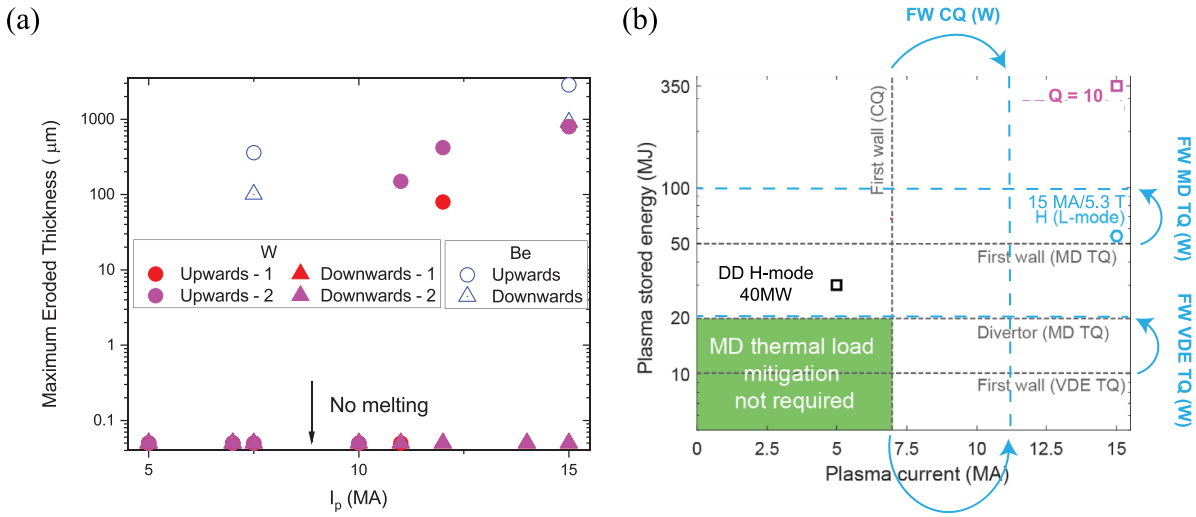

Figure 33. (a) MEMOS-U results for maximum erosion thickness not including the effects vapour shielding for Be [Coburn2022] and W [Chen2022]. For calculations of W at intermediate currents two ways to interpolate the current quench dynamics between 7.5 and 15 MA have been chosen leading to different melt results. (b) Melting thresholds for Be first wall and W divertor during the thermal quench and current quench versus plasma current and thermal plasma energy [Lehnen2015] and revised thresholds for the W first wall in the new baseline.

cooled. The upwards or downwards movement of the plasma during disruptions in ITER depends on the details of the processes taking place during the thermal quench (TQ) (degree of flattening of the current profile) and the current quench (duration of the current quench) and thus both upwards and downwards movements are expected to take place, as shown in figure 34(a). Thus, to achieve the goal that loads are deposited on the first wall and not the divertor, the in-vessel vertical stability control coils will be used to trigger an upwards movement of the plasma in advance of the disruption TQ in SRO. This favours discharge termination on the upper part of the first wall taking place. This requires energisation of the coils some 10's of milliseconds before the TQ takes place as shown in figure 34(b); if the coils are energised at the time of the TQ for a downwards going post-disruption VDE its movement will be slowed down but not prevented. The range of timescales required is similar to the target for disruption TQ mitigation by DMS [Lehnen2023] and it is expected to be demonstrated in SRO. Both for the demonstration of disruption mitigation and to maximise the probability of an upwards movement of the plasma during the disruption current quench extensive experiments are foreseen in SRO starting from low plasma current levels in which the risk of runaway generation (see below) and load damage of W PFCs by disruption loads is negligible.

Once it is ensured that the risk of loads damaging the water cooled divertor is minimised, the goals for the disruption mitigation programme in SRO towards its routine application in DT-1 have been assessed. These are of course linked to the plasma conditions achievable in SRO that include L-mode plasmas up to 15 MA/5.3 T and H-mode plasmas up to 7.5 MA/2.65 T with additional power up to 50 MW. On the basis of the plasma parameters that can be achieved in these plasmas, as shown in figure 35, it is expected that issues related to disruption mitigation at full W_{mag} with a seed of hot electrons ($T_{\mathrm{e}} > 10$ keV, similar to that expected for $Q \geqslant 10$ plasmas) leading to intense runaway production will be fully assessed in SRO with 15 MA plasmas. Similarly, the issues related to shattered pellet penetration in a plasma with multi-keV pedestal temperatures and a hot electron seed will be assessed with 7.5 MA/2.65 T H-modes. As an example of the results that could be expected in the studies of runaway mitigation in such conditions, figure 36 shows the expected final RE current that can be produced in such discharges depending on the TQ duration and onset with respect to shattered pellet fragment arrival as well as the number of injected H pellets [Pusztai2023]. As shown in this figure multi-MA RE discharges can be produced in the experiments required to tune the disruption mitigation and, given the consequences of such loads on W water cooled PFCs [Pitts2025], it is essential that such disruption experiments are terminated on the first wall. This is possible by energizing the in-vessel vertical stability coils in advance of the injection of the shattered pellets, as shown above.

It should be noted that some of the objectives required for disruption mitigation in DT-1 cannot be fully achieved or not achieved at all in SRO. This concerns the demonstration of TQ mitigation at full W_{th} and the mitigation of RE production including the fast electron seeds associated with T β-decay as well as to the Compton scattering of γ rays produced by the irradiated in-vessel components. These can only be demonstrated in DT-1 itself and the NB-IRP in that phase is planned to mitigate the risks associated with this demonstration. Table 2 summarises the plasma parameters that can be achieved in SRO and their relation to the demonstration of the disruption mitigation performance required for DT-1.

While the basic physics processes involved in disruptions together with the associated loads and their mitigation are well established, many of their quantitative descriptions are still

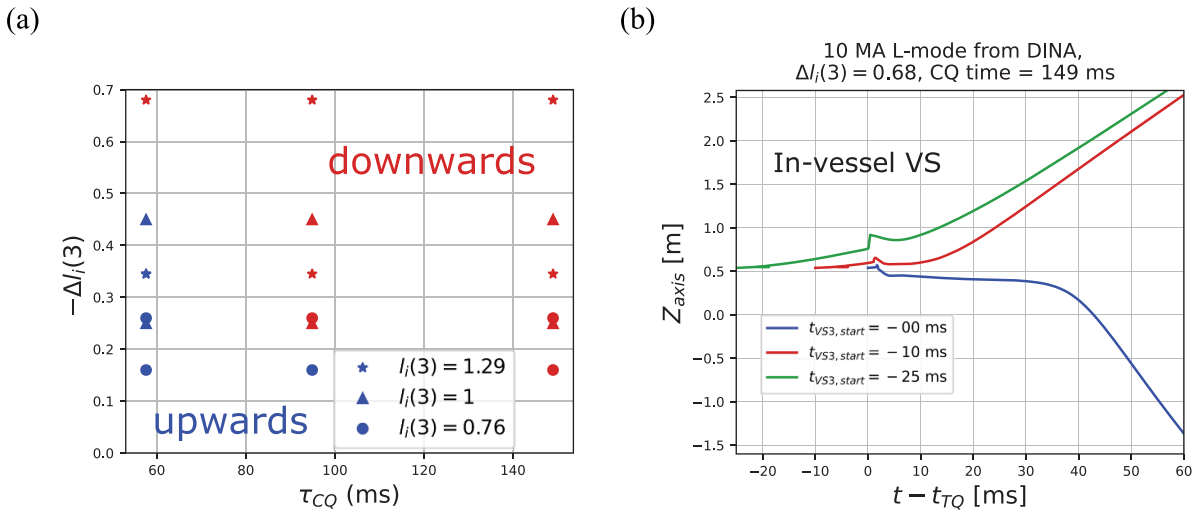

Figure 34. (a) Modelled direction of the plasma movement for 10 MA disruptions as a function of the current profile peaking before the disruption (characterised by $l_i(3)$), the degree of current profile flattening at the thermal quench ($\Delta l_i(3)$) and the duration of the current quench [Artola2024]. (b) Movement of the plasma after the thermal quench for a 10 MA disruption following the energisation of the in-vessel vertical stability coils to move the plasma upwards. In the absence of the energisation of the coils this plasma would move downwards; changing the direction upwards is possible by applying maximum voltage to the in-vessel coils at least 10 ms in advance of the thermal quench. (a) (IMAS SIMDB: 709a9b8-00e6-11f0-b9fb-9440c9e76fd0, 17393ed5- 00eb-11f0-a7fd-9440c9e76fd0, 8ffc3f73-00eb-11f0-b788-9440c9e76fd0, 0fce1cc8-00ee-11f0-46 90a8-9440c9e76fd0, 54c90fd0-00ee-11f0-8720-9440c9e76fd0, 73065487-00ee-11f0-9d9b-9440c9e76fd0, 9a757b02-00ee-11f0-a7aa-9440c9e76fd0, a1d22618-00ee-11f0-85dc-9440c9e76fd0, b66e5eac-00ee-11f0-aacf-9440c9e76fd0, c4d1834e-00ee-11f0-8716-9440c9e76fd0, d2739d1b-00ee-11f0-bf48-9440c9e76fd0, e0393766-00ee-11f0-8165-9440c9e76fd0, f07898fd-00ee-11f0-915e-9440c9e76fd0, 0003dc44-00ef-11f0-a181-9440c9e76fd0, 0fb42975-00ef-11f0-a5e9-9440c9e76fd0,1c992500-00ef-11f0-aee0-9440c9e76fd0, 37b9ac24-00ef-11f0-83b8-9440c9e76fd0, 482324ce-00ef-11f0-913e-9440c9e76fd0). (b) (IMAS SIMDB: e5b26709-00ef-11f0-935c-9440c9e76fd0, 20f33271-00f0-11f0-8be2-9440c9e76fd0, 634979e0-00f0-11f0-bbc5-9440c9e76fd0).

outstanding. The evaluations above are based on modelling efforts with a wide range of physics assumptions and simplifications which impact the conclusions that can be extracted from them. Thus, R&D should be carried out to characterise in detail the spatial structure and time scales of disruption loads, especially for REs. Similarly, 3D MHD non-linear codes that simulate these loads should and are being improved to include all the physics processes involved in disruptions and compared with detailed measurements from experiments along the lines described in [Artola2024]. This is essential to provide a quantitative expectation of loads and mitigation targets that should be set for SRO and the implications for plasma operation, namely the expected damage of the inertially cooled wall.

Diverted L-mode plasma modelling

L-mode plasma stationary conditions have been modelled to determine the operational range with respect to W wall influxes as well as for the viability of complete scenarios. The details of such studies are described in [Pitts2025]. Here we summarise the results of such studies with the JINTRAC code for three typical L-mode plasma conditions which are included in the 15 MA L-mode plasma scenario development path, namely : (a) 5 MA/5.3 T, $P_{ECH} = 5$ MW, $< n_e > \sim 0.3$ n_{GW}; (b) 10 MA/5.3 T, $P_{ECH} = 10$ MW, $< n_e > \sim 0.3$ n_{GW}; *c*) 15 MA/5.3 T, $P_{ECH} = 40$ MW, $< n_e > \sim 0.5$ n_{GW}. We note that for our conservative assumptions (zero prompt W redeposition) and without the addition of Ne for divertor power dissipation, it is necessary to choose higher densities than 0.3

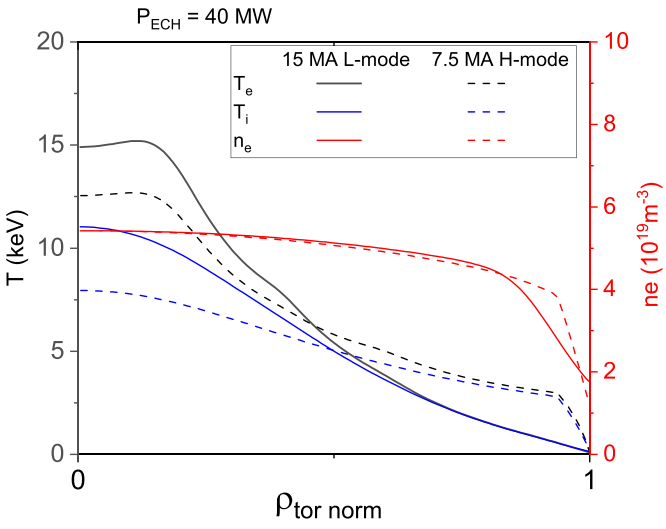

Figure 35. Modelled plasma density and temperature profiles versus square root normalised toroidal flux for L-mode plasmas at 15 MA/5.3 T in H and H-mode plasmas in DD at 7.5 MA/2.65 T achievable in SRO with $P_{ECH} = 40$ MW. 15 MA H L-mode (IMAS SIMDB: 0845d270-00fa-11f0-9661-9440c9e76fd0); 7.5 MA D H-mode (IMAS SIMDB: d20eeee1-00fa- 11f0-bf18-9440c9e76fd0).

n_{GW} when simulating 15 MA with $P_{ECH} = 40$ MW to avoid excessive core radiation from W. In these simulations a fiducial W wall source has been included whose magnitude compared to the divertor source has been scanned. We remind that

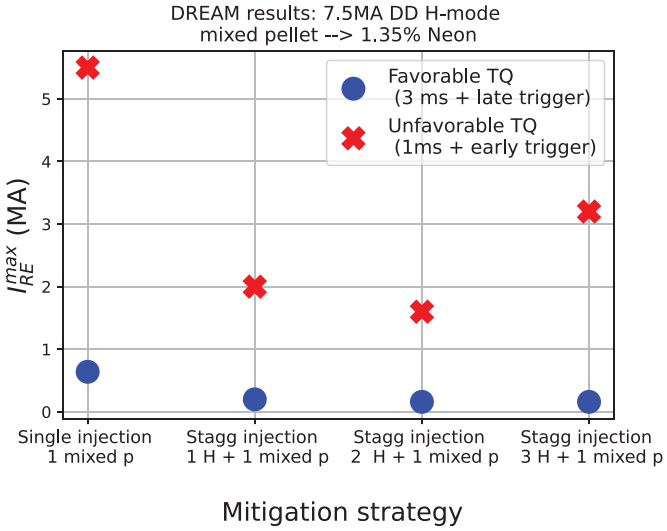

Figure 36. Modelled runaway current produced in the mitigation of plasma disruptions for SRO 7.5 MA/2.65 T with $P_{ECH} = 40$ MW depending on the pellet injection strategy: single mixed H + Ne injection versus staggered injection (pure H pellets followed by a mixed H + Ne pellet) for a range of assumptions related to the TQ trigger time and duration (for more information on TQ conditions see [Vallhagen2024]). In the most unfavourable cases runaway plasma currents of 3–5 MA can be generated. Reproduced from the 49th EPS conference with permission from [Pusztai2023].

Table 2. SRO achievable disruption mitigation goals versus the need for DT-1.

Disruption Phase	CQ	TQ	RE hot tail	RE β decay (T)	RE Compton e^-
DT	15 MA	350 MJ	10–20 keV	*Y*	*Y*
SRO	15 MA **Mitigation for DT-1 fully demonstrated in SRO**	60 MJ ***Mitigation for DT-1 partly demonstrated in SRO***	10–20 keV **Mitigation for DT-1 fully demonstrated in SRO**	*N* Mitigation for DT-1 not demonstrated in SRO	*N* Mitigation for DT-1 not demonstrated in SRO

the typical ratios of wall versus divertor source in experiments is 10%–20%, as shown in figures 10 and 11.

The results of the simulations for low W wall source levels are shown in figure 37; regarding divertor parameters, these plasmas maintain a high ion temperature across most of the divertor target, and the divertor power flux remains under 10 MWm^{-2}. The resulting core W concentrations and radiated power fractions for the range of wall W sources studied is shown in figure 38. For values of the ratio of the wall W-flux to the divertor flux of 10–20%, the W concentration is in the range of 3–4 $\times$ 10^{-5} for the 5 and 10 MA plasmas with $< n_e >$ $\sim$ 0.3 n_{GW}. For the 15 MA plasma with higher plasma density, the W concentration remains at lower values $\sim$ 1–2 $\times$ 10^{-5}. In all cases, the core radiated power fraction remains under 40%, with the 15 MA plasma having the lowest radiated fraction. These results are consistent with the full scenario simulations performed with DINA [Pitts2025].

One interesting feature of these simulations is the relatively high tolerance to W wall influxes and high W concentration of low I_p/low $<n_e>$ L-mode plasmas in ITER. This is due to the fact that such plasmas maintain a high electron temperature (they are ECH heated), which decreases W radiation efficiency, and also have a very low absolute density when $< n_e > \sim 0.3\ n_{GW}$ (e.g. $< n_e >_{5MA} \sim 1.2$ 10^{19}m^{-3}). Since the core W radiation is given by $P_W \sim c_W$ $<n_e>^2 L_W(T_e > 10$ keV), relatively large values of $c_W \sim$ 4–6 10^{-5} are compatible with moderate radiated power fractions $P_{rad}^{core}/P_{aux} \leqslant 50\%$ in these plasmas.

Again here the simulations carried out with JINTRAC can be used to define the guidelines for the SRO L-mode development plan but their details need the validation of the integrated models applied to ITER in present experiments. This includes W production and transport from the PFC surface into the core plasma. We note that these models contain significant simplifications which impact the quantitative results obtained for SRO plasmas.

H-mode plasmas and ELM control in SRO

Initial DD H-mode operation in SRO will start from low levels of plasma current ($I_p \leqslant 5$ MA) to avoid melting of the W divertor by uncontrolled ELMs [Gunn2017] and will expand to 7.5 MA when sufficient degree of ELM control is achieved. As discussed in section 2.1.2, present experiments show that for ELMy H-modes, the W source is dominated by

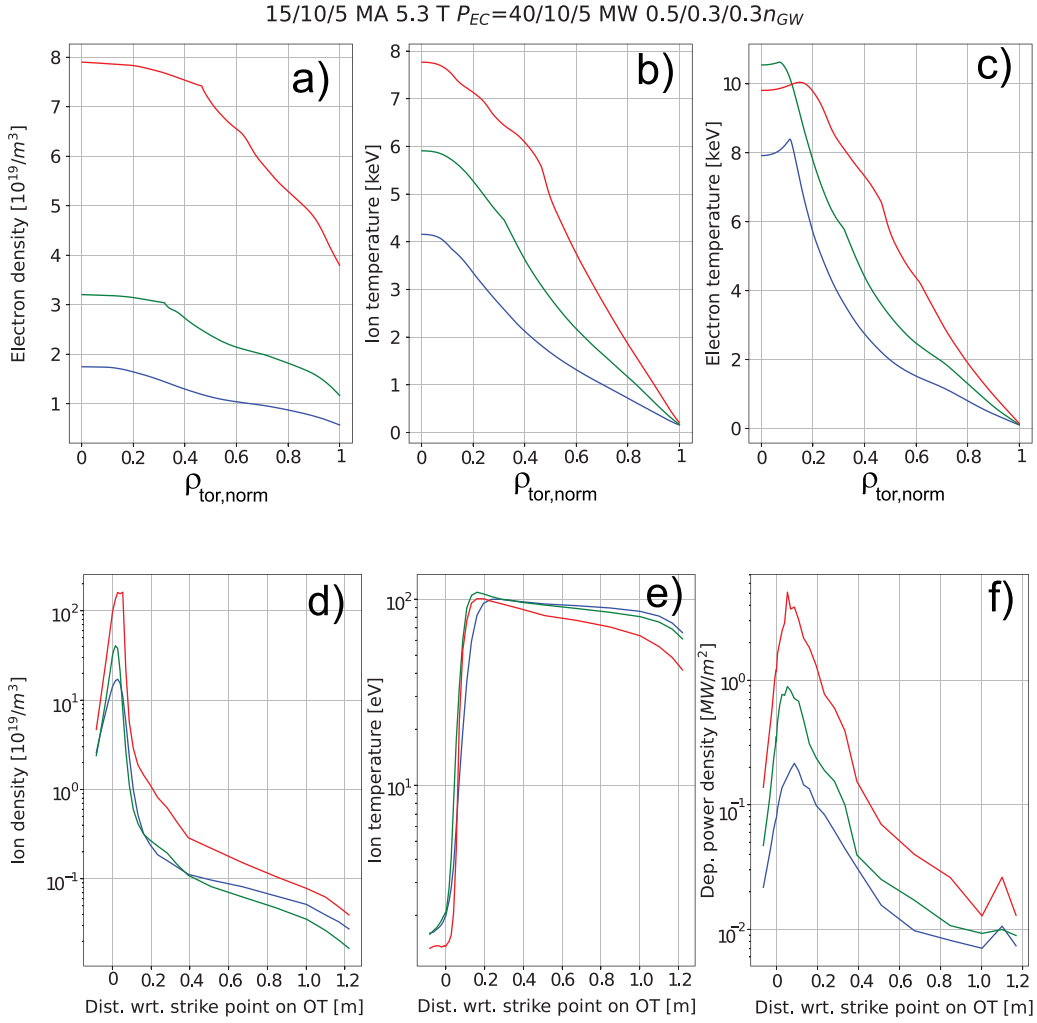

Figure 37. Plasma parameters from JINTRAC integrated modelling for: 5 MA, $P_{\mathrm{ECH}} = 5$ MW, $< n_{\mathrm{e}} > \sim 0.3\ n_{\mathrm{GW}}$ (blue), 10 MA, $P_{\mathrm{ECH}} = 10$ MW, $< n_{\mathrm{e}} > \sim 0.3\ n_{\mathrm{GW}}$; (green) and 15 MA, $P_{\mathrm{ECH}} = 40$ MW, $< n_{\mathrm{e}} > \sim 0.5\ n_{\mathrm{GW}}$ (red). (a) Plasma density vs. square root normalised toroidal flux, (b) electron temperature vs. square root normalised toroidal flux, (c) ion temperature vs. square root normalised toroidal flux, (d) ion density at the outer divertor target vs. distance to the separatrix strike point, (e) ion temperature at the outer divertor target vs. distance to the separatrix strike point and (f) power flux to the outer divertor target vs. distance to the separatrix strike point. 5 MA simulations (IMAS SIMDB: 38d8b02c-ff68-11ef-92d7-9440c9e76fd0); 10 MA simulations (IMAS SIMDB: e197598c-ff62-11ef-9fb5-9440c9e76fd0); 15 MA simulations (IMAS SIMDB: 832554c6-ff63-11ef-9af0-9440c9e76fd0).

sputtering during ELMs when the plasma temperature at the edge is low or the distance between separatrix and W wall is large [Dux2009, Huber2020]. Tungsten produced by ELM interactions with main chamber PFCs is much more effective in contaminating the core plasma than that produced at the divertor.

SRO will be the first phase in which H-modes will be explored in ITER and thus the issues of W sources, W control and the associated requirements on ELM control will be first assessed in this phase. To define the H-mode plasma conditions achievable in SRO and the required ELM control needs (which impact the strategy for ELM control development), two approaches have been followed. The first one is to evaluate the gross divertor W source due to ELMs from SOLPS simulations [Dux2017] and, on this basis, evaluate an equivalent W influx from the wall into the plasma and model the consequences of such an ELM-averaged W flux on H-mode performance. In this approach the W source from the PFCs into the plasma is given by:

$$\Gamma_{\mathrm{W}}^{\mathrm{ELM\text{-}averaged}} = (1 - f_{\mathrm{div,redep}})\,\Gamma_{\mathrm{W,divertor}}^{\mathrm{no\text{-}redep}} + \Gamma_{\mathrm{W,divertor}}^{\mathrm{no\text{-}redep}}/10 \quad (3\text{-}1)$$

where the first term corresponds to the effective W divertor source (including prompt redeposition) and the second term corresponds to the W wall source assumed to be ~10% of the gross divertor one, consistent with experimental findings discussed in section 2.1.2. The resulting ELM-averaged W influx is shown in figure 39 for a range of assumptions regarding the edge power flow level and the fraction of W promptly redeposited at the divertor during ELMs. We note that the divertor prompt re-deposition fraction is found to be larger than 95% in present experiments [Brezinsek2019].

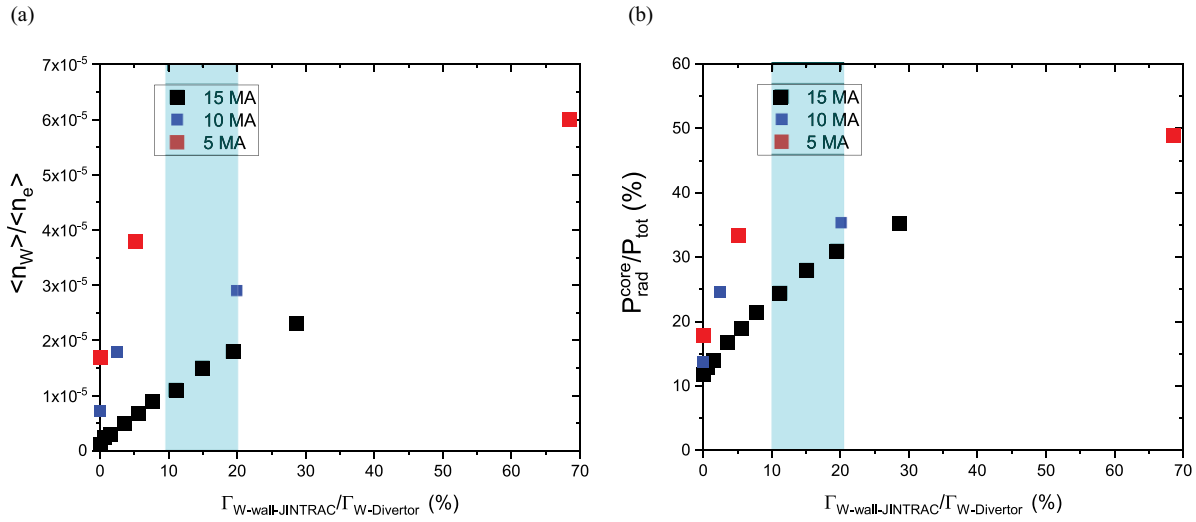

Figure 38. (a) Core W concentration and (b) ratio of core radiated power to total heating power versus the ratio of the effective W wall source to the divertor source in JINTRAC. The cyan shaded region indicates the values for this ratio found in experiment. 5 MA simulations (IMAS SIMDB: 884feca7-006c-11f0-8f81-9440c9e76fd0, 85e932b4-006c-11f0-915e-9440c9e76fd0, c428ec39-006c-11f0-ac92-9440c9e76fd0); 10 MA simulations (IMAS SIMDB: 1a350cb1-0059-11f0-b9c8-9440c9e76fd0, 64b3623a-0059-11f0-a74f-9440c9e76fd0, c764e8e5-006b-11f0-8280-9440c9e76fd0); 15 MA simulations (IMAS SIMDB: e17b5f72-0047-11f0-a0b5-9440c9e76fd0, 5a1b7cdd-0048-11f0-94a0-9440c9e76fd0, e1542d39-0045-11f0-ac51-9440c9e76fd0, 14e20b65-0049-11f0-8a3b-9440c9e76fd0, 30dcd823-0049-11f0-bf12-9440c9e76fd0, bf9d939b-0046-11f0-a084-9440c9e76fd0, 48020712-0058-11f0-bede-9440c9e76fd0, 6010872d-0058-11f0-ba02-9440c9e76fd0, 73ff270a-0058-11f0-aed3-9440c9e76fd0, 82117cf2-0058-11f0-904a-9440c9e76fd0).

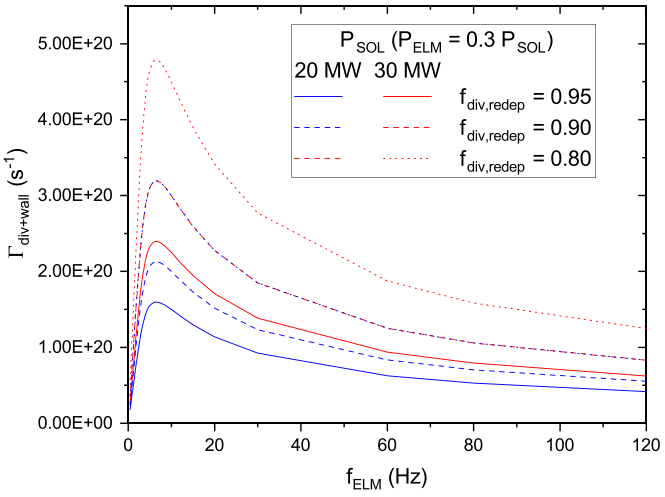

Figure 39. Modelled ELM-averaged W influx into the plasma from the divertor and the main wall versus ELM frequency for typical edge power levels of SRO H-mode operation in ITER and a range of assumptions regarding prompt divertor re-deposition. The W influx is calculated by applying equation (3-1) to the modelling results for the gross W source in [Dux2017].

The impact of the resulting wall influx on SRO H-mode operation has been evaluated with JINTRAC by introducing an effective W wall source (with typical energies of physically sputtered W) whose magnitude has been varied in addition to the W divertor source assuming no prompt redeposition. In these simulations core anomalous plasma transport is modelled with TGLF and neoclassical transport with NCLASS, which provides a suitable description since the toroidal rotation Mach number is low in ITER [Loarte2016]. Pedestal transport is modelled with the so-called continuous ELM model by which the level of anomalous transport is adjusted such that the pedestal pressure remains under the limit evaluated from MHD stability to trigger ELMs. Impurity pedestal transport is assumed to be described by a superposition of neoclassical transport and anomalous transport (with values provided by the continuous ELM model).

The results of these modelling studies are shown in figure 40. We note that for W wall sources corresponding to the largest values, the ELM-averaged W wall influx has a detrimental effect on H-mode sustainment. These critical values of W wall sources in figure 40 are comparable to those corresponding to the wall and the divertor together evaluated from equation (3-1) and shown in figure 39. The modelling results from [Dux2017] thus imply that the effect of ELM-averaged W influxes on initial ITER H-mode operation should not be a concern, provided that low ELM frequencies are avoided. This requires that robust schemes for ELM control be available when such H-mode experiments are performed in ITER and this has been considered to define the machine configuration for SRO which includes the full set of 27 ELM control coils and power supplies as well as 4 pellet injectors that can provide ELM triggering with a frequency up to 60 Hz.

The resilience of these SRO H-modes to wall W influxes comes from the effective screening of W at the pedestal plasma due to neoclassical transport effects, as shown in figure 41, and the high value of the core electron temperature (>10 keV due to poor electron ion thermal coupling and large ion heat transport, see H-mode profiles in figure 35) that maintain the W

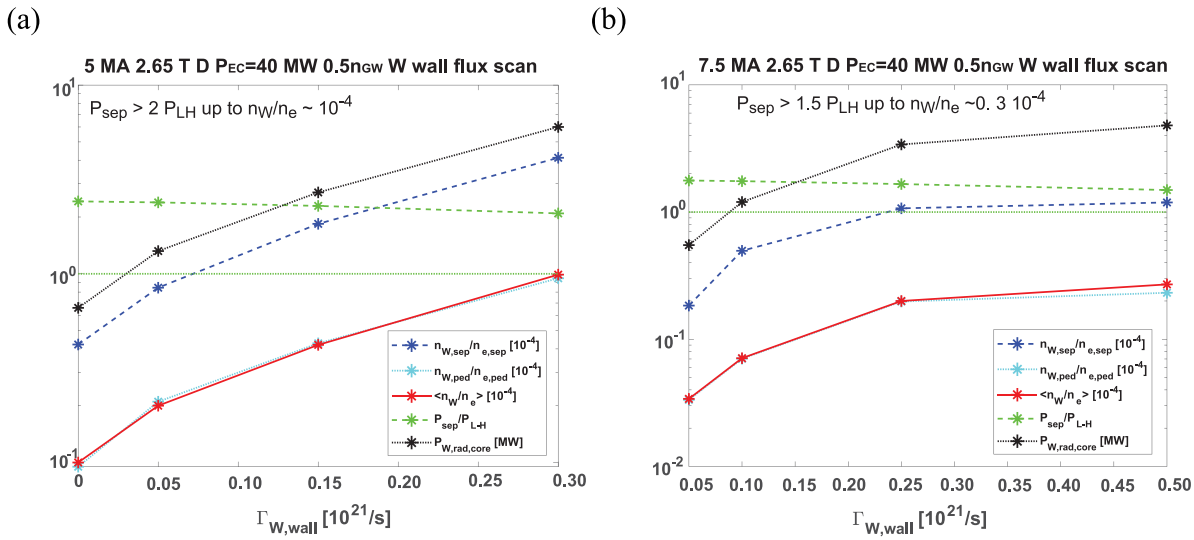

Figure 40. Modelled W concentrations at the separatrix, pedestal top, core plasma, core W radiation and margin of the edge power flow to the L–H transition versus ELM-averaged W wall source for : (a) 5 MA/2.65 T $< n_e \geqslant 0.5$ n_{GW} and (b) 7.5 MA/2.65 T $< n_e \geqslant 0.5$ n_{GW} DD H-mode plasmas with $P_{ECH} = 40$ MW. The red double-headed arrows show the difference between separatrix W concentration (in blue) and core/pedestal W concentration (in cyan/red) due to W screening in the pedestal. 5 MA simulations (IMAS SIMDB: c6c6f8fe-ff66-11ef-9e0b-9440c9e76fd0, f401b079-ff66-11ef-8d4b-9440c9e76fd0, 1374e680-ff68-11ef-98fc-9440c9e76fd0, 36f46257-ff68-11ef-8543-9440c9e76fd0); 7.5 MA simulations (IMAS SIMDB: 5d2e31dd-ff6b-11ef-890e-9440c9e76fd0, 67a997e5-ff6a-11ef-8e70-9440c9e76fd0, f2ac8-ff6a-11ef-8674-9440c9e76fd0, 8d079a05-ff6a-11ef-89e8-9440c9e76fd0).

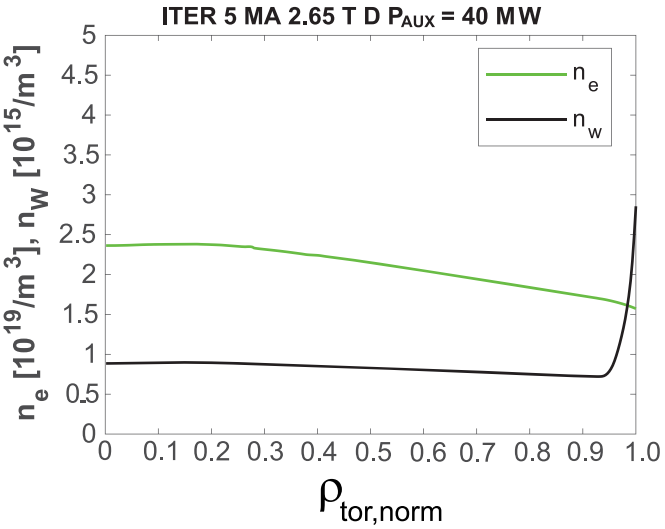

Figure 41. Modelled electron and W density profiles versus square root normalised toroidal flux for a 5 MA/2.65 T $< n_e \geqslant 0.5$ n_{GW} DD H-mode plasma with $P_{ECH} = 40$ MW showing the effective neoclassical screening for W provided by the pedestal plasma with $n_{sep}/n_{GW} = 0.4$ (IMAS SIMDB: 1374e680-ff68-11ef-98fc-9440c9e76fd0).

radiation loss under 10 MW in these plasmas, even for the significant W concentrations of $\sim 10^{-4}$ for $I_p = 5$ MA H-modes. As mentioned in section 2.1.1, the screening effects were identified in previous studies for ITER [Dux2014] and have been recently confirmed at JET [Garcia2022, Field2023].

The second approach followed to evaluate the effect of W influxes driven by ELMs is to perform full ELM-resolved JINTRAC simulations of the effective W influx from the divertor into the plasma and then double its magnitude to mock-up the effect on the W wall source, following the experimental guidance in section 2.1.2 as shown in (figures 10 and 11). In this case the same settings of JINTRAC as those for the calculations above (figures 40 and 41) are used with the difference that, in these studies, the continuous ELM model is not applied to pedestal transport so that the pedestal pressure evolves in time until the MHD pressure limit is reached triggering an ELM. Transport during the ELM is modelled by an increase in particle and heat diffusivities at the plasma edge for a short period ($\sim$1 ms), whose magnitude is adjusted to model the desired particle and energy losses by the plasma during the ELM. The results of such an approach for a 5 MA/2.65 T DD H-mode with $< n_e > \sim 0.5$ n_{GW} and $P_{ECH} = 40$ MW assuming an 80% level of prompt re-deposition at the divertor and a wall source similar to the divertor source, are shown in figure 42. For these conditions, the level of radiation in the core plasma remains low (18% of P_{tot}). However, the instantaneous level of core plasma radiation during the ELM is much larger (15 MW). If this transient radiation exceeds 25 MW, it can trigger an H–L transition for these plasmas. This reinforces the need for appropriate ELM control schemes to be available when these initial H-mode experiments are performed in ITER during SRO.

Since it will not be possible to achieve the required level of ELM control to avoid excessive W contamination in SRO H-modes from the very first H-mode discharges, a risk mitigation strategy has been developed. This is based on the development of 'high-clearance' H-mode plasma scenarios, in which the distance from the plasma separatrix to the wall is increased. This has been performed following two approaches: in the

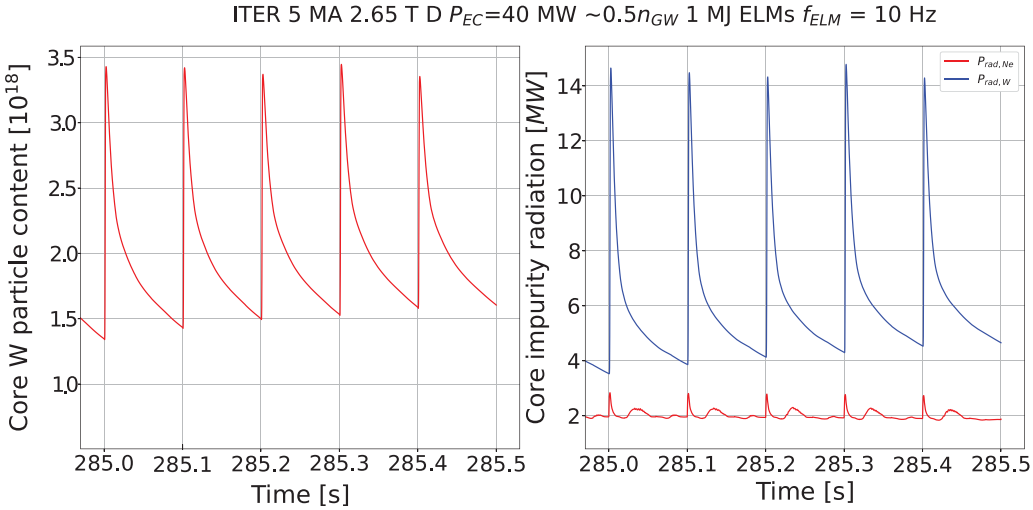

Figure 42. JINTRAC ELM-resolved W modelling for a 5 MA/2.65 T, $< n_e \geqslant 0.5\ n_{GW}$, $P_{ECH} = 40$ MW ECH heated DD H-mode plasma with 1 MJ ELMs and $f_{ELM} = 10$ Hz. The W divertor source is evaluated assuming an 80% prompt re-deposition fraction and the wall source is assumed to be similar to the effective divertor W source. (a) ELM-resolved W influx into the core plasma and (b) ELM-resolved core plasma radiation from W and Ne (IMAS SIMDB: 3531401fff74-11ef-ad2c-9440c9e76fd0).

first, the overall distance from the separatrix to the wall has been increased, whilst in the second, the distance to the outer wall separatrix has been increased at the expense of reducing it elsewhere. The latter is guided by the experimental observation in [Dux2009] that the W source from the LFS wall is more effective in contaminating the core plasma than from the HFS, consistent with ELMs being a key driver for the main chamber W source, as we expect for low I_p H-modes in ITER. The resulting plasma configurations and plasma pressure profiles are shown in figure 43 for 5 MA/2.65 T H-mode plasmas with $P_{ECH} = 40$ MW. With increasing distance to the outer wall, the vertical stability of the plasma worsens and there are increasing demands on the in-vessel vertical stability coils to maintain the plasma vertically stable. For the standard assumption of noise in the dZ/dt diagnostic signal fixed at an RMS value of 0.6 ms^{-1}, the in-vessel coil design limits imply that plasma elongation and triangularity cannot be maintained at the reference values for large outer wall clearances with acceptable vertical stability control through the H-mode scenario and they need to be reduced as clearance to the wall increases. Higher elongations and triangularities would be possible, close to the reference values, if the dZ/dt signal noise can be reduced to 0.2 ms^{-1} [Lukash2017]. The reduction of elongation and triangularity for high wall-clearance impacts the pedestal plasma characteristics (lower pedestal pressures) as shown in figure 43. If the plasma densities are kept as per the reference case for all wall clearances, this will lead to lower pedestal temperatures and worse screening for high clearance configurations. Therefore, an optimisation of the plasma density will be required to optimise screening of W for each wall clearance.

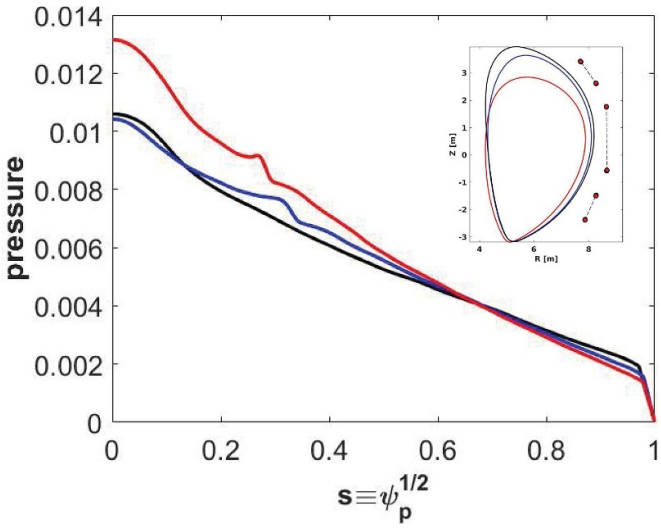

Figure 43. Plasma configurations for DINA 5 MA/2.65 T $< n_e >$ $\sim 0.5\ n_{GW}$, $P_{ECH} = 40$ MW, DD H-mode plasma scenarios in the flat-top phase (reference baseline configuration-black, increased overall wall clearance (15 cm at the outer midplane) configuration-blue and 45 cm outer gap configuration-red) and associated normalised plasma pressure profiles (pressure normalised by B_0^2/μ_0, $B_0 = 2.65$ T) modelled versus square root normalised poloidal flux with JINTRAC including edge MHD plasma stability modelling. Reproduced from [Bai2024]. © IOP Publishing Ltd. All rights reserved. Reference baseline (IMAS SIMDB: 55666971-00d2-11f0-a5a7-9440c9e76fd0); increased overall clearance (IMAS SIMDB: b08e443a-00d3-11f0-88a3-9440c9e76fd0); 45 cm outer gap (69e5f567-00d4-11f0-b236-9440c9e76fd0).

An evaluation of the impact of wall clearance on the W source from the main wall driven by ELMs has been carried out by extrapolation of the AUG observations with a physics-based scaling. As shown in figure 11, the core W concentration in AUG increases by a factor of ~2–3 when the gap to the outer wall is reduced from 8 to 4 cm. The physics-based scaling uses the validated model in [Pitts2007], which relates the ratio of the ELM energy flux to the wall ($\Delta W_{ELM,wall}$) to the total ELM wall + divertor flux (ΔW_{ELM}) with the normalised ELM energy loss ($\Delta W_{ELM}/W_{ped}$) and the ratio of the distance

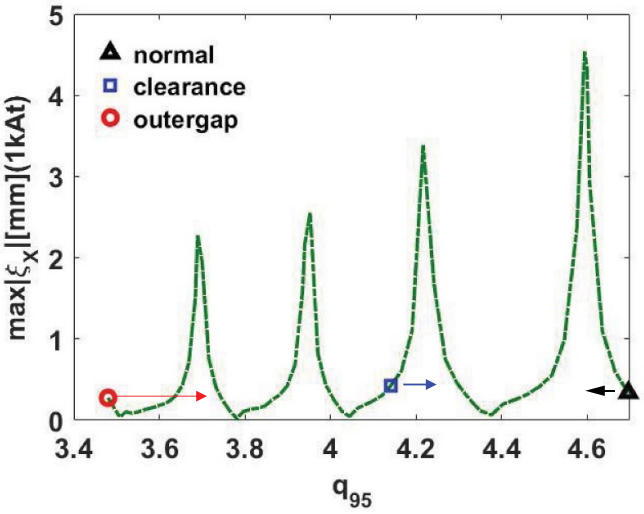

Figure 44. Modelled X-point response in mm per kAt in the ELM control coils showing the change in q_{95} of the resonant windows when the wall clearance is increased. A reduction of a factor of 2 is found from the nominal configuration to that with an outer wall gap of 45 cm [Bai2024] for a constant current level in the ELM control coils. Reproduced from [Bai2024]. © IOP Publishing Ltd. All rights reserved.

of the wall to the device dimensions ($-\Delta R_{\rm wall}/R$). We then further assume that the ELM W wall source is proportional to the ELM wall energy flux such that:

$$\frac{\Gamma_{\rm W\text{-}ELM,wall}}{\Gamma_{\rm W\text{-}ELM}} \sim \frac{\Delta W_{\rm ELM,wall}}{\Delta W_{\rm ELM}} \sim {\rm e}^{\left[-\Delta R_{\rm wall}/R\left(\Delta W_{\rm ELM}/W_{\rm ped}\right)^{-1/2}\right]}. \quad (3\text{-}2)$$

This leads to $\Delta R_{\rm wall} = 15$–30 cm in ITER producing a similar ratio for wall to divertor fluxes by ELMs as those in AUG with 4–8 cm for the same $\Delta W_{\rm ELM}/W_{\rm ped}$. On this basis, plasmas with an outer wall clearance $\Delta R_{\rm wall} \geqslant 30$ cm should have a very low wall contribution to core W contamination and thus provide an effective means to develop H-mode scenarios at low current with low risks regarding the impact of W wall fluxes.

These H-mode plasmas will constitute the workhorse for the development of integration schemes with the W wall and, in particular, ELM control. It is, therefore, essential that the ITER tokamak is equipped with the systems required to support this development. As mentioned above, with four pellet injectors for ELM pacing it should be possible to achieve an ELM frequency of 60 Hz by combining the four injectors for this mission (the maximum pellet injection frequency per injector is 15 Hz) which should lead to acceptable W core plasma influxes for 5–7.5 MA H-mode plasmas according to the analysis in figures 39 and 40. The requirements for ELM control by 3D fields applied with the ELM control coils and increasing clearance have been evaluated with resistive MHD linear modelling (see [Bai2024] for details). The results of these studies are summarised in figure 44 where it is shown that a similar level of X-point displacement (which is experimentally correlated with large ELM mitigation/suppression) can be maintained as the wall clearance is increased if the current in the ELM control coils is doubled. We note that for the reference plasma-wall clearance the design current of the ELM control coils applied with $n = 3$ or 4 toroidal symmetry is 90 kAt for 15 MA H-mode plasmas. For this configuration and plasma current level ELM suppression is expected to be achieved at a coil current level of 45–60 kAt [Hu2021, Becoulet2022], i.e. 3–4 kAt MA^{-1}. On the basis of a linear scaling of this requirement, 30 kAt should be more than sufficient to demonstrate ELM suppression at 5 MA with the reference wall clearance (i.e. 6 kAt MA^{-1}) and, thus, 60 kAt would be required for the highest wall clearances which is well within the capabilities of the ITER ELM control system. We note that the value of the plasma current needs to be tuned to ensure that the q_{95} falls within the windows that provide maximum X-point displacement for each wall clearance, as shown in figure 44 (namely 4.65 MA for the configuration with large outer gap, 4.92 MA for the configuration with increased overall clearance and 4.77 MA for that with the nominal ITER separatrix for 15 MA $Q \geqslant 10$ operation). For 7.5 MA H-modes the wall clearance at which ELM suppression can be demonstrated would be lower than 45 cm both because of limits in ELM control coils current as well as for the in-vessel vertical stability control coils, although the latter depends on the level of noise in the dZ/dt diagnostic signal.

The evaluations discussed in this subsection are based on a combination of physics-based extrapolations of experimental results to ITER plasma conditions and integrated modelling which are subject to large uncertainties. In first place, models to perform integrated modelling studies with a self-consistently generated W source from the divertor and the wall are not yet available and a solid physics basis and detailed experimental characterisation to provide a description of W transport from its source at the surface of the PCS for the core plasma remains to be developed. Therefore, specific experiments on the impact of ELMs and inter-ELM plasma characteristic on the W wall and divertor sources and edge W transport and on the quantification of the effect of wall clearance on W plasma contamination are required. This should be accompanied by the validation of the models used to predict ITER plasmas to ensure the accuracy of the modelling results on which the SRO research plan is based.

3.2.2. Summary and conclusions for SRO. Integrated operation with a large number of tokamak components and ancillary systems in their final baseline configuration and with an inertially cooled tungsten (W) wall in SRO provides substantial minimisation of the risks associated with physics uncertainties and plasma operational aspects for later operation in the DT-1 phase with deuterium–tritium plasmas. In particular, control and investment protection algorithms and systems (PCS, APS, CIS, …) as well as the DMS will be commissioned with plasma during this phase both in L-mode to the nominal

15 MA/5.3 T levels as well as in H-mode up to 7.5 MA/2.65 T. In-vessel components will, thus, already be subject to the highest electromagnetic loads in SRO. This will allow the identification of possible design/manufacturing weaknesses leading to infant failures, which will be possible to solve by hands-on assisted corrective maintenance.

Together with this, the development of the basic building blocks of ITER plasma scenarios (plasma start-up, plasma current ramp-up, flat-top and ramp-down) for both L-mode and H-mode plasmas is the fundamental purpose of this phase. In this phase the schemes to provide and maintain good vacuum conditions foreseen for operation with all-tungsten plasma facing components (GDC and boronisation) and to maintain an acceptable tungsten core plasma concentration will be tested and optimised to minimise impact on machine operations.

Key outcomes of the activities planned in SRO include:

- Demonstration of the capability of superconducting coils and the cryoplant to operate plasma scenarios up to 15 MA/5.3 T in diverted configuration;
- Routine operation with shape and vertical position control up to 15 MA/5.3 T in L-mode;
- Exploration of the H-mode operational space up to 7.5 MA/2.65 T in deuterium plasmas;
- Commissioning of diagnostic systems with plasma and demonstration of their successful integration into the Plasma Control, Interlock and Investment Protection Systems;
- First validation of ITER plasma scenario predictions in L-mode and H-mode (over the range accessible in SRO). This includes (among many key physics and scenario integration issues):
  - o Confirmation of energy and particle confinement expectations for ITER (based on scaling laws and advanced turbulent transport modelling) in L-mode and H-mode,
  - o Confirmation of the additional heating power requirements to access and sustain H-mode plasmas in ITER (presently based on scaling laws),
  - o Assessment of the efficiency of gas fuelling versus pellet fuelling in L-mode and H-mode plasmas,
  - o Demonstration of the requirements for ELM control in H-mode plasmas with low input torque and dominant electron heating (as required for $Q \geqslant 10$ operation),
  - o Quantification of the impact of ELM control on H-mode confinement,
  - o Determination of the scrape-off layer power e-folding length in ITER H-mode plasmas and of its scaling with plasma conditions,
  - o Assessment of the compatibility of H-mode confinement with radiative divertor operation;
  - o Quantification of the tungsten sources (divertor and first wall), of the tungsten transport from the edge to the core plasma and of their impact on L-mode and H-mode plasma scenarios;
- Commissioning of the installed H&CD (ECH and ICH) systems with plasma up to their nominal plasma coupled power levels (40 MW and 10 MW, respectively) for up to 50 s;
- Demonstration of the compatibility of ICH heating with acceptable core plasma tungsten concentrations in L-mode and H-mode plasmas, guiding the decision for an additional 10 MW coupled plasma power upgrade to be installed for DT-1;
- Identification and optimisation of the correction of error fields due to machine assembly and intrinsic non-toroidally symmetric features of ITER's design;
- Demonstration of required divertor and first-wall protection and core impurity control methods, necessary for high-performance H-mode scenarios in DT-1, in deuterium H-mode plasmas up to 7.5 MA/2.65 T;
- Characterisation of disruption loads, to validate safety-related assumptions, and of their effective mitigation by DMS up to 15 MA/5.3 T, including runaway loads;
- Demonstration and optimisation of wall conditioning schemes (GDC, Boronisation, ICWC, ECWC);
- Engineering evaluation of the ITER tokamak as an integrated system with as-built and as-assembled components/systems, including the development of an integrated plant simulator;
- First validation step of the radiation maps by measurements obtained during deuterium operation and testing of safety-related measurements/systems such as the plasma current monitor and the fusion power shutdown system;
- First assessment of fuel (deuterium) retention and removal efficiency, dust production and in-vessel material analysis (first wall samples);
- Elaboration of the first update of the safety-orientated knowledge acquisition programme with regards to plasma transients (disruptions, VDEs, runaways), safety-related diagnostics and systems, dust production, in-vessel fuel retention and corrosion products in the cooling systems.

The demonstration of these objectives is key to minimise risks and to ensure robust operation in DT-1 with D-T, when the facility will begin to operate under the full nuclear licensing rules and activation will make changes or repairs inside the tokamak much more expensive and time consuming.

3.3. Integrated commissioning II

This phase follows the SRO experimental phase and the second phase of assembly (Post-SRO assembly) after SRO. During the Post-SRO assembly phase, additional diagnostics are installed, the ECH system is upgraded with an additional 20–27 MW of power coupled to the plasma, and the ICH heating power may be increased by an additional 10 MW of power coupled to the plasma, if tests at SRO are successful. The TBMs and their ancillary systems and two NBI (HNB-1 and HNB-2) injectors are installed to operate using hydrogen in the ion sources. Regarding in-vessel components, water-cooled W first wall panels will be installed and connected to the blanket shield modules. The capabilities of the diagnostic set will be expanded from those available in SRO, in particular, to measure fusion products. Prior to the start of the IC-II phase a calibration of the neutron diagnostics will be performed. A high-level description of the IC-II activities is shown in figure 45.

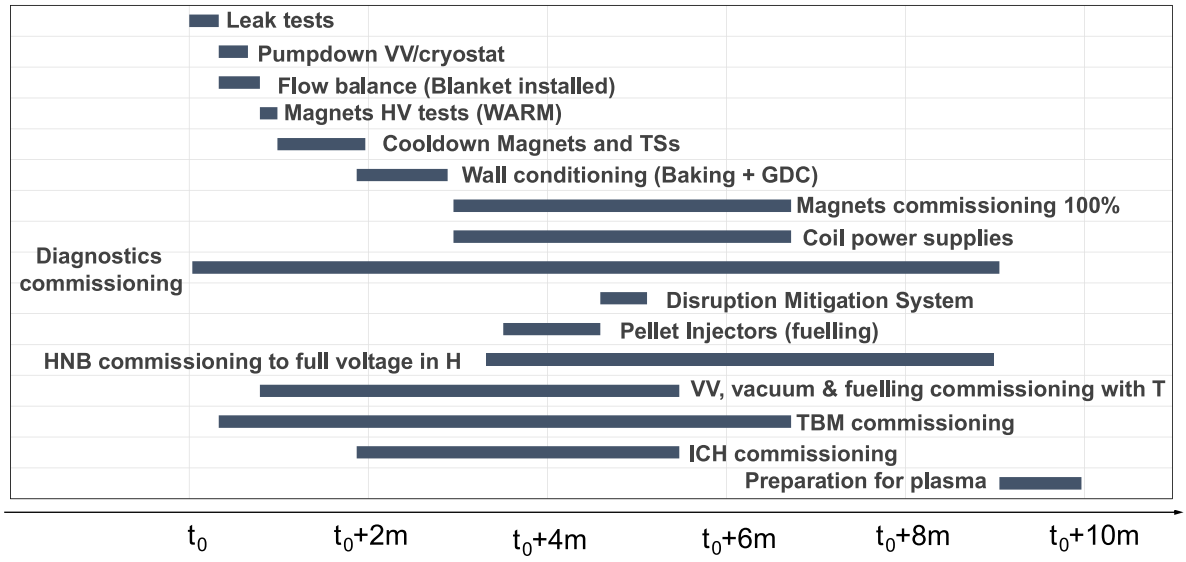

Figure 45. Overall schedule and main activities for Integrated Commissioning II.

The objective of this phase is to re-commission the systems already available from IC-I and to commission the newly available systems together with additional control, interlock and safety systems required for them and for later operation in DT-1. Of particular importance in this phase is the integrated commissioning of TBMs, NBIs and of the Tritium Plant connected to the tokamak. By this phase, the Tritium Plant will have been commissioned stand-alone, which requires the reception of tritium on-site during Post-SRO assembly, and will be followed by the connection of the plant to the tokamak systems. Lessons learnt from the previous IC-I phase will be included in the preparation of the detailed plan for IC-II.

The licensing process to allow the introduction of tritium into the tokamak and to perform D-T plasmas shall be completed during this phase in advance of DT-1 operations. This will require the timely submission of the first conclusions of the safety-orientated knowledge acquisition programme including those from dust and in-vessel material sample analysis. The IC-II phase is planned to last 10 months and proceeds directly to the DT-1 phase.

Key outcomes of planned activities in the IC-II phase include:

- Commissioning of the NBIs (excluding the NBI ducts) using hydrogen in the ion sources to accelerating voltages ∼870 kV;
- Commissioning of the four TBMs and associated subsystems;
- Commissioning of the controls, safety and interlock systems required for DT-1 operation;
- Commissioning of the Tritium Plant connected to the tokamak systems;
- Update of the safety-orientated knowledge acquisition programme including analysis of SRO results and samples as well as of the qualification and commissioning test results during IC-II.

3.4. First deuterium–tritium phase (DT-1)

The objective of the first deuterium–tritium (DT-1) phase is to achieve the first Project's goals in the demonstration of the scientific and technological feasibility of fusion power production foreseen in the ITER Project. For the fusion power production goal, this is the demonstration of 500 MW of fusion power production with $Q \geqslant 10$ for lengths longer than 300 s. To meet the goals, the research programme in this phase addresses key scientific and technical issues for the demonstration of nuclear fusion as an energy source, including the self-heating of deuterium–tritium plasmas by alpha particles from the fusion process, the demonstration of operation with efficient tritium management, the demonstration of tritium-breeding by performing the TBM Program [Giancarli2024], the validation of assumptions in the nuclear safety licence in DT-1 and the provision of the operational basis to define the licence details for the second deuterium–tritium (DT-2) phase.

The DT-1 phase is divided into five two-year operational cycles with 16 months of plasma operation followed by 8 months long term maintenance plus commissioning periods. The achievement of the DT-1 goals requires installation of new systems or upgrades, in addition to those already available in SRO, particularly of the H&CD systems (ECH, ICH and NBI), the water-cooled W first wall, diagnostics and the TBMs with their ancillary systems, as summarised in table 1. In particular, an extensive set of diagnostics to characterise fusion products will be available.

Before the start of DT-1 the licencing process for ITER to start deuterium–tritium operation should be completed. Of particular importance for the DT-1 phase is the availability of

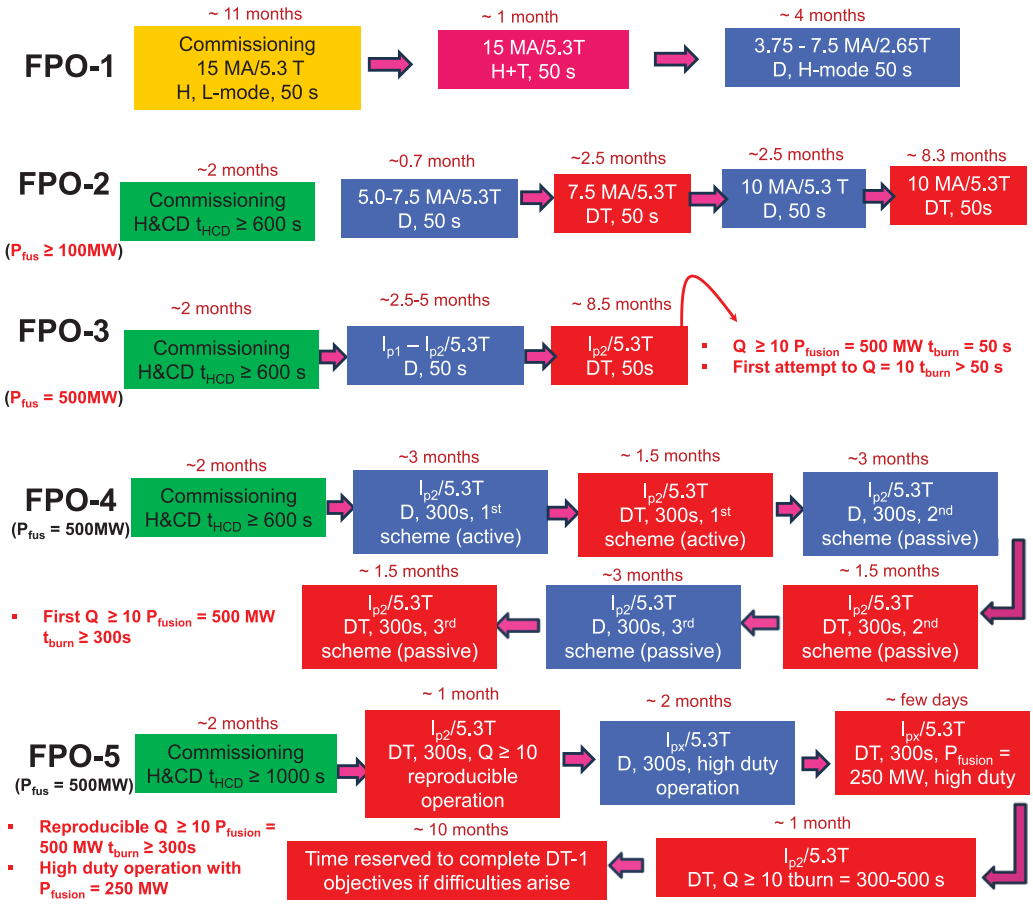

Figure 46. Sequence of main experimental research activities and foreseen time allocation for the DT-1 phase which includes five operational campaigns (FPO-1 to FPO-5). Note that in FPO-4 several approaches will be followed to extend the burn length; these include the use of H&CD systems to control the current profile and, thus, MHD stability (active) while others are based on pre-forming the current profile before the high Q phase is accessed (passive).

the Tritium Plant to reprocess tritium and deuterium for fuelling and to stand ready to handle releases of tritium into the secondary containment during long-term maintenance. The neutron fluence in this phase will be limited to enable the performance of maintenance activities in the corresponding long-term maintenance periods, while respecting shutdown dose rate requirements for workers. This fluence is evaluated to be ~3.5 10^{25}; this is of the order of ~1% of the ultimate project fluence goal, namely 0.3 MW yr^{-1} m^2, which corresponds to 3 10^{27} DT neutrons. This fluence limitation has a clear impact on the definition of the goals of DT-1 itself as well as on the strategy proposed to achieve them. It is essential to ensure that sufficient fluence is available for the development and demonstration of the $Q \geqslant 10$ $t_{\rm burn} \geqslant 300$s goal as well as for the TBM related goals in the last campaigns of DT-1. Otherwise, there is a risk that the DT-1 fluence limit is reached before these goals are achieved and that the goals themselves would have to be postponed to DT-2. The proposed strategy is designed to minimise this risk but, in addition, the execution of the experimental strategy will have to implement specific actions (e.g. shortening of pulses showing performance much lower than expected) to ensure that neutron fluence is not wasted. This is already standard practice in present tokamaks when DT experiments have been performed (e.g. see [Piron2019] for JET DT experiments).

The overall plan for the DT-1 phase is shown in figure 46 and the H-mode scenario development path followed in DT-1 is shown in figure 47. Emphasis is given to the achievement of $Q \sim 10$ plasmas as soon as possible (i.e. in short ~50 s burn lengths) and, once demonstrated, to the extension of high Q scenarios to 300–500 s burn. The choice of ~50 s for the first $Q \geqslant 10$ demonstration target is based on the requirement to achieve stationary plasma conditions (except for current diffusion), including DT fusion-produced helium content in the plasma, as part of this first $Q \geqslant 10$ demonstration. The foreseen neutron fluence production in DT-1 per FPO campaign and the accumulated fluence are shown in figure 48.

3.4.1. Fusion power operation-1. The objective of the FPO-1 campaign is to re-establish operation with the newly installed and upgraded systems in the Post-SRO assembly phase, first in H and then in DD plasmas. This will require the re-commissioning of existing systems and the commissioning for short plasma pulses (~50 s flat-top length) of the new/upgraded systems, controls, interlocks, protection, diagnostics,

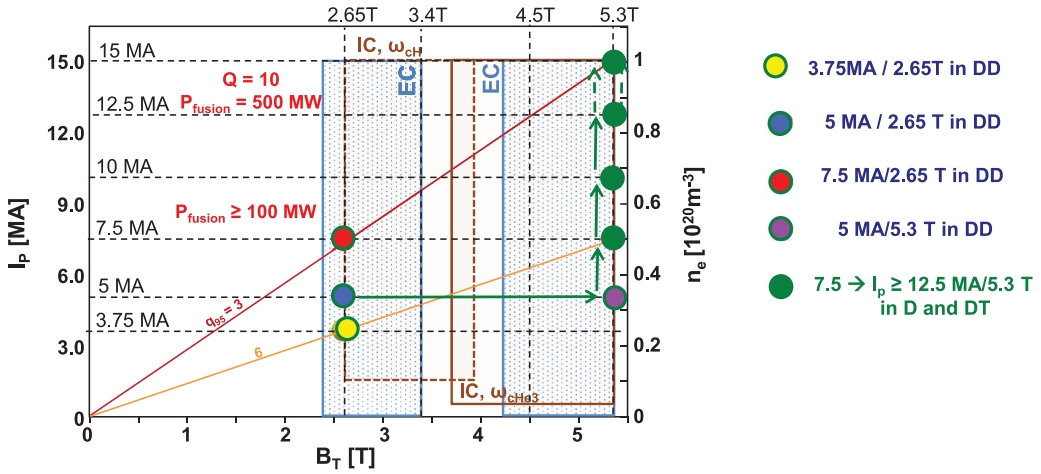

Figure 47. Sequence of H-mode plasma scenarios to be explored in DT-1 in DD and DT plasmas in terms of plasma current, toroidal field and electron density, assuming a typical value of ∼85% of the Greenwald limit.

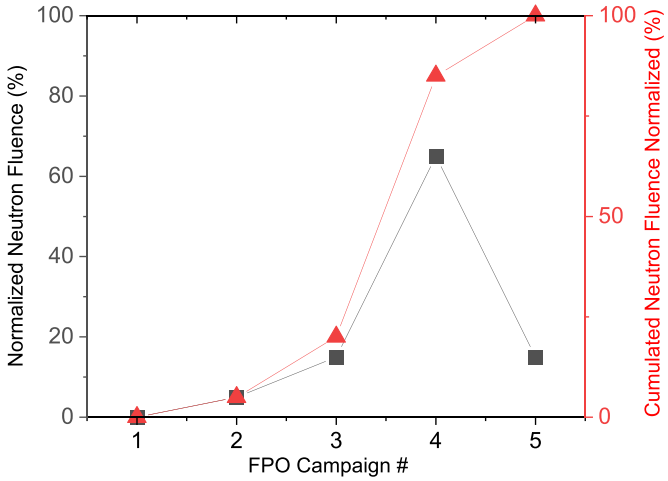

Figure 48. Foreseen neutron fluence consumption in the 5 FPO experimental campaigns in DT-1 as percentage of the fluence limit of 3.5 10^{25} neutrons. The left vertical axis applies to the fluence consumed per campaign while the right vertical axis corresponds to the cumulated fluence consumed up to and including a given FPO campaign.

etc., specially of the NBI, which will operate (with H in the ion source) for the first time in ITER.

The scenarios developed in SRO (15 MA/5.3 T—L-mode in hydrogen and 7.5 MA/2.65 T H-mode in deuterium) will be reproduced and their operational ranges extended taking advantage of the new systems and the newly available capabilities. This will include the determination of the effects of new sources of error fields on plasma scenarios, such as those due to the TBMs, as well as their minimisation. Similarly, the optimisation of wall conditioning schemes (GDC, boronisation, ICWC, ECWC) in their final configuration will be carried out. The newly installed/operational water-cooled in-vessel components (blanket shield modules and first wall panels) will be subject to the highest electromagnetic loads, as well as to power fluxes comparable to those in $Q \geqslant 10$ operation, already in the H phase of FPO-1. This is ensured by operation in H plasmas with additional heating power up to 103–120 MW (depending on upgrades implemented by DT-1) and with plasma current/toroidal field up to 15 MA/5.3 T in this campaign. This will allow the identification of possible design/manufacturing weaknesses of these water-cooled components leading to infant failures, which would be possible to solve by hands-on assisted corrective maintenance before deuterium operation starts.

Before the change-over from hydrogen to deuterium, tritium will be introduced in the tokamak and plasmas with varying hydrogen/tritium contents will be performed. This will require the use of the fuelling and T plant connected to the tokamak, injecting tritium into the plasma for the first time. These experiments will allow a first quantification of tritium retention in ITER. These T containing plasmas will be used to commission the DMS system, including the presence of high energy electrons from β-decaying tritium during disruptions, and to demonstrate its effectiveness in suppressing runaways up to 15 MA/5.3 T with pure T plasmas. The DMS commissioning experiments will be followed by tests of the fuel (tritium) removal schemes for DT-1 to assess their efficiency and guide their optimisation.

The logic for the strategy behind the proposed steps in the DT-1 research plan is as follows:

L-mode scenario development to 15 MA/5.3 T in H plasmas. The purpose of this first part of the campaign is to re-develop the L-mode plasma scenarios already explored in SRO now including the new components (W water-cooled first wall) and systems (e.g. NBI, increased ECH power, TBMs etc.). This will require a re-assessment of error fields and their correction since the new systems include ferromagnetic materials leading to new sources of error fields as well as a re-tuning of the plasma control, protection and disruption mitigation systems to account for the effects of the new H&CD schemes and the

largely increased (at least doubled) level of additional heating power. It is important to note that in this phase the W water-cooled first wall will already be installed and it is important to avoid large loads on the PFCs during disruptions, i.e. mitigation of disruption loads should be routinely achieved when operating at high I_p and W_{th} ($\sim$100 MJ) which will be accessible in this phase thanks to the increased additional heating. Special emphasis in this phase will be given to the commissioning with plasma of the new H&CD systems installed in the post-SRO assembly phase (e.g. assessment of shine-through limits for NBI) as well as to the new diagnostics (not yet those for fusion products since this first part is in H).

Assessment of T effects on disruption loads and mitigation up to 15 MA/5.3 T in H + T plasmas and assessment of T removal efficiency.
The purpose of the second (short) part of the campaign is to assess the impact of high energy electrons from β-decay of T on disruption dynamics and in the requirements for mitigation and to assess T removal efficiency.

The impact of T on disruptions mostly concerns the generation of REs in the current quench of the disruption. In SRO the mitigation of RE focuses on the hot tail of high energy electrons that may remain in the plasma after the TQ. Mitigation of such runaway source could be achieved through pre-TQ densification, which ensures the thermalisation of high-energy electrons before the electric field exceeds the critical threshold for RE generation. Such mitigation strategy is applicable, in principle, for β-decay electrons but its practicalities are very different to those in SRO. Increasing the electron density has been shown to thermalise β-decay electrons during the CQ; however, the required densities to achieve the same mitigation level increase by an order of magnitude compared to those for hot tail in SRO [Vallhagen2024]. Given these uncertainties and the potential risk that substantial damage to PFCs may occur while runaway mitigation is being optimised, the FPO-1 NB-IRP includes these targeted experiments as soon as all the systems of the machine are fully operational and before DD operation, leading to machine activation preventing in-vessel human intervention, starts. Should PFCs need to be replaced because of inefficient disruption mitigation during tests in T-containing plasmas, this could be potentially done with human support for in-vessel operations. We note that, as described in section 3.4.6, the proposed plan to address the impact of T on disruptions and their mitigation includes a range of T concentrations from 1% to 100% and is designed to, as far as possible, minimise the risks of RE damage to water cooled W PFCs.

During this operational phase the assessment of T removal efficiency of the strategies developed in SRO will be, for the first time, carried out with T containing plasmas and re-tuned for maximum efficiency. This is an important step before DT operation starts and routine T removal must be carried out.

H-mode scenario development in DD plasmas 3.75–7.5 MA/2.65 T (q_{95} = 3–6).
In this third and last part of the FPO-1 campaign H-mode scenarios at 2.65 T, already explored in SRO, will be re-developed. As mentioned before, new H&CD systems with increased power and improved diagnostics for H-mode and DD plasmas will be available, as well as new sources of error field. ITER tokamak operation will thus need to be re-developed with substantial re-tuning of plasma control and protection systems as well as re-development of the scenarios themselves. As an example, the increased H&CD power will require re-tuning and application of the control systems to prevent excessive power fluxes on the water cooled PFCs. Similarly, the use of NBI for heating of H-modes will lead to an increased level of ion heating and plasma rotation compared to SRO. This together with the increased plasma β will impact H-mode plasma parameters as well as core and pedestal plasma MHD stability, requiring the re-tuning of the ELM control and NTM control schemes developed in SRO. In addition, the H-mode plasmas developed in this part will serve as a reference to plan the experiments for H-mode development in FPO-2 at 5.3 T with the same range of q_{95}.

3.4.2. Fusion power operation-2. The objective of the FPO-2 campaign is to perform the first D-T plasmas in ITER and to demonstrate fusion power production in excess of 100 MW with $Q \geqslant 1$ for durations of, at least, 50 s. To minimise neutron fluence consumption, D–D and D–T plasma scenarios, with a range of tritium concentrations up to their optimum value for fusion power production, will be developed with plasma currents/fields in the range of 7.5–10 MA/5.3 T. Besides neutron fluence minimisation interleaving DD and DT scenarios, which is possible thanks to the available additional $P_{aux} \geqslant 100$ MW, provides a robust path for the development of scenarios in ITER by:

- Separating scenario development issues associated with high I_p, P_{aux} and W_{th} operation in ITER from those related to DT burning plasmas with substantial alpha heating;
- Allowing a gradual increase of T content in the plasma and thus a gradual build of alpha heating, fast electron seeds for REs (β-decay and Compton from γ emission due to wall activation) and T throughput (and associated fuel retention).

This approach minimises the risk that large variations in plasma parameters leading to loss of control (e.g. large excursions of edge power flow, W_{th}, runaway seeds, alpha particle densities) may occur when expanding the operational space of DD and DT plasmas towards high $I_p/P_{aux}/Q$ operation.

From the results obtained in these experiments the plasma scenarios (i.e. I_p, optimum H&CD mix, etc.) with the potential to deliver 500 MW of fusion power with $Q \geqslant 10$ will be identified. Experiments in this phase will be accompanied by the application, further development and validation of plasma scenario models to ensure that they can reproduce the plasma parameters obtained in this phase. This should ensure the provision of reliable predictions for the required plasma scenarios to be explored to demonstrate the 500 MW of fusion power with $Q \geqslant 10$ goal, which is the goal of FPO-3.

The development foreseen in FPO-2 will require the re-tuning of the plasma control and protection schemes already commissioned (or re-commissioned) in FPO-1, in particular those required to provide acceptable power fluxes to PFCs and core impurity content. The DMS will also be re-tuned to account for the increasing levels of plasma energy and tritium content in H-mode plasmas. First studies of T fuelling in H-mode plasmas will be performed in this phase and their results be used for the optimisation of plasma fuelling and of the fuel cycle. Helium exhaust from deuterium–tritium fusion will be explored for the first time in ITER. Similarly, the schemes to remove tritium, provide good wall conditions, error field correction, etc., will be re-tuned/optimised and applied to the plasma scenarios with increasing levels of I_p, P_{aux}, tritium content and P_{fusion}. In this phase burn control experiments will be carried out to commission with plasma the systems to be later applied with high fusion power levels in FPO-3.

Prior to FPO-2, a decision will be made to maintain the NBI system using H in the ion sources or to change to D. As part of the initial phase of this campaign the capabilities of the H&CD systems to support burning deuterium–tritium plasmas with durations of, at least, 300 s will be assessed. This assessment will require operation at maximum plasma coupled power for each of the systems for durations of, at least, 600 s.

By this time of the programme significant neutron production and fusion power will be produced for the first time in ITER. Therefore, experiments to confirm the calibration of the associated diagnostics (neutrons and alpha particles) will be performed before fusion power production at a level of ∼100 MW is attempted. These plasmas will have a significant fast particle pressure from NBI while fast alpha pressure will remain moderate. Despite this, since the fast particle drive for Toroidal Alfvén Eigenmodes scales with q^2, this may lead to Alfvén Eigenmodes being driven in these plasmas (we note that damping terms also scale with q^2) [Pinches2015]. Therefore, it may be necessary at this stage, and in advance of FPO-3, to develop means to control AEs if the associated fast particle transport or losses are excessive.

The logic for the strategy behind the proposed steps in the FPO-2 research plan is as follows:

H-mode scenario development 5 MA/5.3 T in DD plasmas ($q_{95} = 9$)
Estimates of the tolerable ELM size for uncontrolled ELMs in ITER avoiding divertor melting (edges and surface of monoblocks) correspond to those for 5 MA plasmas with $q_{95} = 3$ [Gunn2017] so that operation at 7.5 MA/5.3 T has significant risks in terms of divertor melting. ELM control schemes are expected to require significant re-tuning from those developed for 3.75 −7.5 MA/2.65 T H-modes for 7.5 MA/5.3 T H-modes. Therefore, discharges with uncontrolled ELMs will unavoidably have to be executed before ELM control can be achieved. As discussed in section 3.4.6 the pedestal pressure and, thus ELM energy loss, in ITER may scale almost linearly with B_t at fixed I_p, which implies that 5 MA/5.3 T H-modes in FPO-2 will have similar ELM sizes to those for 7.5 MA/2.65 T in FPO-1 leading, potentially, to edge divertor monoblock melting. However, operation at very high values of q_{95} is known to facilitate H-mode regimes with small/grassy ELMs and, thus, 5 MA/5.3 T with $q_{95} = 9$ is chosen as the first step in the development of 5.3 T H-modes in ITER. This is expected to minimise the risk of edge divertor melting by avoidance of large Type I ELMs through operation in such grassy ELM/small ELM regime without the need for active ELM control techniques. Should this not be sufficient, lower I_p (∼3.75 MA or lower, if needed) would need to be explored for H-mode plasmas development in this first step at 5.3 T. We note that besides a first confirmation of the scaling of plasma parameters with B_t, the scaling of the H-mode threshold with B_t will also be first assessed in ITER at this time by comparing these plasmas with those in FPO-1 (5 MA/2.65 T).

H-mode scenario development 7.5 MA/5.3 T in DD and DT plasmas ($q_{95} = 6$)
The first step in 5.3 T scenario development done in DD and DT is carried out at 7.5 MA. This will confirm the scaling of pedestal and core plasma parameters with I_p at full B_t and, for the first time, the impact of T on these parameters. This should provide an initial assessment of the potential of high q_{95} plasmas to achieve high confinement and high fusion production in ITER including the specificities of ITER's plasma parameters as well as of its H&CD systems, as discussed in section 3.4.6.

Besides providing a high B_t reference for 7.5 MA/2.65 T, the choice of 7.5 MA for this first step also ensures that the risks in runaway production due to electron seeds from β-decay are low, as shown in section 3.4.6. 7.5 MA/5.3 T plasmas in FPO-2 have a very wide operational space for both DD and DT H-modes over a wide range of T concentrations and this will be explored. We note that the H-mode power threshold for DD plasmas at 7.5 MA/5.3 T and $<n_e> \sim 0.9\, n_{GW}$ is ∼55 MW compared to an additional heating power of ∼100 MW and that this threshold decreases with main hydrogenic ion isotopic mass.

H-mode scenario development 10 MA/5.3 T in DD and DT plasmas ($q_{95} = 4.5$)
The second step in 5.3 T scenario development in DD and DT is carried out at 10 MA since this is the reference value for $Q \geqslant 5$ steady-state operation in ITER [Polevoi2020, Kim2021]. Exploration of this scenario early in the programme, even if not extending it to very long burn durations at this stage, will provide very valuable information on access to high Q operation and moderately elevated q_{95} in ITER. The W_{th} in these plasmas is expected to increase by ∼30%–50% compared to 7.5 MA/5.3 T while, obviously, W_{mag} will be a factor of ∼ 1.8 higher. This will require tuning of the control and protection systems from those for 7.5 MA/5.3 T DD plasmas and, with increasing T concentration, in DT plasmas.

As for the step above, although more restricted, a wide operational space in both DD and DT H-modes over a wide range of T concentrations will be accessible. We note that

the H-mode threshold for DD plasmas at 10 MA/5.3 T and $<n_e> \sim 0.68\, n_{GW}$ is ∼55 MW compared to an additional heating power of ∼100 MW and that this threshold decreases with main hydrogenic ion isotopic mass. At this stage, if not earlier, fusion power production in excess of 100 MW with $Q \geqslant 1$ will be demonstrated in ITER. Besides this fusion production goal, the main outcome of FPO-2 is the validation of models to predict plasma parameters and performance in both DD and DT plasmas at 7.5–10 MA/5.3 T with several 10's MW of alpha heating. These validated models will then be used to predict the plasma conditions, in particular the value of I_p, for which $Q \geqslant 10$ will be achievable in ITER in DT and the equivalent plasma conditions in DD, which will be investigated in FPO-3. We note that these 10 MA/5.3 T plasmas DT will have characteristics close to those foreseen for the ITER non-inductive steady-state $Q = 5$ plasmas and will thus provide an initial assessment of the plasma performance that is expected in these conditions.

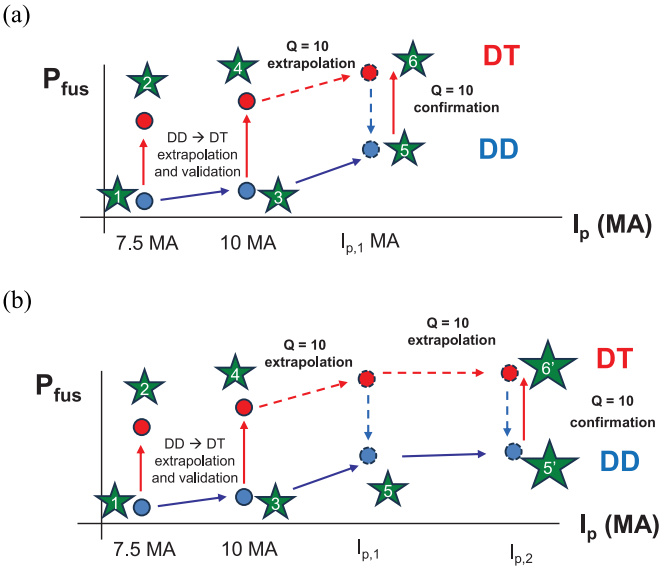

Figure 49. Experimental steps towards $Q \geqslant 10$ in FPO-3 following the steps (1–4) in FPO-2. Full arrows correspond to experiments that will be carried out while dashed lines correspond to modelling predictions. (a) Represents the case in which $Q \geqslant 10$ DT predictions are made on the basis of FPO-2 (6) and the corresponding DD predictions (5) are verified by experiment. In this case, once step 5 is verified, the programme in FPO-3 will proceed to step 6. (b) Represents the case in which $Q \geqslant 10$ DT predictions are made (6) and the corresponding DD predictions (5) are not verified by experiment. In this case the models will be re-validated with the results of step 5 and a new prediction for $Q \geqslant 10$ conditions (6′) will be made together with the corresponding DD predictions (5′). In this case, once step 5′ is verified, the programme in FPO-3 will proceed to step 6. If step 5′ is not verified, the cycle of model re-validation and prediction will be repeated.

3.4.3. Fusion power operation-3. The objective of the FPO-3 campaign is to demonstrate fusion power production of 500 MW with $Q \geqslant 10$ for, at least, 50 s including stationary helium exhaust. This campaign will provide the first D–T plasmas in ITER dominated by alpha heating and a wealth of new physics and operational results. To minimise neutron fluence consumption, D–D and D–T plasma scenarios, with a range of tritium concentrations up to their optimum value for fusion power production, will be developed. This development will start from the plasma scenario identified by the models validated in FPO-2 (foreseen to provide $Q \geqslant 10$ in D–T) to confirm the expected plasma performance in D–D plasmas. If the performance is confirmed this scenario will be explored in D–T. If the D–D plasma performance is not confirmed, new scenarios will be developed in D–D plasmas up to the performance level required and, then, explored in D–T. The schematic representation of the experimental strategy to be followed towards the achievement of $Q \geqslant 10$ in FPO-3 is shown in figure 49. We note that this strategy has been successfully applied to plan and execute experiments in the JET DTE-2 campaign [Garcia2023, Maggi2024, Rimini2024]. The FPO-3 experimental strategy is focused on the achievement of $Q \geqslant 10$ at the lowest I_p (<15 MA) possible since this has significant benefits from the point of view of MHD plasma stability and disruption loads and facilitates their mitigation.

The associated expansion of the operational space in FPO-3 will require the gradual re-tuning of the plasma control and protection schemes already commissioned FPO-2, as well as of the DMS with increasing levels of plasma energy and tritium content in H-mode plasmas. Similarly, the schemes to remove tritium, provide good wall conditions, etc., will have to be optimised to sustain high Q operation as well. By the end of this campaign all ancillary systems and control schemes necessary to perform high Q operation in DT plasmas will be routinely utilised. These include those needed for the integration of core plasma confinement and purity requirements with acceptable first wall and divertor plasma power and particle fluxes. In this respect, the duration of the $Q \geqslant 10$ phase, with target of ∼50 s will have to be adjusted to that required to demonstrate stationary helium exhaust. A duration of ∼50 s is required to demonstrate this goal on the basis of modelling predictions discussed in section 3.4.6. Besides considerations of neutron fluence consumption, it is advantageous to maintain the $Q \geqslant 10$ phase as short as possible while providing stationary plasma parameters including helium concentration. As discussed in section 3.4.4, the current profile in ITER relaxes on timescales of 100's of seconds and this may lead to the triggering of MHD instabilities as the burn length increases. Thus, it is expected that burn extension to timescales of 100 s and longer will require substantial experimental time beyond that available in FPO-3. The strategy for FPO-3 aims at the achievement of the $Q \geqslant 10$ goal at the lowest I_p value possible. For values of I_p significantly lower than 15 MA the achievement of $Q \geqslant 10$ relies on the demonstration of higher-than-H-mode confinement in ITER, along the findings in present experiments based on the so-called advanced inductive or hybrid scenario [Luce2014], which have provided record DT fusion power at JET [Maslov2023]. To this end, the experiments in FPO-3 will explore the optimisation of the current profiles, especially on H-mode entrance, to maximize confinement at $I_p < 15$ MA. If the confinement achieved at

$I_p < 15$ MA is not high enough for $Q \geqslant 10$, then scenarios with $I_p = 15$ MA (i.e. the so-called ITER baseline scenario) will be used for $Q \geqslant 10$ demonstration.

In addition to the access to alpha heating dominated DT plasmas, the FPO-3 campaign will provide key results for the validation of fusion-product diagnostic measurements and safety-related evaluations for D-T operation in ITER, in particular: (a) full validation of the radiation maps in nominal fusion power operating conditions, (b) confirmation of the applicability of the in-vessel retained T management approach in $Q \geqslant 10$ plasmas (50 s duration), (c) evaluation of the dust production rates for $Q \geqslant 10$ plasmas (50 s duration), etc. These will be used to refine the licencing requirements details in the follow-up DT-2 phase and for the plans of the FPO-4 and FPO-5 campaigns. The FPO-3 campaign will conclude with the first attempt to extend the stationary burn duration at 500 MW fusion power with $Q \geqslant 10$ beyond 50 s. This is performed at this stage to determine the physics processes that may lead to the termination of the burn before 300 s, which is essential for the refinement of the plans for burn extension in FPO-4.

Prior to FPO-3, and if the NBI system has been maintained with H in the ion sources in FPO-2, a decision may be taken to maintain the NBI using H in the ion sources or to change to D. Similarly, the capabilities of the H&CD systems to support burning DT plasmas with durations of, at least, 300 s will be confirmed (if FPO-2 tests were successful) or re-assessed at the beginning of this campaign. We note that the impact of operating the NBI with H ion sources on fusion performance for high Q plasmas is very minor, as discussed in section 3.4.6. Therefore, the decision to maintain the ion sources in H or change to D will be made on the basis of operational reliability of the NBI system with one or other isotope rather than on plasma physics considerations. Strategies to maximize Q at this stage will include optimisation of the H&CD mix in the scenarios explored. For instance, the role of ion heating in the high Q access phase and in the maximum Q achievable will be explored by maximizing the use of NBI (which deposits 1/3 of the power in the ions in ITER) and ICH in these scenarios and compared to those using NBI and ECH. It is well known that ICH heating in DT plasmas can lead to an increase of Q by $\Delta Q \leqslant 1.5$ in ITER [Wagner2010] and this will be tested in this phase. We note that extensive experiments to explore the impact of H&CD mix on ITER high Q operation are foreseen in DT-2 (see section 3.5) once the licence to operate ITER to its full neutron fluence of 3.0 10^{27} is in place.

3.4.4. Fusion power operation-4. The objective of the FPO-4 campaign is to demonstrate fusion power production of 500 MW with $Q \geqslant 10$ for burn times of up to, at least, 300 s. Progress in the extension of burn duration from 50 to 300 s is foreseen to take most of the experimental time in this campaign. It is, thus, expected that the number of pulses demonstrating 500 MW fusion power with $Q \geqslant 10$ for 300 s in this campaign will be small. The extension of the burn from ~50 s to longer timescales is expected to be limited by the development of MHD instabilities as seen in present experimental devices such as DIII-D [Turco2024]. These consists of tearing modes which become unstable when the current profile relaxes after the L–H mode transition following the build-up of the pedestal plasma and the ensuing bootstrap current. This causes the formation of a 'well' in the current profile which, in its relaxation in time, can lead to the triggering of tearing modes, as shown in figure 50.

As shown in section 3.4.6 these instabilities may appear in longer time intervals in ITER since the profile of the plasma current relaxes in timescales of several 100 s of seconds. This current profile evolution can also affect plasma transport and, thus, impact the parameters of the plasma and its fusion performance. To control or avoid these instabilities both active control and passive avoidance strategies will be employed. The former will make use of the H&CD capabilities of ITER for active MHD control, in particular of the ECH upper launchers which can deposit up to 20–27 MW of power and current drive in the region of $\rho = 0.4$–0.88 to prevent tearing modes from growing [Poli2018]. The main drawback of such approach is that, if a significant amount of power needs to be deposited in the external part of the plasma to provide tearing mode stabilisation, this may limit the achievable Q to values lower than 10. Passive avoidance strategies rely on shaping of the current profile in the L-mode and early H-mode phases to avoid such instabilities developing when the profile of the current in the plasma relaxes as demonstrated in DIII-D [Turco2024]; an example is shown in figure 50.

To minimise neutron fluence consumption, D–D and D–T plasma scenarios, with the optimum tritium concentration, will be developed. This development will start from the DD plasma scenario identified in FPO-3 (providing $Q \geqslant 10$ in D–T plasmas for 50 s) by extending it to a high-performance duration of, at least, 300 s using active and passive MHD control strategies. The schemes providing a high-performance D–D plasma scenario with a duration of, at least, 300 s will then be explored in D–T. In this exploration the MHD control strategies will be re-tuned to account for D–T effects, alpha particle effects, etc., up to the demonstration of the project goal of 500 MW fusion power with $Q \geqslant 10$ for 300 s. This will enable the study of burning plasma physics and associated control challenges with $Q \geqslant 10$ operating conditions over timescales of, at least, 300 s. The performance of many systems/schemes required to support burning plasmas for long timescales will be studied, such as: (a) the assessment of the effects of fusion neutrons and nuclear heating on diagnostics and superconducting magnets in nominal $Q \geqslant 10$ operating conditions, (b) the demonstration of in-vessel tritium management by the optimisation of wall conditioning and tritium removal schemes in nominal $Q \geqslant 10$ operating conditions and (c) an update of the safety-orientated knowledge acquisition programme including, for the first time, measurements of dust production, tritium retention, activated corrosion products and TBM operation with nominal fusion power of 500 MW, $Q \geqslant 10$ and burn duration of 300 s, as well as the associated maintenance activities.

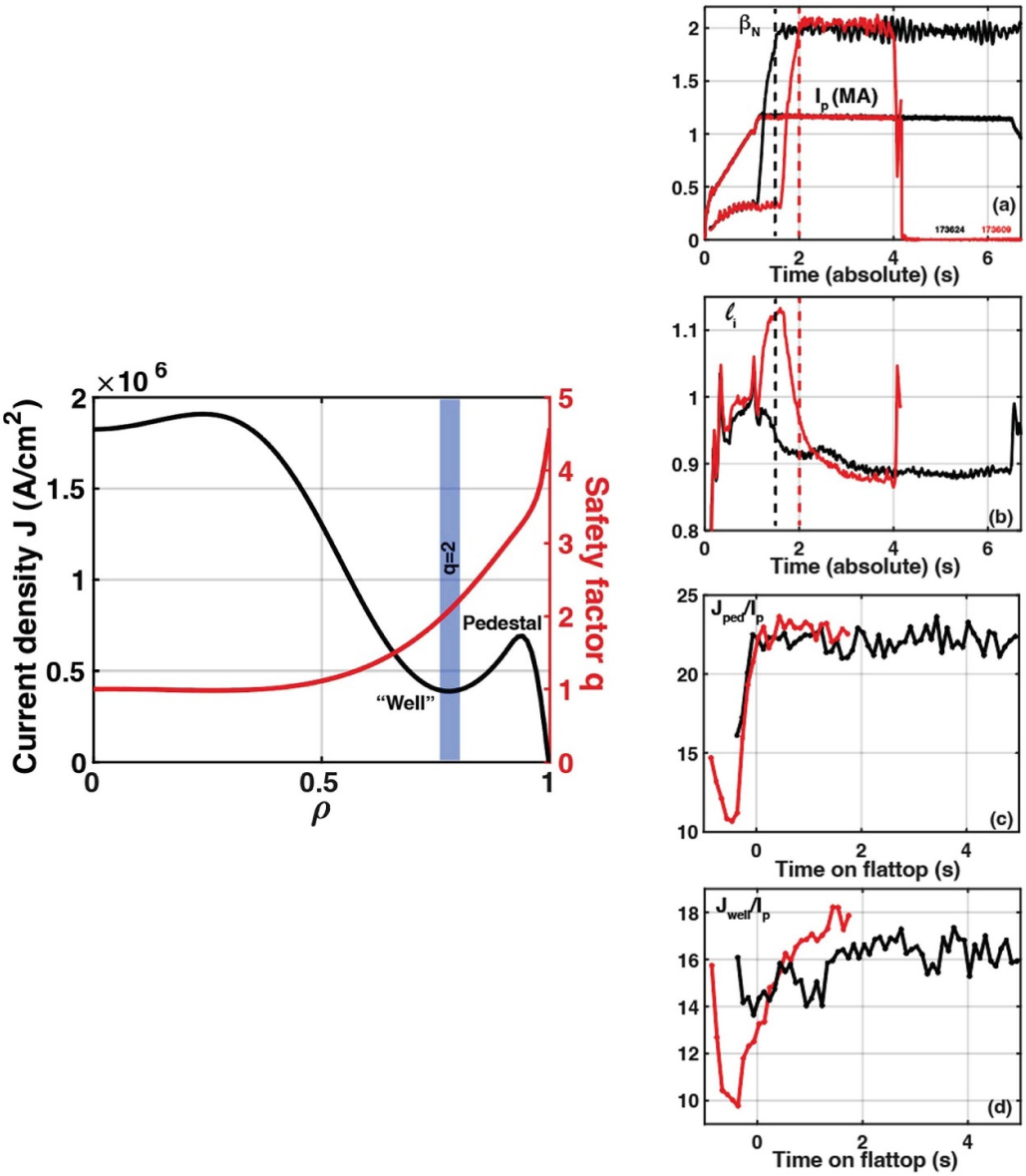

Figure 50. Left) Typical current density (black) and safety factor (red) profiles for an ITER Baseline Shape (IBS) discharge in DIII-D, with the indication of the q = 2 rational surface, the current pedestal and the current 'well'where tearing modes can become unstable. Right) Time histories of β_N and plasma current (a), internal inductance (b), pedestal current (c), and'well' current (d), for two IBS shots comparing a delayed to an early H-mode transition (red and black respectively) showing that an early H-mode transition avoids MHD instabilities being triggered later in the pulse. Reproduced from [Turco2024]. CC BY 4.0.

3.4.5. Fusion power operation–5 (FPO-5). The objective of the FPO-5 campaign is to demonstrate reproducible fusion power production of 500 MW with $Q \geqslant 10$ for burn times of, at least, 300 s. In addition, some dedicated experimental days of high-duty (1 pulse every 30 min) fusion power production of 250 MW for burn times of, at least, 300 s will be demonstrated. The experimental programme in this campaign follows the path started in the FPO-4 campaign and will initially focus on the demonstration of reproducible fusion power production of 500 MW with $Q \geqslant 10$ for burn times of, at least, 300 s. In DT-1, reproducible $Q \geqslant 10$ operation with 500 MW fusion power and burn times of, at least, 300 s is quantitively formulated as the demonstration of pulses meeting these fusion performance requirements with a repetition time of, at most, 60 min (1 pulse every 60 min). Together with this, scenarios to demonstrate high-duty (1 pulse every 30 min) with fusion power production goal of 250 MW for burn times of, at least, 300 s will be identified from those developed in FPO-2 through to FPO-4 (or additionally developed, if needed). Scenarios that can potentially provide this level of fusion power in a reliable way (i.e. not using the full capability of ITER's actuators, especially the H&CD systems) have been preliminarily identified; some examples are shown in figure 51 [Kim2024] but other options are possible if ICH

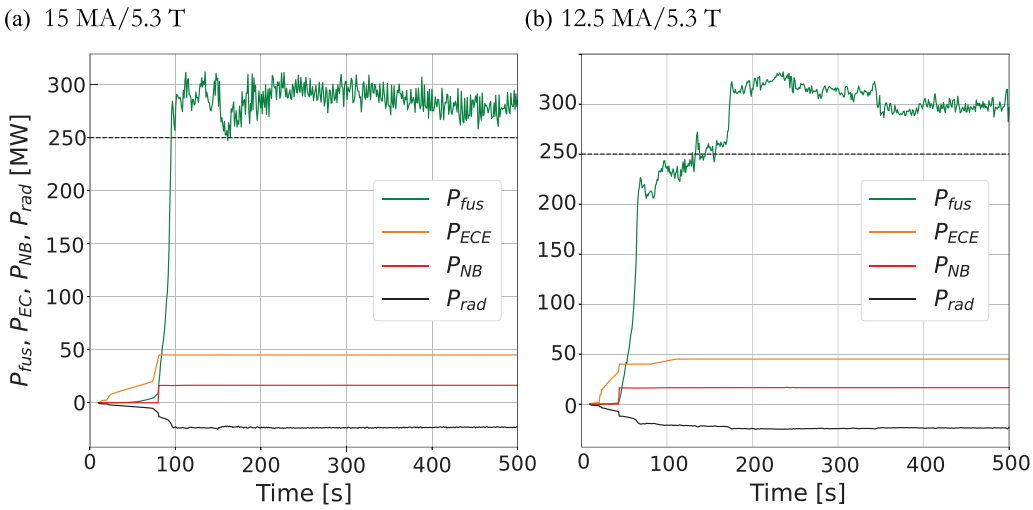

Figure 51. Time-dependent JETTO simulations of DT H-modes with $P_{\text{fusion}} \geqslant 250$ MW providing a burn length longer than 300 s. For both cases $P_{\text{ECH}} = 45$ MW and $P_{\text{NBI}} = 16.5$ MW is applied leaving a reserve power of 15–22 MW in ECH and 16.5 MW in NBI to provide reliable high duty operation. Note that for 15 MA plasmas $<n_e> \sim 0.5\, n_{\text{GW}}$ while for 12.5 MA plasmas $<n_e> \sim 0.7\, n_{\text{GW}}$ [Kim2024] (12.5 MA simulations IMAS SIMDB: ebaf12e5-ff73-11ef-9426- 9440c9e76fd0;; 15 MA simulations IMAS SIMDB: c0ef6a3c-ff73-11ef-9727-9440c9e76fd0).

proves to be efficient in SRO. Pulses of such scenarios will be repeated back-to-back in dedicated experimental days during which high-duty operation will be demonstrated. These days will provide important technical information for the high-duty operation foreseen in DT-2 as well as key results for the TBM research plan [Giancarli2024], particularly the demonstration of tritium breeding.

Once the key goals of this campaign have been demonstrated, depending on the neutron fluence available and the priorities of the ITER Project at the time, any remaining time in the FPO-5 campaign may be dedicated to the extension of the burn of the $Q \geqslant 10$ scenario to, at least, 500 s or to the further exploitation of high-duty operation, for instance. Alternatively, the FPO-5 campaign may be terminated at this stage to proceed to the 2nd deuterium–tritium phase (DT-2).

3.4.6. Physics evaluations supporting the DT-1 research plan and open R&D issues. To define the steps in the development of the ITER operational scenarios in DT-1, as well as the strategy for most effective mitigation/retirement of operational risks, a series of modelling studies have been carried out. In this section we summarise the main outcome of these studies as well as the associated R&D issues.

Disruption loads and mitigation in DT-1

The main objective of the H campaign in FPO-1 is to restart and re-commission the tokamak with all post-SRO components and systems installed. It is executed with H plasmas to minimise in-vessel activation in case human access to the vacuum vessel is required as a result of issues arising during commissioning with plasma. A specific experiment carried out towards the end of the H phase of the FPO-1 campaign is targeted to retire the risks associated to β-decay during disruption mitigation. These have not been addressed in SRO and can materialise during DT operation. If this is the case, significant damage to first wall panels may occur needing their replacement in an activated environment during DT. Modelling studies show that schemes that provide disruption mitigation with moderate RE production by hot tail fail to do so when T and Compton seeds are included, as shown in figure 52 (comparison of orange diamond and black square symbols).

To retire this risk it is thus considered to perform a short campaign (∼1 operational month) in H plasmas up to 15 MA/5.3 T with increasing levels of T, starting from trace-T up to ∼100% T, in which the disruption mitigation schemes developed for SRO are re-tuned to account for both hot electrons and β-decay electrons. If successful, the risk associated with β-decay electrons from T will be largely retired at this stage. It cannot be ruled out, however, that in the execution of the disruption mitigation programme to retire the T β-decay risk in FPO-1, significant REs are produced causing significant damage to the water cooled first wall panels, even if their design is being improved to sustain as high as possible RE impacts. The proposed strategy to minimise the possibility of substantial RE damage occurring consists in starting the T scan from low to high T fraction (up to $\sim$ 100%) in conditions in which large RE production is low, such as with 7.5 MA plasmas. To evaluate this condition, we have considered the results in figure 51 [Vallhagen2024] which show that the typical secondary RE avalanche process [Rosenbluth1997] in ITER can be described by

$$\log_{10}\left(\frac{I_{\text{RE}}}{I_{\text{seed}}}\right) = \alpha_{\text{av}} I_{\text{p}}, \text{ with } \alpha_{\text{av}} \sim 0.7 - 1.4\ \text{MA}^{-1}. \quad (3\text{-}3)$$

Considering that for 7.5 MA the avalanche gain is lower than $10^{5.25}$–$10^{10.5}$, that the expected β-decay T-seeds are typically 10 mA for 15 MA DT plasmas in ITER [Martín-Solis2017], and the fact that the plasma density scales with I_{p},

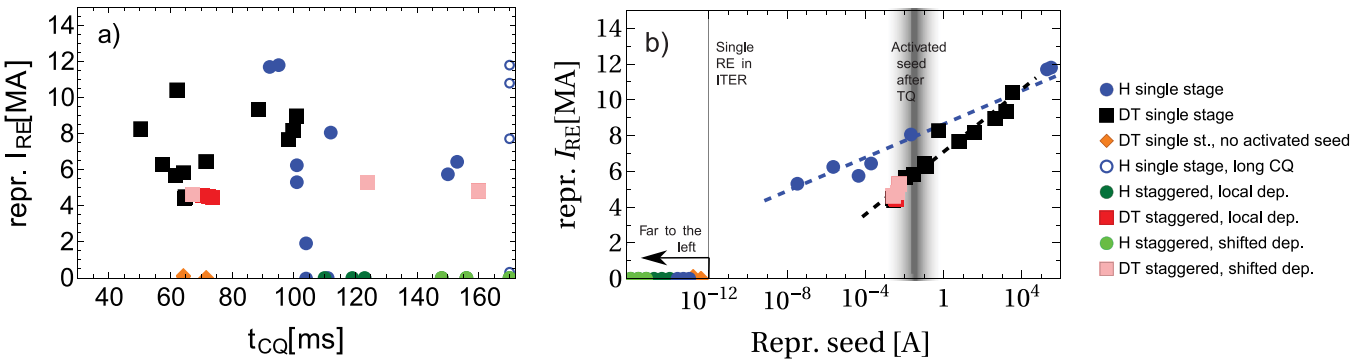

Figure 52. Resulting RE current following the application of the DMS for L-mode H plasmas and DT H-mode plasmas with $Q \geqslant 10$ at 15 MA in single stage or double stage mitigation [Vallhagen2024]. The various symbols correspond to different assumptions related to the disruption mitigation by shattered pellet injection and plasma conditions (H or DT plasma). For the DT plasmas a comparison is made in which the nuclear RE seeds of high energy electrons is removed (labelled DT non-act) to show the effect of these sources on the generated RE current (orange diamond). (a) Resulting RE current versus CQ duration. (b) Resulting RE current versus the representative RE seed. The seed corresponding to a single relativistic electron is marked by a vertical line; all points to the left of that line are far to the left of the scale plotted range; these points are plotted there to illustrate that the final RE current in those cases is negligible. The typical range of activated seed generated after the TQ is indicated by the grey shaded region. Reproduced from [Vallhagen2024]. CC BY 4.0.

the level of runaway current in these plasmas will be limited to ∼2–300 kA for Tritium concentrations up to 100% at 7.5 MA. Such levels of REs should not pose a major issue for W water cooled first wall integrity unless the toroidal asymmetry of RE deposition is extreme [Pitts2025].

In these relatively low-risk 7.5 MA plasma conditions RE mitigation schemes will be developed for a range of %T in the plasma. This process is repeated at higher I_p starting with low %T first. By adjusting the steps in I_p and the % T in the plasma it is possible to ensure that the maximum number of RE that can be generated by avalanche is the same at lower I_p and higher %T that at the next step with higher I_p and lower %T. This is because the product $I_{\text{T-seed}} \times G_{\text{avalanche}}$, i.e. the maximum potential number of RE generated, remains constant across steps ($I_{\text{T-seed}}$ is the production rate of β-decay electrons in T and $G_{\text{avalanche}}$ is the secondary electron amplification factor, which scales as $G_{\text{avalanche}} \sim 10^{\alpha\, v\text{Ip}}$ [Rosenbluth1997]), as illustrated in figure 53. This approach to RE mitigation is foreseen to be used first in the FPO-1 campaign in H plasmas. If successful, it will be adapted to successive campaigns where DD and DT plasmas will be sequentially explored with increasing levels of I_p in L- and H-mode. We note that at the highest I_p levels operation may be limited to L-mode plasmas for DD or D + low% T because the required power for H-mode operation is likely to exceed the installed P_{aux}.

It cannot be ruled out that in the execution of the disruption mitigation programme to retire the T β-decay risk in FPO-1 sizeable REs are produced causing significant damage to the W water-cooled first wall panels. If this damage is considered excessive for the remaining DT-1 programme, the affected first wall panels will need to be removed after this phase of FPO-1. The advantage of the proposed approach with regards to not addressing this risk until later operation in DT-1 is that this replacement will be done with low activation in-vessel since the hydrogen plasmas have very moderate

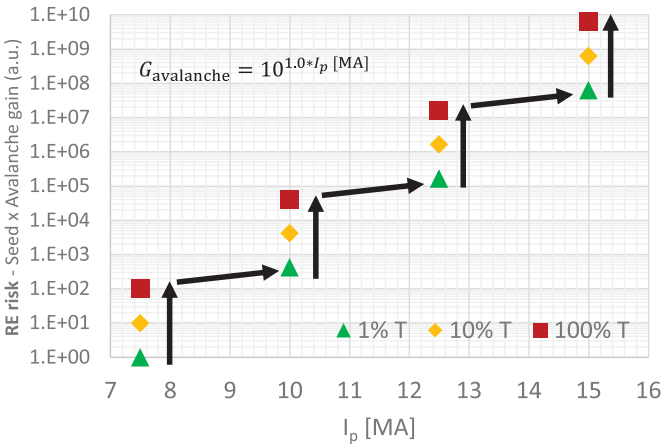

Figure 53. Expected $I_{\text{T-seed}} \times G_{\text{avalanche}}$ versus the I_p and %T steps foreseen in the $H + T$ plasmas in FPO-1 to develop RE mitigation. By adjusting the step in I_p and % T it is possible to ensure that $I_{\text{T-seed}} \times G_{\text{avalanche}}$ is similar at lower I_p and higher %T that at the next step with higher I_p and lower %T. Thus, the RE mitigation effectiveness should remain constant across these steps. It should be noted that within an I_p level, the %T can be varied in as small steps as needed, 1–10–100% are given in the figure for illustration only.

neutron production [Polevoi2023] and the proton-tritium reaction ($p + T \rightarrow n + \text{He}^3$) has an energy threshold above 1 MeV.

We note that the evaluations above have been carried out with plasmas whose position does not change in time as the current decay proceeds and runaways are produced, which does not reflect the real situation in ITER. As the plasma current decreases the ITER plasmas will displace upwards or downwards, as discussed in section 3.2.1. Including this effect in simulations of current quenches with RE in ITER leads to a significant reduction of the generated RE current compared to static plasma simulations [Wang2024] so that the evaluations

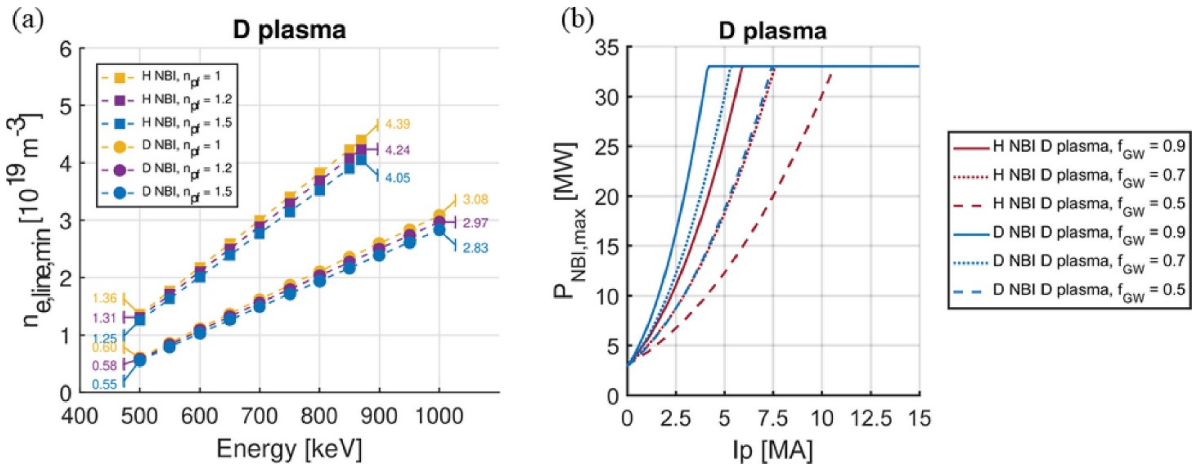

Figure 54. (a) Minimum line-averaged electron density $n_{e,line,min}$ for unrestricted D and H NBI heating in ITER D plasmas, for different values of density peaking factors, as a function of beam injection energy. (b) H and D NBI available power in a D plasma versus plasma current at different Greenwald density fractions f_{GW}. Reproduced from [Vincenzi2024b]. CC BY 4.0.

presented here are conservative. Verifying this theoretical finding experimentally remains an open R&D issue with potentially significant consequences for ITER in terms of RE risk reduction.

NBI shine-through loads and implications for scenario development

Since the ITER NBI system operates with neutrals injected at very high energy (500–870 keV for H and 500–1000 keV for D), its use at low plasma densities is limited by shine-through loads. The operational range for NBI heating in ITER was evaluated originally in [Singh2017] and has been recently re-evaluated taking into account improved modelling for the NBI as well as the latest design of the ITER W first wall and blanket modules that intersect the beams. The results of this study are described in [Vincenzi2024b], here we report on the major conclusions and implications for the research plan.

In first place, as expected, the use of H neutrals in the NBI increases significantly the shine-trough loads for given plasma parameters compared to D neutrals. This is shown in figure 54 [Vincenzi2024b] and restricts the amount of power that can be delivered by the NBI system for some plasma conditions. On the contrary, the isotope of the main plasma (H or D) has a minor influence on the resulting shine through loads. For commissioning of the NBI system in the initial phase of FPO-1, in which H neutrals will be used, the L-mode plasma scenarios considered will take into account these operational restrictions. Later in DT-1 when DD and DT scenarios are developed, the impact of using H neutrals will be more noticeable (especially at low $I_p/<n_e>$) if the NBI system is maintained in H to $Q \geqslant 10$ operation. To ensure robust H-mode operation, the reduced power from the NBI implies that more power will need to be provided by RF systems [Vincenzi2024a]. To quantify these requirements, the RF power needed to supplement that by H-neutrals NBI to access and sustain H-mode operations has been assessed for low density H-modes ($<n_e> \sim 0.5\ n_{GW}$) in which NBI shine-through restrictions are highest. The results are shown in figure 54 demonstrating

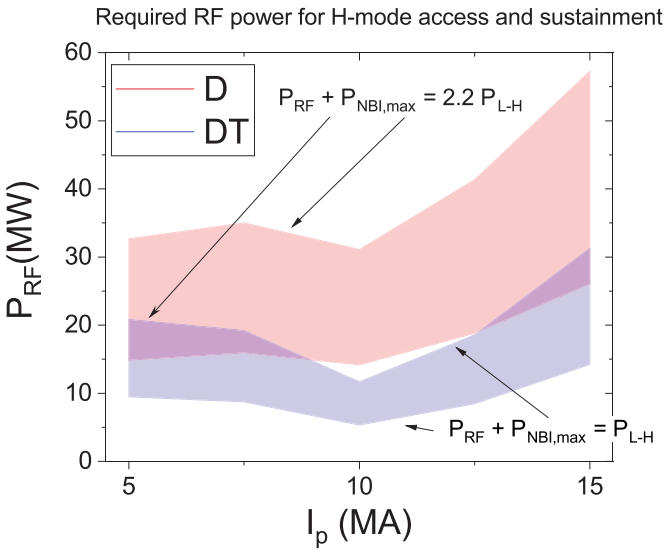

Figure 55. Required RF power to access and sustain ITER H-modes in DD and DT plasmas (excluding alpha heating) versus plasma current for $<n_e> \sim 0.5\ n_{GW}$. For H-modes access $P_{aux} = P_{LH}$ is assumed while for H-mode sustainment $P_{sep} = 1.5\ P_{LH}$ is assumed, with core radiation being 30% of the heating power (this is equivalent to $P_{H,sustainment} = 2.2\ P_{LH}$).

that the installed RF power in DT-1 (70 MW with a possible upgrade to 87 MW) is sufficient to implement the research plan even with the restrictions imposed in NBI power imposed by operation with H neutrals [Vincenzi2024a]. If the NBI were to operate with D neutrals these restrictions would be smaller and the required RF power lower than that in figure 55.

High q_{95} impact on pedestal and plasma performance

Within the usual peeling ballooning limit for pedestal plasma parameters, the pedestal in ITER is expected to be dominantly limited by peeling instabilities when operating at high Q [Snyder2011]. This is the consequence of the expected plasma parameters themselves (e.g. low collisionality and

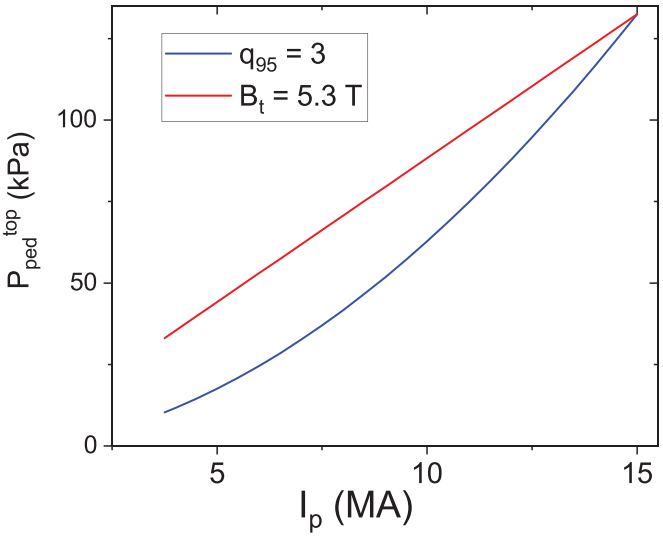

Figure 56. Plasma pedestal pressure versus I_p in ITER H-modes for $B_t = 5.3$ T H-modes versus those for which B_t is gradually increased to maintain $q_{95} = 3$.

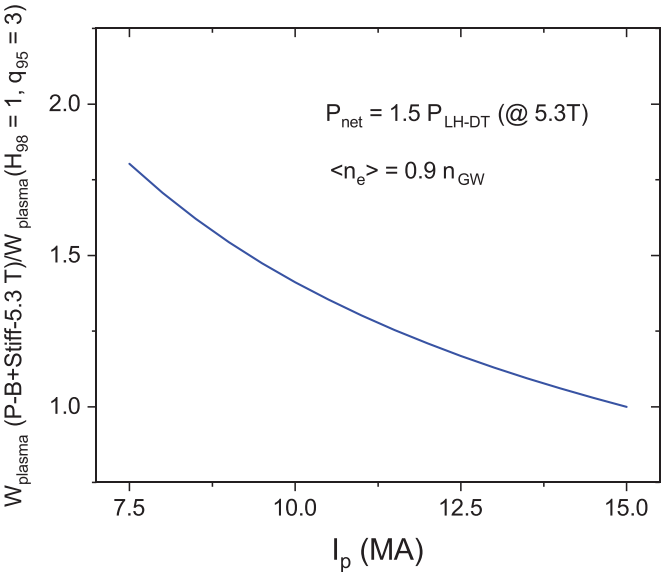

Figure 57. Ratio of the plasma energy evaluated with the $H_{98y,2}$ scaling law with $q_{95} = 3$ and an alternative approach assuming an additional dependence $T \sim B_t^{0.84}$, versus I_p for ITER H-modes with $<n_e> \sim 0.9\, n_{GW}$ and with $P_{net} = P_{tot}$–$P_{rad} = 1.5\, P_{LH\text{-}DT}$(@ 5.3 T).

pedestal width) as well as of the shallow density gradient in the pedestal resulting from the requirements for fusion performance ($<n_e> \geqslant 0.85\, n_{GW}$) and the need to operate in a high divertor radiation regime ($n_{sep} \geqslant 0.5 <n_e>$, [Pitts2019]) [Polevoi2017]. As a result, the stability limit for the pedestal pressure in ITER scales as

$$p_{ped} \sim I_p \times B_t^{0.84}. \quad (3\text{-}4)$$

This has a wide range of consequences with respect to the pedestal plasma parameters achievable as H-mode scenarios are developed in the IRP from low towards high I_p, as well as on the resulting plasma energy/energy confinement time. In particular for scenarios with the same f_{GW} :

$$\beta_{ped} \sim (n_{ped} \times T_{ped})/I_p^2 \sim B_t^{0.84}/I_p \quad (3\text{-}5)$$

$$\nu^*_{ped} \sim (n_{ped} \times q_{95})/T_{ped}^2 \sim 1/B_t^{0.68} \quad (3\text{-}6)$$

$$\rho^*_{ped} \sim T_{ped}^{1/2}/B_t \sim 1/B_t^{0.58}. \quad (3\text{-}7)$$

This implies that the variation of pedestal poloidal β, normalised gyroradius and pedestal collisionality over the range of H-modes to be explored in DD and DT plasmas in DT-1 (except the 5 MA/5.3 T scenario) will be less than a factor of ~2. Since $\beta_{p,ped}$, ν^*_{ped} and ρ^*_{ped} are important parameters for the processes that impact pedestal physics [Beurskens2011], moderate variations are expected in ITER scenarios as current and field are varied. The exception are those variations associated with plasma shape and q_{95} which, obviously, affect pedestal plasma stability. To illustrate the effect on pedestal pressure of ITER DT-1 H-modes being peeling-limited and the resulting dependence of the pedestal pressure on B_t, figure 56 compares the pedestal pressure expected in ITER when I_p is increased while maintaining a constant q_{95} compared to that in which B_t is kept constant. The pedestal plasma pressure at 15 MA/5.3 T is taken as normalisation point. When the field is kept constant $p_{ped} \sim I_p$, while when q_{95} is kept constant $p_{ped} \sim I_p^{1.84}$ resulting in very large differences in pedestal pressure at $I_p \leqslant 7.5$ MA for full B_t plasmas compared to those with $q_{95} = 3$.

This elevated pressure at low I_p for $B_t = 5.3$ T can potentially impact the achievable plasma energy and fusion power at low I_p compared to that derived applying the ITER $H_{98y,2}$ scaling. The magnitude of the impact depends on the degree of stiffness in the core plasma transport in ITER. If a large stiffness would be found in ITER H-modes (i.e. $T_{core} \sim T_{ped}$) this would lead to a much stronger dependence of the plasma energy on B_t than that from the ITER $H_{98y,2}$. To quantify this, as a zeroth-order estimate, we take the $H_{98y,2}$ scaling at $q_{95} = 3$ as reference to evaluate the plasma energy in ITER H-modes and we compare with the resulting plasma energy assuming that in, addition, there is a temperature dependence on B_t as $T \sim B_t^{0.84}$ for $f_{GW} \sim$ constant. The results of this comparison are shown in figure 57, illustrating that 7.5 MA plasmas in ITER have the potential to achieve very high normalised energy confinement times and, thus, plasma energies and fusion powers. While these evaluations are consistent with present experimental results [Ding2024], whether they will materialise in ITER or not remains an open R&D issue. We note that NBI heated plasmas at 7.5 MA in ITER can have a large fraction of the current driven non-inductively (~60%) [Maget2013, Polevoi2023] and, since NBI is the main contributor, the compatibility of stiff core transport and the resulting MHD stability of these high β_p plasmas with the associated current profiles needs to be considered.

Impact of W wall source on the $Q \geqslant 10$ scenario

While the impact of the W wall on H-mode plasmas has been assessed for SRO plasmas, this impact is quantitatively and qualitatively different in Q 10 plasmas. For SRO plasmas the

main impact concerns the radiation of the core plasma and the associated H-mode operational range for additional heating powers up to 50 MW. In $Q \geq 10$ plasmas, in which alpha heating is dominant, the effect of excessive W radiation in the core is amplified since a decrease in plasma temperature caused by this excessive radiation also decreases the alpha heating power. Therefore, the impact of the W wall source on ITER high Q operation has been quantified by JINTRAC simulations including core and SOL plasmas and plasma-wall interactions. At high Q, ELMs must be suppressed in ITER to avoid melting of the W divertor [Gunn2017] and thus do not contribute to the W wall source. ELM suppression in JINTRAC is reproduced by means of the so-called continuous ELM model in which the pedestal transport coefficients are adjusted so as to obtain the values of pressure (density and temperature) expected from ideal MHD modelling. Under these conditions without ELMs, the W wall source is generated by the impact of plasma ion flux (including impurities) and charge exchange neutral (CXN) wall fluxes. Presently, no integrated model exists that can perform full integrated simulations including a proper description of the plasma-wall interactions with the main wall. In JINTRAC the edge simulation grid is restricted to the first field line that intercepts the wall, starting from the divertor area (target + baffle) and, thus, an effective W source at the edge of the grid has been applied in the simulations for ITER.

To define the magnitude of this effective source, the W wall source and its transport into the SOL have been modelled with the 2D version of the WallDYN code [Schmid2015] for a selected set of edge plasma conditions for $Q \geqslant 10$ plasmas and single null magnetic configuration. The WallDYN simulations provide the W wall influx and the penetration of W up to the far-SOL region that can be modelled with JINTRAC. These WallDYN studies have been described in [Schmid2024], below we summarise the main results and high-level conclusions for ITER.

The W source has been evaluated with WallDYN using plasma backgrounds previously utilised for Be wall erosion estimates [Khan2019], with a neon (Ne) concentration of up to 1.8% at the separatrix, corresponding to a high seeding case. The total W gross erosion wall source ranges from 10^{19} to few $\times 10^{21}$ W atoms s^{-1}, depending on SOL flow and far-SOL plasma parameter and radial transport assumptions. The highest wall source corresponds to a SOL with stagnant flows concurrent with Ne fluxes in high ionisation states to the wall. The latter is determined by the far-SOL electron temperature which has been considered to be in the range of 10–20 eV in these simulations. A summary of results obtained in [Schmid2024] is shown in figure 58. Similar evaluations have been previously carried out using ERO 2.0 with the same plasma backgrounds and various erosion/deposition modelling assumptions [Eksaeva2022]. Assuming no impurities to be present in the plasma, the gross erosion rate for the W wall in ITER is found to be more than 10^4 times lower than for Be walls, i.e. in the range of 10^{19} W atoms s^{-1} (we note that Be gross erosion rates are in the range of 1.5–3.5 $\times$ 10^{23} [Romazanov 2022]). Including Ne impurity in the simulations

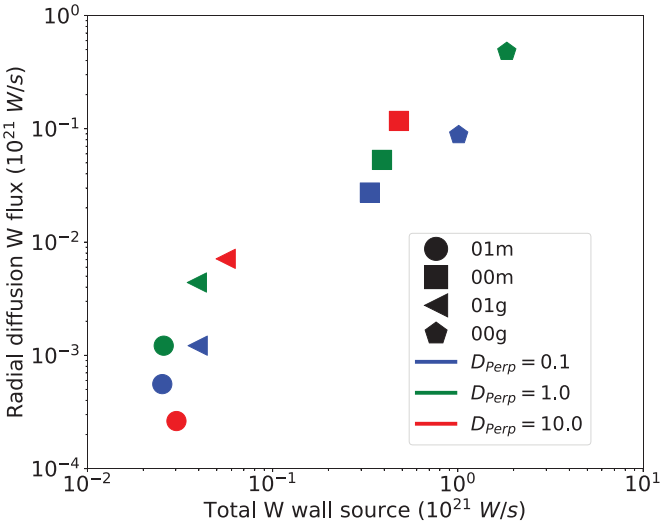

Figure 58. WallDYN modelled radial diffusion driven flux of W across the edge modelling calculation grid boundary for ITER $Q \geqslant 10$ plasmas versus total W wall source, which includes influx due to erosion and reflection from both main chamber wall and divertor for a range of far-SOL W transport diffusion coefficients. Reproduced from [Schmid2024]. CC BY 4.0.

increases the gross source by around an order of magnitude compared to that for pure plasmas, a somewhat lower increase than in [Schmid2024].

In both [Eksaeva2022] and [Schmid2024], the dominant mechanism for the W source is Ne sputtering and the ensuing W self-sputtering, which is dominant for far-SOL electron temperatures of 20 eV, while CXN sputtering is negligible. However, CXN sputtering of W in these studies is modelled by estimating the average energy of the neutrals on the wall. This can lead to a large underestimate of the sputtered W source when there is a significant number of high energy neutrals but the low energy contribution dominates so that the neutral average energy falls under the W sputtering threshold. To account for this effect, dedicated simulations have been carried out to estimate an upper limit for the W wall source using available modelled neutral energy spectra from Eirene for $Q \geqslant 10$ edge plasma parameters [Khan2019, Romazanov2022] and double MC [Babenko2020], as shown in figure 59. We have further assumed that the largest value at the wall poloidal cross section applies to the whole wall to provide an upper W CXN wall source estimate. The results of these evaluations compared to those obtained with an average energy for the neutrals [Schmid2024] are shown in table 3. As expected, considering the high energy tail of the neutrals increases the CXN W source significantly. However, the associated source remains under 10^{20} W atom s^{-1} and, thus, is a non-dominant contributor compared to the Ne + W-self sputtering source of few $\sim 10^{21}$ W atom s^{-1} mentioned above.

To evaluate the effect of the W wall source on high Q operation, JINTRAC simulations have been carried out. As described above, JINTRAC cannot simulate the W wall source

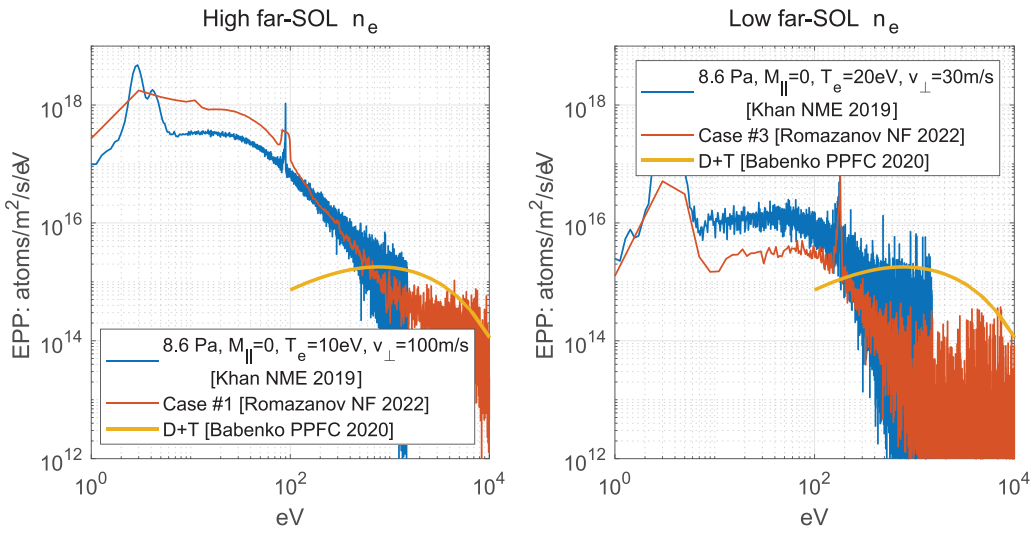

Figure 59. Eirene and DOUBLE-MC calculated CXN neutral energy spectra for ITER $Q \geqslant 10$ plasma conditions [Khan2019, Romazanov2022, Babenko2020]. The lower flux at higher energy in the EIRENE spectra is due to SOL neutral screening, which is absent in the DOUBLE-MC code since the latter does not include the SOL plasma in the evaluation of neutral wall fluxes.

Table 3. WallDYN calculated gross W source from sputtering by CXN for ITER $Q \geqslant 10$ plasma backgrounds compared to the evaluations combining EIRENE and DOUBLE-MC spectra to reflect the role of sputtering by neutrals in the energetic tail of the CXN distribution, as well as the energy and angular dependent W sputtering yield.

Case	$W_{C\text{-}X<E>}(10^{20}\,s^{-1})$	$W_{C\text{-}X}{}^{max}(10^{20}\,s^{-1})$
High far-SOL n_e and low T_e	0.073	0.8
Low far-SOL n_e and high T_e	0.0053	0.14

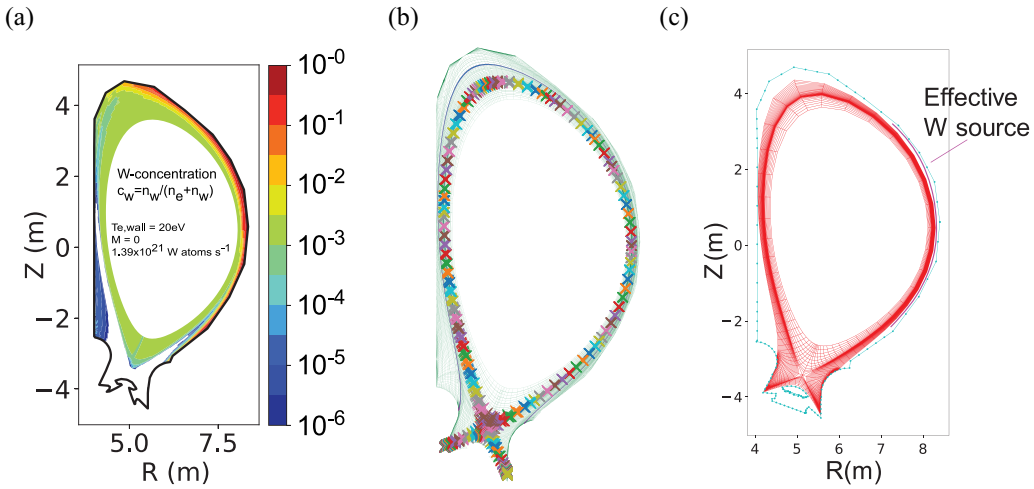

Figure 60. (a) Edge W concentration from WallDYN for a typical ITER $Q \geqslant 10$ case [Schmid2024], (b) WallDYN simulation grid and c) JINTRAC edge simulation grid and effective W source angular extent (the core plasma is also simulated by JINTRAC but it is not shown in this figure).

due to technical limitations of the grids used for the edge/SOL simulation module (EDGE2D-Eirene). An effective W wall source has therefore been implemented in JINTRAC which provides W atoms with typical energies of physically sputtered W at the edge of the computational grid (∼9 cm from the separatrix at the outer mid-plane for the particular magnetic equilibrium used in the WallDYN calculations) within an angle of $\sim +/45°$ around the midplane, as shown in figure 60. The magnitude of this effective source is then varied so as to obtain the values of the W density predicted by WallDYN at the JINTRAC computational grid edge (see figure 60). The impact of such effective source is then modelled, together with the W divertor source, in a self-consistent way. As a conservative approach, it is assumed that prompt-re-deposition does not

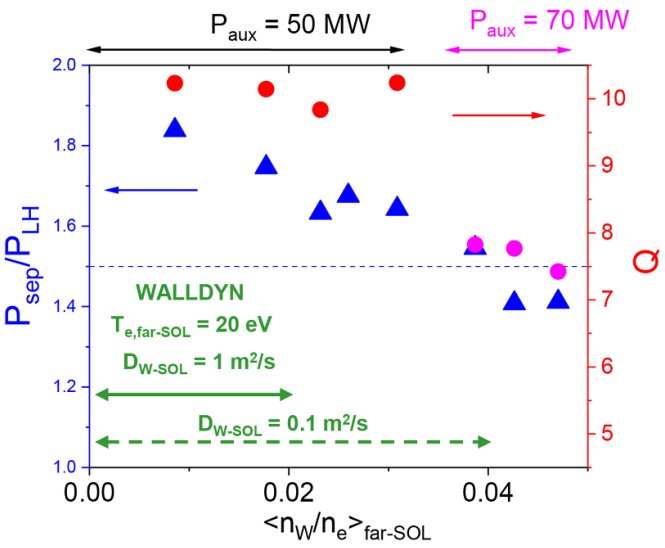

Figure 61. JINTRAC modelled Q and margin of edge power flow above the L–H transition versus average W density in the far-SOL compared to predictions from WallDYN for 15 MA/5.3 T DT plasmas with additional power heating levels of 50 MW ($Q \geqslant 10$) and 70 MW for the highest W density range. 50 MW simulations (IMAS SIMDB: c5bd554f-d82d-11ef-9d5e-9440c9e7706c, ebee9b5c-d85e-11ef-b07c-9440c9e7706c, fd6127f6-d85e-11ef-ab5a-9440c9e7706c, e2f85f48-d8c3-11ef-b93f-9440c9e7706c, 8743dad6-d7f2-11ef-8fd5-9440c9e7706c); 70 MW simulations (IMAS SIMDB: 3c5ee4dc-d830-11ef-9055-507c6f614884, 42cc46e5-d830-11ef-9d40-507c6f614884, 00a58ff2-d8c4-11ef-8f15-507c6f615d1a).

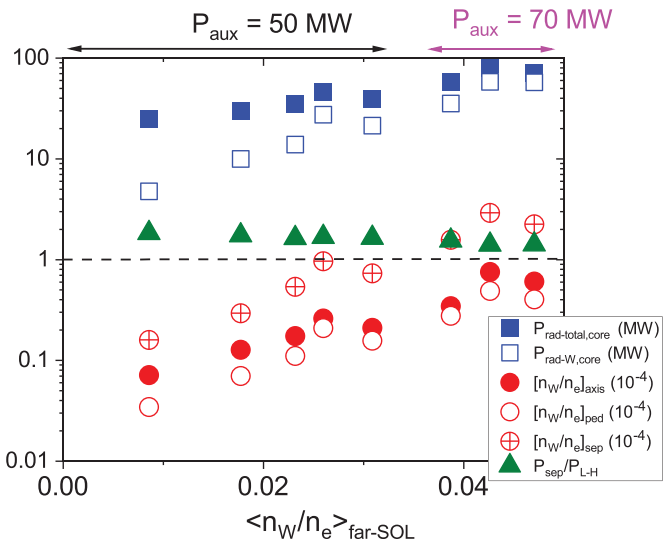

Figure 62. JINTRAC modelled W concentrations at the separatrix, pedestal top and core averaged, W-caused and total radiation and margin of edge power flow above the L–H transition versus W density in the far-SOL for 15 MA/5.3 T DT plasmas with additional power heating levels of 50 MW ($Q \geqslant 10$) and 70 MW for the highest W density range. 50 MW simulations (IMAS SIMDB: c5bd554f-d82d-11ef-9d5e-9440c9e7706c, ebee9b5c-d85e-11ef-b07c-9440c9e7706c, fd6127f6-d85e-11ef-ab5a-9440c9e7706c, e2f85f48-d8c3-11ef-b93f-9440c9e7706c, 8743dad6-d7f2-11ef-8fd5-9440c9e7706c); 70 MW simulations (IMAS SIMDB: 3c5ee4dc-d830- 11ef-9055-507c6f614884, 42cc46e5-d830-11ef-9d40-507c6f614884, 00a58ff2-d8c4-11ef-8f15- 507c6f615d1a).

occur for either the wall-injected W or for the W produced at the divertor.

The resulting consequences for high Q plasma operation in ITER modelled with JINTRAC, with the core plasma being described by the TGLF-SAT2 model and pedestal transport with the continuous ELM model, are summarised in figure 61 showing that $Q \geqslant 10$ operation can be maintained up to the largest W far-SOL densities calculated by WallDYN if W far SOL transport remains significantly turbulent ($D_{\text{W-SOL}} = 1$ m^2 s^{-1}). However, if the typical values for near-SOL transport in H-mode ($D_{\text{W-SOL}} = 0.1$ m^2 s^{-1}) would also apply in the far-SOL the additional heating power would need to be increased to 70 MW. This is required to compensate the increased W radiation to maintain the plasma in high H-mode confinement and, thus, Q would be reduced to ~7.5–8. We note that there is ample experimental evidence showing that for H-mode plasmas turbulence is only reduced in the near-SOL while the far-SOL remains turbulent as in L-mode [Boedo2009] and, thus, this second case is not likely in ITER. More detailed information on the W density concentrations and resulting radiated powers and edge power flows is shown in figure 62. An important outcome of these studies is that the key physics process that enables high Q operation in ITER with a W wall (for the highest W influxes modelled) is the screening of W in the pedestal. This provides a reduction of a factor of ~3–4 for the core W concentration, which drives core plasma radiation and lowers confinement and Q, compared to that at the separatrix, which is determined by the W wall source and SOL W transport.

More details of the core plasma parameters modelled with JINTRAC for these high Q plasmas are given in figure 63. In particular, no core W accumulation is observed in these modelling studies, which is in agreement with other studies [Fajardo2024a, Fajardo2024b]. The increase of W wall influxes and W density deteriorates plasma confinement and reduces Q in ITER but this is driven by a decrease in edge power flow and not by uncontrolled W accumulation. This is due to the dominance of anomalous W transport over neoclassical transport in the core of these ITER high Q plasmas, as shown in figure 63, as also identified in [Fajardo2024a, Fajardo2024b]. As mentioned above, moderate W screening is found in the pedestal with the continuous ELM model (a decrease of the W density by a factor ~4 from the separatrix to the pedestal). In this pedestal transport model, it is assumed that the W diffusion coefficient (D_{W}) and pinch velocity (v_{W}) are given by:

$$D_{\text{W}} = D_{\text{turb}} + D_{\text{W}}^{\text{neo}} \tag{3-8}$$

$$v_{\text{W}} = v_{\text{W}}^{\text{neo}} \tag{3-9}$$

where the D_{turb} and $D_{\text{W}}{}^{\text{neo}}$ are the anomalous and neoclassical W diffusion coefficients, while $v_{\text{W}}{}^{\text{neo}}$ is the neoclassical pinch velocity. D_{turb} is assumed to be the same for all ion species and its value is adapted in the model to provide stationary pedestal

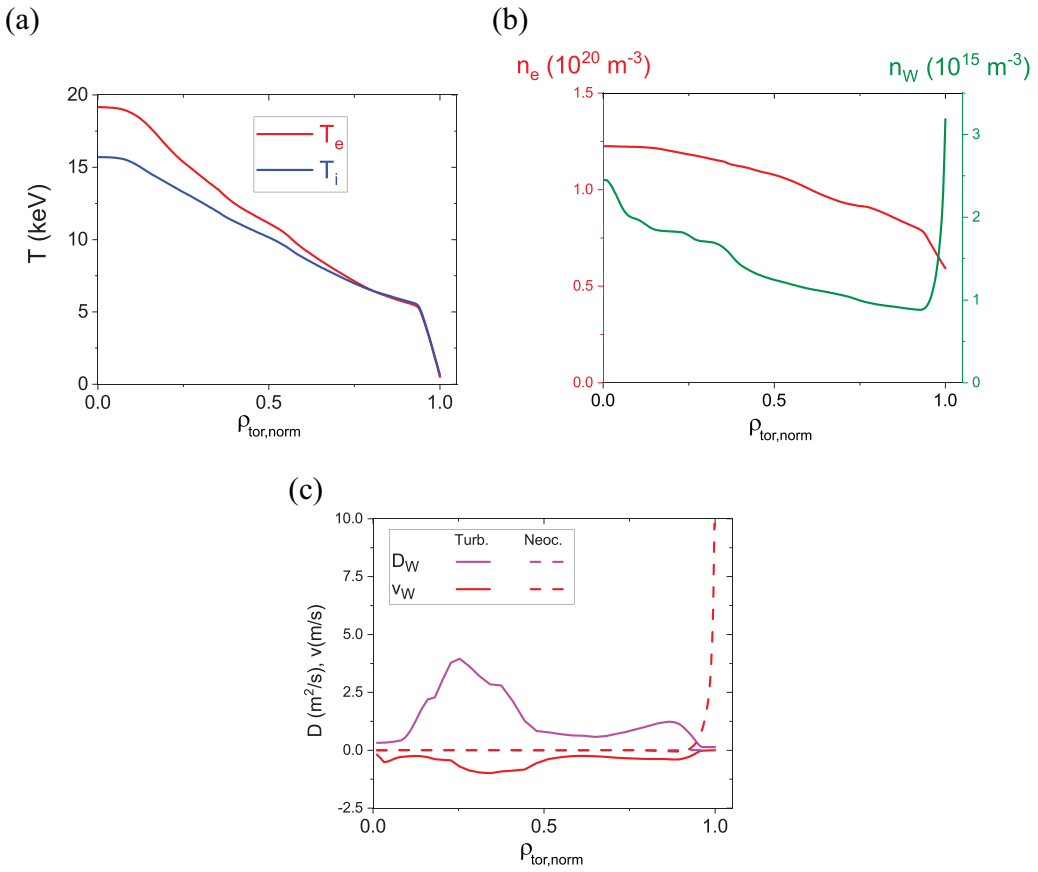

Figure 63. JINTRAC modelled core and pedestal plasma parameters and W transport coefficients versus square root normalised toroidal flux for $Q \geqslant 10$ plasmas modelled with the core transport model TGLF-SAT2 and the continuous ELM model for pedestal transport: (a) electron and ion temperatures, (b) electron and W densities and, (c) W transport coefficients (diffusion and pinch velocity) showing the reduction of anomalous transport in the pedestal and dominance of the outwards neoclassical W pinch and the absence of significant core peaking for the W density due to the dominance of turbulent diffusion(IMAS SIMDB: 8743dad6-d7f2-11ef- 8fd5-9440c9e7706c).

conditions. This attempts to mock-up the transport effects of ELM suppression by RMPs or small/no-ELM regimes in the pedestal.

These assumptions lead to a scale length for the W density profile in the pedestal $\lambda_W \sim D_W/v_W \sim D_{turb}/v_W{}^{neo}$ and to a resulting W screening determined by Δ_{ped}/λ_W where Δ_{ped} is the pedestal width. If we had applied assumptions more suitable for inter-ELM transport in present experiments with low D_{turb}, then $\lambda_W \sim D_W/v_W \sim D_W{}^{neo}/v_W{}^{neo}$ and the resulting W screening in ITER would have been much larger (orders of magnitude) than in these JINTRAC calculations. This much smaller λ_W's for conditions between ELMs in Type I ELMy H-modes are in line with experimental observations [Pütterich2011]. We note that modelling of ITER edge plasmas with the SOLPS-ITER code for $Q \geqslant 10$ plasmas including drifts also shows a decrease of the Ne impurity concentration (from the separatrix to the pedestal top), confirming that ITER neoclassical impurity screening predictions are robust [Kaveeva2020].

Obviously, the simulations presented in this section represent a first attempt to quantify the impact of the additional W influxes in the plasma due to its use as plasma facing material in the NB ITER first wall. While the modelling tools and assumptions have been successfully applied to model present experiments, significant improvements from the modelling point of view are required to refine the ITER predictions. The simulations have to be extended to higher fidelity and to ensure that self-consistent plasma parameters and assumptions are used across all modelling codes applied; this is presently progress. To achieve this, self-consistent plasma backgrounds obtained with the SOLPS-ITER wide grid version and a detailed and consistent description of the CXN fluxes to the wall should be used to model the W wall source for ITER and these W wall source and far-SOL transport results also be used with the same assumptions in the JINTRAC simulations.

These improved simulations will then eventually be self-consistent but this does not guarantee that the ITER predictions will be accurate. To ensure this a focused effort should be carried out in present experiments to validate the physics basis for the models applied to ITER predictions and to compare them quantitatively with experiment. In the area of plasma-wall interactions and SOL plasmas this concerns the models to predict the W wall source and its transport across the SOL to determine the expected W concentration at the ITER plasma separatrix. In the areas of pedestal and core plasma

the emphasis should be put on the characterisation of high Z impurity pedestal and core transport with special focus on ELM-suppressed/no-ELM regimes for the pedestal plasma. Only after this effort has come to fruition can the results discussed in this section be considered solid. It is important to reach this point in the near future in order to define the precise mitigation operational strategies (and feasible upgrades) to be implemented in the NB-IRP to achieve $Q \geqslant 10$ in DT-1. Presently, these are based on experimental guidance described in section 2.1 and the modelling results presented in this section.

Achievement of stationary $Q \geqslant 10$ conditions in ITER

The objective of the DT-1 campaign is to demonstrate $Q \geqslant 10$, $P_{\text{fusion}} = 500$ MW operation over times of, at least, 300 s. As an intermediate target, $Q \geqslant 10$ for timescales sufficient to achieve stationary plasma parameters except the current profile is to be achieved in FPO-3. To determine these timescales as well as the expected evolution of the plasma parameters and of the current profile, core-edge integrated simulations have been carried out with JINTRAC. These include the core and pedestal plasma as well as the edge plasma and the associated plasma-wall interaction. Modelling of these processes is essential to correctly address the timescales for the processes at hand since they are impacted both by core + pedestal timescales as well as edge timescales; a prototypical example is the time evolution of the core helium density considering the available pumping capabilities and operation in a radiative divertor regime required to sustain $Q \geqslant 10$ in ITER.

Simulations to determine the timescale to achieve $Q \geqslant 10$ and stationary plasma parameters, except the current profile, show that all plasma parameters except the helium density in the core plasma are achieved in timescales of ∼30 s after the L–H transition. To achieve stationary helium density profiles in the core plasma requires an additional ∼50 s, as shown in figure 64 [Köchl2020]. This time of 50 s has been taken as the target to reach $Q \geqslant 10$ operation in FPO-3 with all plasma parameters (except current profile) in stationary conditions. To ensure that such ITER estimates are accurate the validation of the capabilities of the ITER applied codes to reproduce the dynamics of the L–H transition and of helium exhaust are required in present experiments. This validation has been performed to a reasonable extent for the former with JET data [Köchl2017] as well as for helium exhaust and transport [Groth2002, Kappatou2019].

Simulations have also been performed for longer timescales to resolve the evolution of the current profile [Köchl2018]. Similar to the DIII-D results discussed in section 3.4.4 and shown in figure 50, the current profile in ITER relaxes from the relatively peaked profile typical of L-mode ($\text{li}_3 \sim 1.0$) to that of an H-mode with much lower current profile peaking due to a substantial pedestal bootstrap current. As shown in figure 65, the timescale of current profile relaxation for $Q \geqslant 10$ plasmas in ITER as measured by the internal inductance li_3 is ∼ 115 s. This implies that, at least, 300s of $Q \geqslant 10$ operation (corresponding to time ∼400 s in figure 65) are required to achieve a stationary current profile in ITER. The current

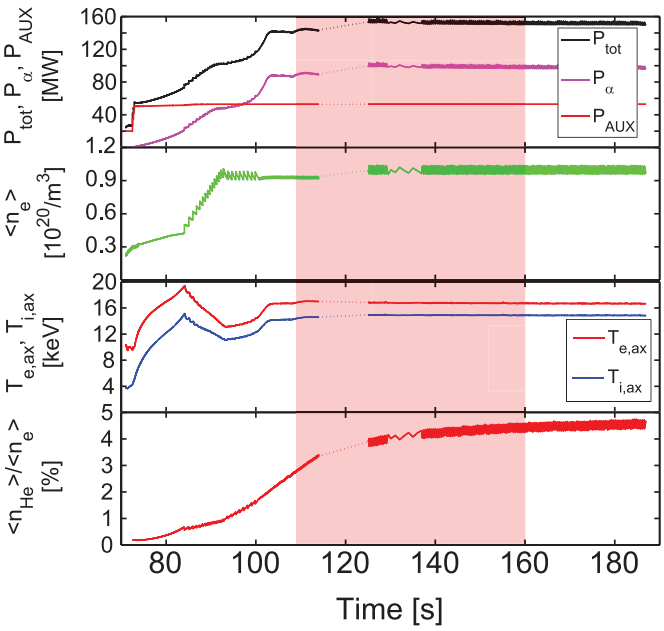

Figure 64. JINTRAC core-edge integrated simulations of $Q \geqslant 10$ access in ITER. From top to bottom time evolution of: (a) total heating power (P_{tot}), Alpha heating power (P_α) and auxiliary heating power (P_{AUX}), (b) line average density ($<n_e>$), (c) Central electron ($T_{e,ax}$) and ion ($T_{i,ax}$) temperatures and, (d) core plasma helium concentration ($<n_{He}>/<n_e>$). The band highlighted in red marks the interval of ∼50 s from the achievement of $Q \geqslant 10$ to that of stationary helium concentration [Köchl2018, Köchl2020] (IMAS SIMBD: be1013d6-ffa6-11ef-9f65- 9440c9e76fd0).

profile relaxation process is shown in detail in figure 66(a) with the q profile in the outer half of the plasma increasing as the plasma current profile relaxes, except in the pedestal where the dynamics are determined by the bootstrap current. This leads to the formation of a current well similar to DIII-D at the beginning of the H-mode phase (see figure 66(b)) that relaxes as the current profile relaxes and can potentially lead to the triggering of tearing modes in ITER.

While the current profile evolution predicted for ITER is in reasonable qualitative agreement with experimental observations, a quantitative evaluation of its accuracy remains outstanding. This is essential to predict whether or not tearing modes will be triggered on long time scales in ITER $Q \geqslant 10$ plasmas. To progress in this direction a quantitative validation of the models used to predict current profile evolution in ITER against present experiments, such as those of DIII-D in section 3.4.4, is required. Then the validated models should be applied to ITER and tearing mode stability be analyzed along the lines of the studies in [Turco2024].

Impact of hydrogen NBI on the $Q \geqslant 10$ scenario

In the hydrogen campaign in FPO-1 the NBI injectors will be commissioned with plasma injecting H neutrals. NBI operation with H neutrals is considered to have a lower risk for ITER because negative ion current density levels compared to those required in ITER have already been demonstrated in present facilities with hydrogen beams [Fantz2020] and because the

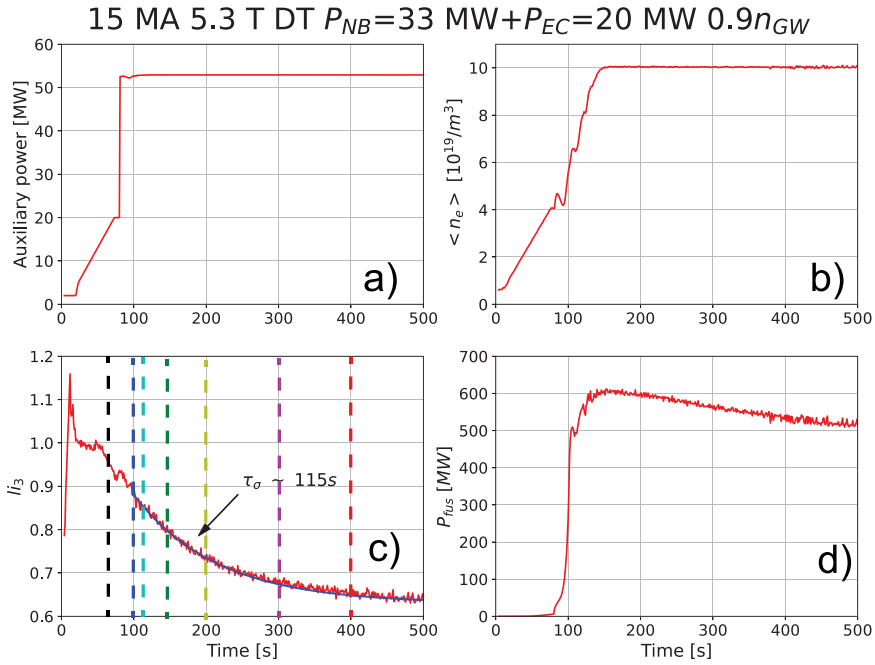

Figure 65. Time evolution of plasma parameters in JINTRAC core-edge integrated simulations of $Q \geqslant 10$ plasmas in ITER: (a) auxiliary power, (b) electron average density, (c) plasma internal inductance (li_3) (vertical dashed lines correspond to those for which the q profile is shown in figure 64) and, (d) Fusion power [Köchl2018, Köchl2020] (IMAS SIMDB: 8c9575de-ff9e-11ef-a181-9440c9e76fd0, 9e4eaca5-ff9f-11ef-a979-9440c9e76fd0, 3d87dedc-ffa0-11ef-8eee-9440c9e76fd0).

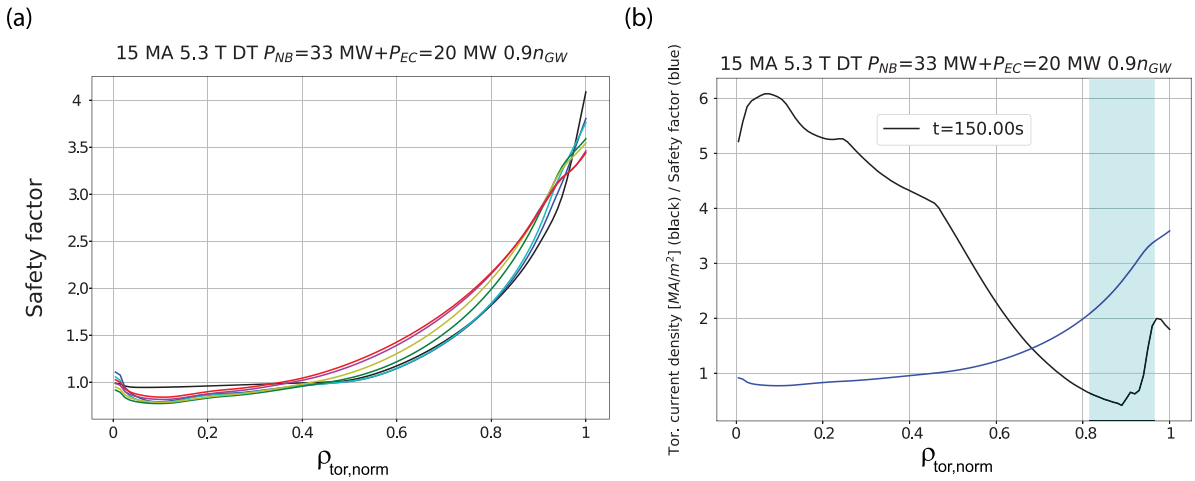

Figure 66. (a) Profiles of the safety factor for the time slices marked in figure 65 versus square root toroidal flux showing the changes to the q profile as the current profile relaxes in $Q \geqslant 10$ plasmas. (b) Current (j_{plasma}) and q profiles versus square root toroidal flux at the start of the $Q \geqslant 10$ phase with stationary plasma parameters (except current profile). This corresponds to $t = 150$ s in figure 65 [Köchl2018] (IMAS SIMDB: 8c9575de-ff9e-11ef-a181-9440c9e76fd0, 9e4eaca5-ff9f-11ef-a979-9440c9e76fd0, 3d87dedc-ffa0-11ef-8eee-9440c9e76fd0).

required acceleration voltage to provide 33 MW is 870 keV in H versus 1 MeV in D. Depending on results obtained in FPO-1, H NBI operation could be extended to the end of the DT-1 campaigns as a risk mitigation for NBIs, if problems in D beam development are encountered in the Neutral Beam Test Facility.

Therefore, the impact on fusion performance for $Q \geqslant 10$ plasmas of plasmas heated by H compared to D beams has been evaluated with fully integrated JINTRAC simulations. The main outcome of these studies is that the impact of H versus D NBI heating in high Q scenarios is very low, in the few percent range, as shown in figure 67. The fusion power for H NBIs is found to decrease by 10 MW because of the lack of fast-NBI-D + T reaction and an additional reduction of a similar size due to core plasma dilution by ∼1% H concentration. We note that the alpha particle source for 500 MW $Q \geqslant 10$ operation is ∼1.8 10^{20} s^{-1} while the H neutral source provided by 33 MW of 870 keV H neutrals is ∼2.4 10^{20} s^{-1}. Therefore, comparable (somewhat higher) H and He densities would be expected on this basis. However, H exhaust is

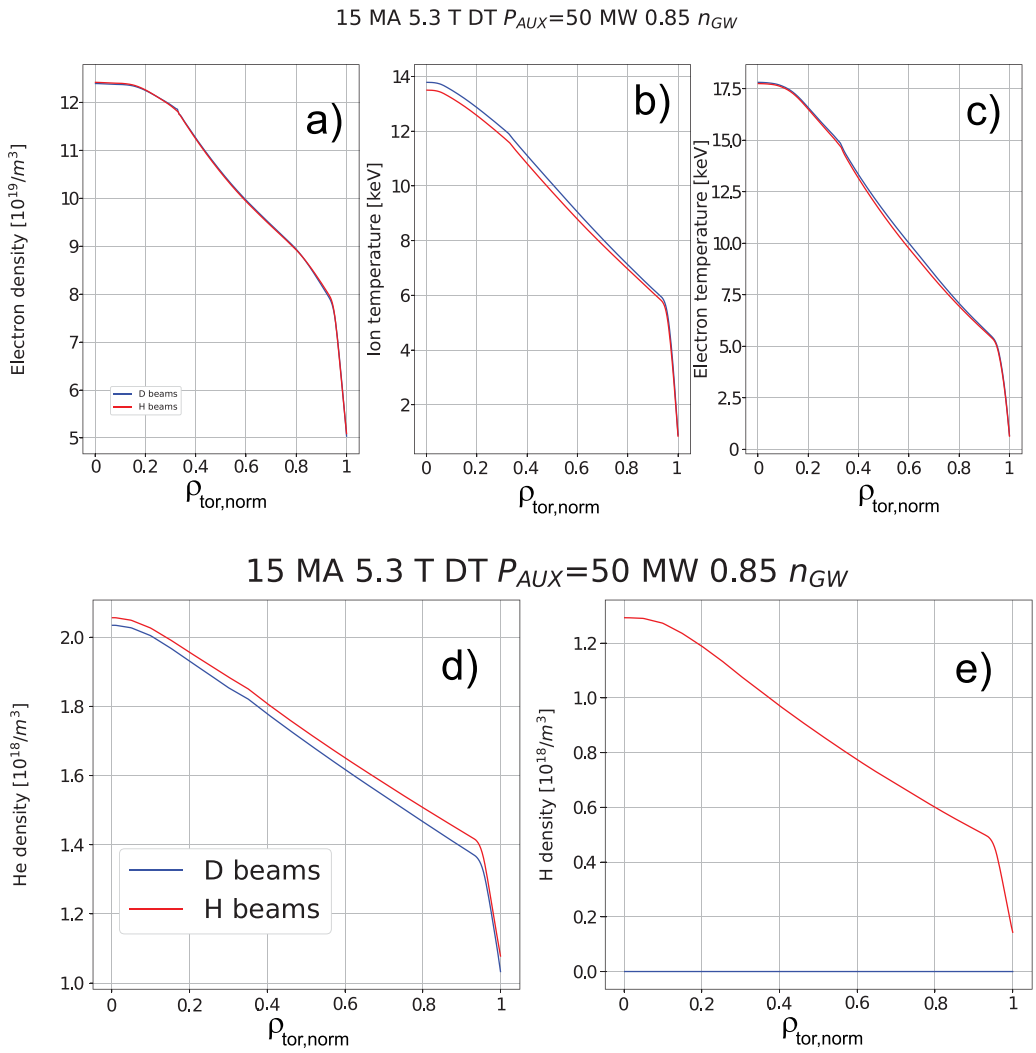

Figure 67. Profiles of plasma parameters for two 15 MA/5.3 T Q $\geqslant$ 10 ITER plasmas one heated by H (in red) and the other by D NBIs (in blue) versus square root toroidal flux: (a) plasma density, (b) ion temperature, (c) electron temperature, (d) He density and (e) H density. D-NBI simulation (IMAS SIMDB: fe3d54c1-ff7b-11ef-9730-9440c9e76fd0); H-NBI simulation (f0b7aa16-ff7b-11ef-aea2-9440c9e76fd0).

much more efficient than for He, since there is a considerable de-enrichment for He at the ITER divertor [Kukushkin2001, Loarte2001]. This results in a factor of ∼2 lower H than He density in the main plasma and to a very reduced impact of H NBIs on fusion performance in ITER high Q plasmas compared to D NBIs.

Therefore, we can conclude that the main impact of executing the DT-1 research plan with H NBIs concerns the restrictions associated with the higher shine-through loads discussed above in this section and not a large reduction of the fusion power. As discussed above the restrictions associated with higher shine-through loads can be reasonably overcome in DT-1 by the more intensive use of RF heating schemes, within their installed heating power, for low I_p/low $<n_e>$ scenarios in which the H neutral NBI shine-through loads are highest.

3.4.7. Summary and conclusions from DT-1. Tokamak operation and research carried out in DT-1 concludes the demonstration of the capabilities of ITER to operate at $Q \geqslant 10$ with $P_{fusion} = 500$ MW in a reproducible way both from the scientific as well as the technical point of view. Understanding of the behaviour of alpha heating dominated plasmas, their control and actuator needs (leading to disruption free operation) as well as their integration with wall/divertor requirements and effective load mitigation (e.g. disruptions) will be demonstrated to $P_{fusion} \leqslant 500$ MW. The data collected in this phase (e.g. activation, tritium retention, dust production, etc.) will provide the basis for the DT-2 safety case to exploit ITER's capabilities in full, namely $P_{fusion} \leqslant 700$ MW and a total neutron fluence of 3 10^{27}.

Key outcomes of the activities in DT-1 include :

- Demonstration of reproducible operation with fusion power of 500 MW with $Q \geqslant 10$ for, at least, 300 s, demonstrating the main Project's fusion power goal for DT-1;
- Demonstration of high duty operation with fusion power of 250 MW for, at least, 300 s;
- Complete assessment of the effects of fusion neutrons and nuclear heating on diagnostics and superconducting magnets

in nominal $Q \geqslant 10$ operating conditions ($P_{\text{fusion}} = 500$ MW, burn duration of, at least, 300 s);
- Extended characterisation of burning plasmas physics and associated control challenges in nominal $Q \geqslant 10$ operating conditions over timescales of, at least, 300 s;
- Demonstration of in-vessel tritium management, dust production rates, etc., in nominal $Q \geqslant 10$ operating conditions to confirm the licencing requirement details in the second deuterium- tritium phase that will follow DT-1;
- Final report of the safety-orientated knowledge acquisition programme in the DT-1 phase including results from operation with nominal fusion power of 500 MW, $Q \geqslant 10$ and burn duration of, at least, 300 s and from high-duty operation with fusion power of 250 MW for, at least, 300 s, as well as of the associated maintenance activities;
- First operation of the TBMs systems (TBSs) in reproducible nominal $Q \geqslant 10$ operating conditions and in high- duty operation with fusion power of 250 MW for, at least, 300 s. This will demonstrate the achievement of coolant thermo-hydraulics conditions relevant for high-efficiency electricity production and of tritium breeding to confirm the tritium breeding ratio (TBR) in demonstration fusion power reactors.

3.5. Second deuterium–tritium phase (DT-2)

The objective of this phase is twofold:

(a) To demonstrate all the Project's fusion power production goals. These goals are the demonstration of 500 MW of fusion power with $Q \geqslant 10$ for lengths of 300–500 s, in high duty operation, and of long pulse and non-inductive steady-state scenarios with $Q \geqslant 5$ and burn lengths of 1000 s and 3000 s, respectively. They are presently foreseen to be achievable with the DT-1 H&CD mix at 12.5 MA for the 1000's goal [Kim2016] but will require the upgrade of the 3rd NBI for the demonstration of steady-state operation at 10 MA [Polevoi2020, Kim2021], and;

(b) To support the ITER Members' demonstration fusion reactor programmes including both scenario development issues (e.g. heat flux exhaust), design basis/operational issues (e.g. optimum H&CD mix, minimum sensor and actuator set for fusion reactors, etc.) and their TBM programmes, in principle, up to neutron fluences of, at least, 0.3 MW yr m^{-2} (3 10^{27} neutrons), assuming this is confirmed by the licence for DT-2. We note that variants of the ITER long-pulse and steady-state scenarios to address the Project's fusion power production goals above are presently considered as prime candidate operational scenarios for several demonstration fusion reactors and, thus, the research in this area is not only to fulfil the Project's goals but also to support the ITER Members' demonstration fusion reactor programmes.

The detailed research programme for this phase will be defined during DT-1, once high fusion power/high Q DT plasmas have been produced in ITER and the licencing requirements for DT-2 have been defined in detail. The development of long pulse and non-inductive steady-state scenarios with $Q \geqslant 5$ with burn lengths of 1000 s and 3000 s, respectively, is expected to follow the path identified in the 2016 baseline IRP [ITR-2024-005]. The final experimental strategy to be implemented in DT-2 will be strongly influenced by the results obtained in FPO-2 and FPO-3 during which the candidate plasmas for these high Q scenarios will be explored (in short burn 50 s).

The DT-2 phase is foreseen to last up to 10 yrs, i.e. it includes 5 experimental campaigns. It is presently considered to share the experimental time, starting from the first experimental DT-2 campaign, between the development of the two scenarios to demonstrate the Project's fusion power goals with that dedicated to operation/scenario development to address the needs of the ITER Members' demonstration fusion reactor programmes.

As an example of research that could be done to address these needs figure 68 shows the expected level of core radiation compatible with H-mode operation (assuming $P_{\text{sep}} \geqslant 4/3\ P_{\text{L–H}}$) and the resulting Q from zeroth-order scalings of low core radiation integrated simulations. This shows that by applying the installed power in ITER it will be possible to demonstrate DEMO-like power exhaust with $P_{\text{fusion}} \geqslant 500$ MW albeit with $Q < 10$. To evaluate more precisely the achievable Q at high radiation/high P_{aux} in ITER requires integrated modelling that takes into account in a more precise way the effect of impurities into plasma performance.

Similarly, the flexibility of the installed H&CD systems in ITER will allow testing of the impact of various H&CD mixes on operation at high Q. This can be used, for instance, to define the minimum or optimum set of H&CD schemes required in a DEMO reactor. As an example of the fusion-reactor-targeted research that could be done in ITER during DT-2 to address this issue, figure 69 shows the waveforms of H&CD power and plasma density to access $Q \sim 10$ conditions for a range of H&CD mixes. Noe that the temporal evolution of the plasma density in this figure corresponds to the fastest density rise that ensures access to $Q \sim 10$. If the density is increased faster after the step-up of the additional heating power the plasma returns to L-mode or to a low confinement H-mode in ITER [Köchl2017]. This is due to the total power produced in the plasma (including alpha heating) being insufficient to maintain the plasma in a high confinement H-mode at high density if this is increased too fast; namely, T_i falls under 10 keV and P_α decreases strongly. The results show that the use of H&CD schemes that provide some level of direct ion heating (NBI and ICH) provides a faster access to burning plasma conditions and a higher Q for ITER, as already identified in [Wagner2010]. We note that the latter effect is not relevant at fusion reactor Q's ($\sim$30) due to the strong dominance of alpha heating. When only ECH is applied the

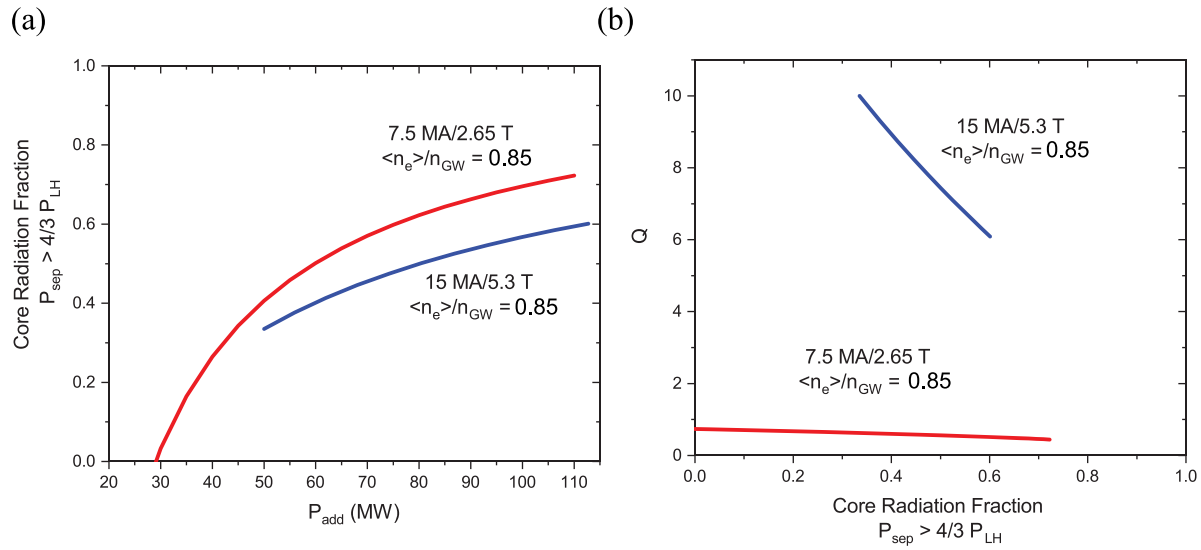

Figure 68. (a) Level of core radiation fraction versus additional heating power, $P_{\rm add}$, for $<n_{\rm e}>/n_{\rm GW} = 0.85$ in DT plasmas with 15 MA/5.3 T and 7.5 MA/2.65 T (extrapolated from integrated plasma simulations for 50 MW additional heating and a simple 0-D model with $H_{98y2} = 1$ plus constant impurity and helium fractions independent of radiation fraction level). (b) Fusion gain, Q, for the two cases as a function of the core radiation fraction.

density rise is much slower than for other H&CD schemes as a result of the lack of direct ion heating by this additional heating scheme. Despite this, $Q \sim 10$ conditions can be achieved solely with ECH heating once alpha heating starts to dominate.

Operation and testing of different TBSs could be envisaged in this phase, including more advanced TBS designs (depending on the evolutions of the demonstration fusion reactor studies). Similarly, specific system upgrades may be implemented before DT-2, such as: (a) installation of a third NBI (HNB-3) for the demonstration of full non-inductive, steady-state operation with $Q \geqslant 5$, (b) the expansion of the tritium plant capabilities to support long pulse/steady-state scenarios, high duty operation and, (c) the expansion of the Hot Cell capabilities to manage the increasing amount of radwaste. Prior to the start of DT-2 a specific integrated commissioning campaign, whose details will be defined during DT-1, will be carried out to recommission the available systems by the end of DT-1 and those that may be installed/upgraded before the start of DT-2 tokamak operation.

4. Summary and conclusions

The NB proposed by the ITER Organisation to ensure a robust achievement of the Projects' goals is described in this paper as well as its associated research plan. The NB includes modifications to ITER 2016 baseline systems and components and to their installation sequence (taking advantage of opportunities provided by delays in core tokamak components' assembly due to manufacturing issues) in order to ensure a more robust and reliable path to the achievement of the Project's goals. This paper has described the evaluations and assessments performed to define the optimised ITER machine and ancillary systems configuration to achieve these goals taking into account the expected learning curve in tokamak operation as well as the difficulties encountered in nuclear licencing with the 2016 ITER baseline. These assessments are based on a wide base of experimental results obtained in the ITER Members fusion devices together with extensive modelling studies with state-of-the-art codes from their fusion research institutes.

Together with the new arrangement of ITER systems and components, a new research plan has been developed to define the main experimental approaches that will be followed to achieve the Project's goals. The NB research plan takes into account progress in understanding since the 2016 ITER baseline was developed. It is structured to address and retire ITER operational risks as soon as feasible and to minimise their impact on experimental availability should the risks materialise. To achieve these two objectives specific components are installed (inertially cooled W wall in SRO, higher additional heating power) and operational strategies have been revised (e.g. DD operation for H-mode robust access in SRO, assessment of T β-decay risk in H plasmas in FPO-1, etc.).

While the strategy of the new ITER baseline and research plan are well founded on experimental results and sound modelling predictions, the details of the research plan remain to be developed. These details are subject to uncertainties since, in some cases, the experimental results in today's fusion devices cannot be empirically extrapolated to ITER and because the models used to predict plasma behaviour have not been validated to the level required for ITER predictions to be considered quantitatively accurate. This requires targeted R&D to be undertaken whose specific focus has been described in the relevant sections of this paper.

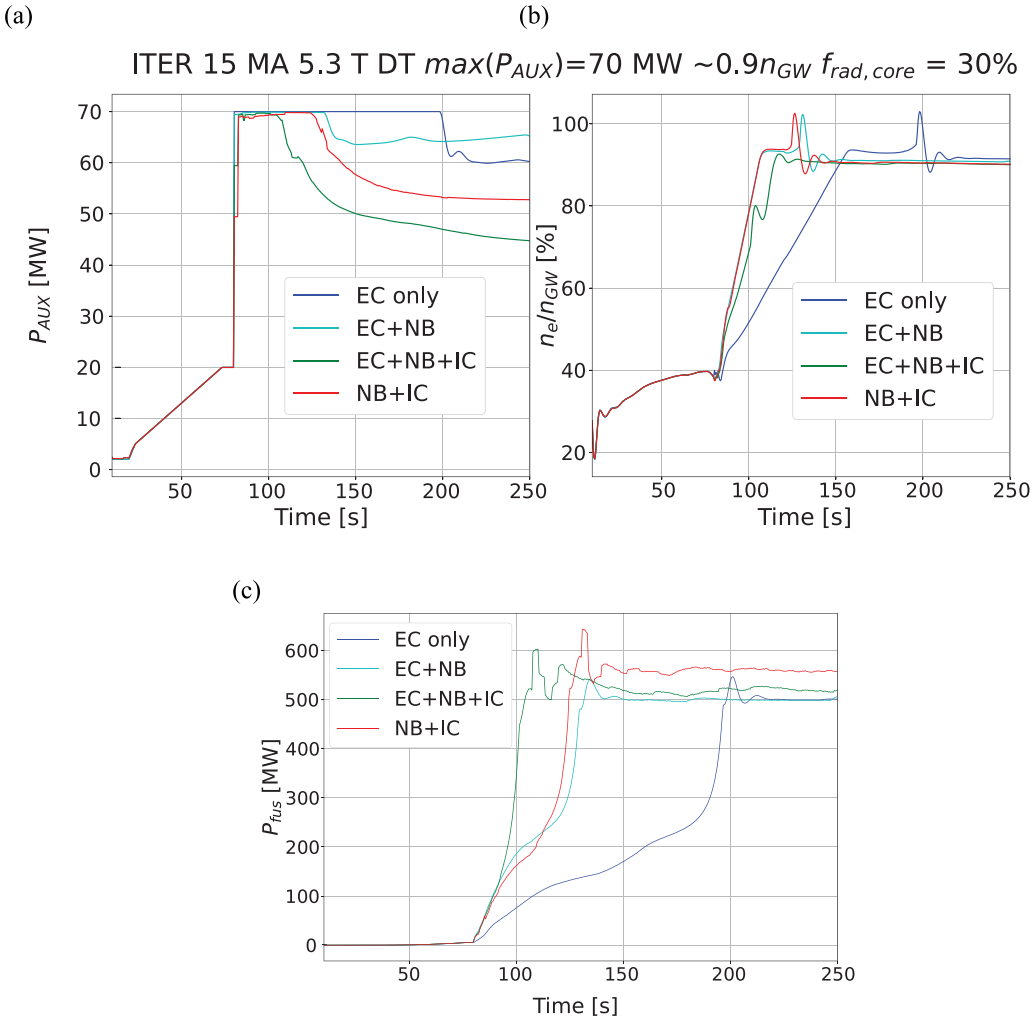

Figure 69. (a) Additional heating power waveform to achieve Q $\sim$ 10 in ITER assuming a core radiated power level $\sim$ 30% of the total heating power (alpha + additional heating) for a range of H&CD mixes in ITER. (b) Density waveform including the fastest rise to stationary burning conditions with robust access to Q $\sim$ 10. (c) Resulting fusion power in these scenarios. EC only simulation (IMAS SIMDB: 8d6ba811-ff79-11ef-b662-9440c9e76fd0); EC + NB simulation (IMAS SIMDB: 6877fed1-ff79-11ef-903a-9440c9e76fd0), EC + NB + IC (IMAS SIMDB: fee45250-ff79-11ef-b418-9440c9e76fd0), NB + IC (IMAS SIMDB: 71143c1f-ff7a-11ef-9c01-9440c9e76fd0).

The assessments presented and the NB research plan described at high level in this paper will continue to be elaborated in close collaborations between the ITER Organisation and the ITER Member's fusion research institutes in both the experimental and theory/modelling areas. This collaboration will continue to be essential for the successful implementation and execution of the NB IRP once machine assembly is completed.

Data availability statement

All data that support the findings of this study are included within the article (including the IMAS references for the computational results).

Acknowledgment

The authors wish to thank a large number of colleagues (too many to be cited individually) in the fusion communities of the ITER Members for constructive discussions and criticisms in the elaboration of the new ITER baseline and of its Research Plan.

Disclaimer

ITER is the Nuclear Facility INB No. 174. This paper describes evaluations and plans for the scientific exploitation of ITER; nevertheless, the nuclear operator is not constrained by the results of this paper. The views and opinions expressed herein do not necessarily reflect those of the ITER organisation.

Data access

Original data contained in the figures produced by ITER organisation co-authors can be made available on request. The data that appears in the figures has been written to the IMAS

scenario SIMSDB database. Each simulation is assigned a unique reference.

ORCID iDs

A Loarte https://orcid.org/0000-0001-9592-1117
R A Pitts https://orcid.org/0000-0001-9455-2698
T Wauters https://orcid.org/0000-0002-2941-7817
P de Vries https://orcid.org/0000-0001-7304-5486
M Lehnen https://orcid.org/0000-0001-6043-8803
X Bai https://orcid.org/0000-0002-0911-9935
I S Carvalho https://orcid.org/0000-0002-2458-8377
M Schneider https://orcid.org/0000-0003-4881-6861
S D Pinches https://orcid.org/0000-0003-0132-945X
F Poli https://orcid.org/0000-0003-3959-4371
G Suarez Lopez https://orcid.org/0000-0001-9009-0027
L Chen https://orcid.org/0000-0003-4233-5936
P Veltri https://orcid.org/0000-0002-0625-1201
R Michling https://orcid.org/0009-0008-2666-1516
A Fossen https://orcid.org/0009-0007-1139-7284
A Becoulet https://orcid.org/0000-0002-6918-9249
G Zhuang https://orcid.org/0000-0002-6048-8568
G Xu https://orcid.org/0000-0001-8495-8678
J Huang https://orcid.org/0000-0001-5662-809X
M Jia https://orcid.org/0000-0002-1672-9782
R Ding https://orcid.org/0000-0003-2880-9736
Y Sun https://orcid.org/0000-0002-9934-1328
Q Yang https://orcid.org/0000-0002-6354-1408
M Xu https://orcid.org/0009-0001-3059-7026
S Brezinsek https://orcid.org/0000-0002-7213-3326
J Stober https://orcid.org/0000-0002-5150-9224
J Hobirk https://orcid.org/0000-0001-6605-0068
F Rimini https://orcid.org/0009-0001-2917-0455
J Garcia https://orcid.org/0000-0003-0900-5564
J Ghosh https://orcid.org/0000-0002-4369-1900
B Magesh https://orcid.org/0009-0003-6953-5580
H Urano https://orcid.org/0000-0001-8740-8954
K Ogawa https://orcid.org/0000-0003-4555-1837
G Motojima https://orcid.org/0000-0001-5522-3082
C K Sung https://orcid.org/0000-0002-8122-0018
Y M Jeon https://orcid.org/0000-0002-7374-3759
S Lebedev https://orcid.org/0000-0001-5979-5344
N Bakharev https://orcid.org/0000-0002-8147-4739
X Chen https://orcid.org/0000-0002-8718-6877
L Casali https://orcid.org/0000-0003-2924-3674
R Maingi https://orcid.org/0000-0003-1238-8121
F Turco https://orcid.org/0000-0002-3723-0438
Y Liu https://orcid.org/0000-0002-8192-8411
J R Martín-Solís https://orcid.org/0000-0003-0458-4405
C Angioni https://orcid.org/0000-0003-0270-9630
I Pusztai https://orcid.org/0000-0001-5412-4090
D Fajardo https://orcid.org/0000-0001-5802-4572
D Mateev https://orcid.org/0000-0001-6129-8427
E Lerche https://orcid.org/0000-0003-4584-3581
D van Eester https://orcid.org/0000-0002-4284-3992
P Vincenzi https://orcid.org/0000-0002-5156-4354

References

[Angioni2014] Angioni C *et al* (JET EFDA Contributors) 2014 *Nucl. Fusion* **54** 083028
[Angioni2017] Angioni C, Sertoli M, Bilato R, Bobkov V, Loarte A, Ochoukov R, Odstrcil T, Pütterich T and Stober J (The ASDEX Upgrade Team) 2017 *Nucl. Fusion* **57** 056015
[Angioni2021] Angioni C 2021 *Plasma Phys. Control. Fusion* **63** 073001
[Angioni2023] Angioni C, Citrin J, Loarte A, Polevoi A R, Kim S H, Fable E and Tardini G 2023 *Nucl. Fusion* **63** 126035
[Artola2024] Artola F J, Schwarz N, Gerasimov S, Loarte A and Hoelzl M 2024 *Plasma Phys. Control. Fusion* **66** 055015
[Babenko2020] Babenko P Y, Mironov M I, Mikhailov V S and Zinoviev A N 2020 *Plasma Phys. Control. Fusion* **62** 045020
[Bai2024] Bai X, Loarte A, Liu Y Q, Pinches S D, Koechl F, Li L, Dubrov M and Gribov Y 2024 *Plasma Phys. Control. Fusion* **66** 055017
[Barabaschi2023] Barabaschi P *et al* 2023 *Proc. 29th IAEA Fusion Energy Conf.* (*London, UK*) PaperOV/1–3
[Barabaschi2025] Barabaschi P *et al* 2025 *Proc. 33rd SOFT* (*Dublin, Ireland*) **215** 114990
[Becoulet2022] Becoulet M *et al* (the JOREK Team) 2022 *Nucl. Fusion* **62** 066022
[Beurskens2011] Beurskens M N A *et al* 2011 *Phys. Plasmas* **18** 056120
[Bigot2022] Bigot B 2022 *Nucl. Fusion* **62** 042001
[Bobkov2010] Bobkov V *et al* (ASDEX Upgrade Team) 2010 *Nucl. Fusion* **50** 035004
[Bobkov2017] Bobkov V *et al* 2017 *Plasma Phys. Control. Fusion* **59** 014022
[Bobkov2024] Bobkov V *et al* 2024 *Proc. 26th PSI Conf.* (*Marseille, France*) **41** 101742
[Boedo2009] Boedo J A 2009 *J. Nucl. Mater.* **390–391** 29–37
[Brezinsek2019] Brezinsek S *et al* (JET contributors) 2019 *Nucl. Fusion* **59** 096035
[Bucalossi2022] Bucalossi J *et al* 2022 *Nucl. Fusion* **62** 042007
[Buzhinskij1997] Buzhinskij O I and Semenets Y M 1997 *Fusion Technol.* **32** 1
[Chen2022] Chen L *et al* 2022 *Proc. 25th Plasma Surface Interactions Conf.* (*Jeju, Korea*)
[Chomiczewska2024] Chomiczewska A *et al* (JET Contributors) 2024 *Nucl. Fusion* **64** 076058
[Coburn2022] Coburn J *et al* 2022 *Nucl. Fusion* **62** 016001
[Colas2024] Colas L *et al* 2024 *Proc. 26th PSI Conf.* (*Marseille, France*) 42 101831
[Ding2024] Ding S *et al* 2024 *Nature* **629** 555–60
[Dux2009] Dux R *et al* 2009 *J. Nucl. Mater.* **390–391** 858
[Dux2011] Dux R, Janzer A and Pütterich T (ASDEX Upgrade Team) 2011 *Nucl. Fusion* **51** 053002
[Dux2014] Dux R, Loarte A, Fable E and Kukushkin A 2014 *Plasma Phys. Control. Fusion* **56** 124003
[Dux2017] Dux R, Loarte A, Angioni C, Coster D, Fable E and Kallenbach A 2017 *Nucl. Mater. Energy* **12** 28
[Eksaeva2022] Eksaeva A, Kirschner A, Romazanov J, Brezinsek S, Linsmeier C, Maviglia F,

Siccinio M and Ciattaglia S 2022 *Phys. Scr.* **97** 014001
[Ennaceur2000] Ennaceur M M and Terreault B 2000 *J. Nucl. Mater.* **280** 33
[Fajardo2024a] Fajardo D *et al* 2024 *Plasma Phys. Control. Fusion* **67** 015020
[Fajardo2024b] Fajardo D, Angioni C, Fable E, Tardini G, Bilato R, Luda T, McDermott R M and Samoylov O (the ASDEX Upgrade Team) 2024 *Nucl. Fusion* **64** 104001
[Fantz2020] Fantz U, Wünderlich D, Riedl R, Heinemann B and Bonomo F 2020 *Fusion Eng. Des.* **156** 111609
[Field2023] Field A R *et al* (JET Contributors) 2023 *Nucl. Fusion* **63** 016028
[Gao2009] Gao X *et al* 2009 *J. Nucl. Mater.* **390–391** 864
[Garcia2022] Garcia J *et al* 2022 *Phys. Plasmas* **29** 032505
[Garcia2023] Garcia J *et al* (JET Contributors) 2023 *Nucl. Fusion* **63** 112003
[Garzotti2019] Garzotti L *et al* 2019 *Nucl. Fusion* **59** 026006
[Giancarli2024] Giancarli L *et al* 2024 *Fusion Eng. Des.* **203** 114424
[Gong2024] Gong X *et al* 2024 *Proc. 50th EPS Conf. on Plasma Physics* (*Salamanca, Spain*)
[Groth2002] Groth M *et al* 2002 *Nucl. Fusion* **42** 591
[Gunn2017] Gunn J P *et al* 2017 *Nucl. Fusion* **57** 046025
[Hagelaar2015] Hagelaar G J M, Kogut D, Douai D and Pitts R A 2015 *Plasma Phys. Control. Fusion* **57** 025008
[Henderson2015] Henderson M *et al* 2015 *Phys. Plasmas* **22** 021808
[Helou2023] Helou W *et al* 2023 *Proc. 29th IAEA Fusion Energy Conf.* (*London, UK*)
[Hong2011] Hong S-H *et al* 2011 *J. Nucl. Mater.* **415** S1050
[Hu2021] Hu Q M, Park J-K, Logan N C, Yang S M, Grierson B A, Nazikian R and Yu Q 2021 *Nucl. Fusion* **61** 106006
[Huber2020] Huber A *et al* 2020 *Nucl. Mater. Energy* **25** 100859
[Huijsmans2013] Huijsmans G T A and Loarte A 2013 *Nucl. Fusion* **53** 123023
[ITR-24-004] Loarte A *et al* 2024 Initial evaluations in support of the new ITER baseline and Research Plan *ITER Organization Technical Report*
[ITR-24-005] Campbell D J 2024 *ITER Research Plan within the Staged Approach, (Level III—Final Version), ITER Organization Technical Report*
[Jia2024] Jia M *et al* 2024 *Proc. 50th EPS Conf. on Plasma Physics* (*Salamanca, Spain*)
[Joffrin2014] Joffrin E *et al* 2014 *Nucl. Fusion* **54** 013011
[Kahn2019] Khan A, De Temmerman G, Lisgo S W, Bonnin X, Anand H, Miller M A, Pitts R A, Schmid K and Kukushkin A S 2019 *Nucl. Mater. Energy* **20** 100674
[Kallenbach2005] Kallenbach A *et al* 2005 *Plasma Phys. Control. Fusion* **47** B207
[Kallenbach2009] Kallenbach A *et al* (ASDEX Upgrade Team) 2009 *Nucl. Fusion* **49** 045007
[Kappatou2019] Kappatou A *et al* (the ASDEX Upgrade Team) 2019 *Nucl. Fusion* **59** 056014
[Kaveeva2020] Kaveeva E *et al* 2020 *Nucl. Fusion* **60** 046019
[Kim2016] Kim S H, Bulmer R H, Campbell D J, Casper T A, LoDestro L L, Meyer W H, Pearlstein L D and Snipes J A 2016 *Nucl. Fusion* **56** 126002
[Kim2021] Kim S H, Polevoi A R, Loarte A, Medvedev S Y and Huijsmans G T A 2021 *Nucl. Fusion* **61** 076004
[Kim2024] Kim S H *et al* 2024 *Proc. 2nd IAEA Technical Meeting on Long-Pulse Operation of Fusion Devices* (*Vienna, Austria*)
[Köchl2017] Köchl F *et al* (JET Contributors) 2017 *Nucl. Fusion* **57** 086023
[Köchl2018] Köchl F *et al* 2018 *Proc. 27th IAEA Fusion Energy Conf.* (*Gandhinagar, India*)
[Köchl2020] Köchl F *et al* 2020 *Nucl. Fusion* **60** 066015
[Korving2024] Korving S Q, Mitterauer V, Huijsmans G T A, Loarte A and Hoelzl M 2024 *Phys. Plasmas* **31** 052504
[Kovtun2023] Kovtun Y *et al* 2023 *Nucl. Mater. Energy* **37** 101521
[Kukushkin2001] Kukushkin A S, Janeschitz G, Loarte A, Pacher H D, Coster D, Reiter D and Schneider R 2001 *J. Nucl. Mater.* **290–3** 887
[Lehnen2015] Lehnen M *et al* 2015 *J. Nucl. Mater.* **463** 39–48
[Lehnen2023] Lehnen M *et al* 2023 *Proc. 29th IAEA Fusion Energy Conf.* (*London, UK*)
[Li1999] Li J *et al* 1999 *Nucl. Fusion* **39** 973
[Lin2020] Lin Y, Wright J C and Wukitch S J 2020 *J. Plasma Phys.* **86** 865860506
[Loarte2001] Loarte A 2001 *Plasma Phys. Control. Fusion* **43** R183
[Loarte2015] Loarte A *et al* 2015 *Phys. Plasmas* **22** 056117
[Loarte2016] Loarte A *et al* 2016 *Proc. 26th IAEA Fusion Energy Conf.* (*San Diego, USA*)
[Loarte2017] Loarte A and Neu R 2017 *Fusion Eng. Des.* **122** 256–73
[Loarte2021] Loarte A *et al* 2021 *Nucl. Fusion* **61** 076012
[Luce2014] Luce T C *et al* (the ITPA Integrated Operation Scenario Topical Group Members, the ASDEX-Upgrade Team, the DIII-D Team, JET EFDA Contributors and the JT-60U Team) 2014 *Nucl. Fusion* **54** 013015
[Lukash2017] Lukash V E 2017 *Proc. 44th EPS Conf.* (*United Kingdom*)
[Maget2013] Maget P, Artaud J-F, Bécoulet M, Casper T, Faustin J, Garcia J, Huijsmans G T A, Loarte A and Saibene G 2013 *Nucl. Fusion* **53** 093011
[Maget2022a] Maget P *et al* 2022 *Proc. 48th EPS Conf. on Plasma Physics*
[Maget2022b] Maget P *et al* 2022 *Plasma Phys. Control. Fusion* **64** 045016
[Maggi2024] Maggi C F *et al* 2024 *Nucl. Fusion* **64** 112012
[Manas2021] Manas P *et al* 2021 *Proc. 28th IAEA Fusion Energy Conf.*
[Martin2008] Martin Y R *et al* 2008 *J. Phys.: Conf. Ser.* **123** 012033
[Maslov2023] Maslov M *et al* (JET Contributors) 2023 *Nucl. Fusion* **63** 112002
[Martín-Solís2017] Martín-Solís J R, Loarte A and Lehnen M 2017 *Nucl. Fusion* **57** 066025
[Mateev2023] Matveev D *et al* (JET Contributors) 2023 *Nucl. Fusion* **63** 112014
[Neu2009] Neu R *et al* 2009 *Phys. Scr.* **T138** 014038
[Park2023] Park J-S, Bonnin X, Pitts R, Gribov Y, Wauters T, Kavin A A, Lukash V E and Khayrutdinov R R 2023 *Nucl. Fusion* **63** 076027
[Pinches2015] Pinches S D, Chapman I T, Lauber P W, Oliver H J C, Sharapov S E, Shinohara K and Tani K 2015 *Phys. Plasmas* **22** 021807

[Piron2019] Piron L, Challis C, Felton R, King D, Lennholm M, Lomas P, Piron C, Rimini F and Valcarcel D 2019 *Fusion Eng. Des.* **146** 1364–8
[Pitts2007] Pitts R A *et al* (JET EFDA Contributors) 2007 *Nucl. Fusion* **47** 1437
[Pitts2019] Pitts R A *et al* 2019 *Nucl. Mater. Energy* **20** 10069
[Pitts2021] Pitts R A *et al* Progress in the understanding of plasma-wall interactions in support of the ITER research plan *47th EPS Conf. on Plasma Physics* (*21–25 June 2021*) (virtual) I1.001
[Pitts2023] Pitts R A *et al* 2023 *Proc. 29th IAEA Fusion Energy Conf.* (*London, UK*)
[Pitts2025] Pitts R A *et al* 2025 *Nucl. Mater. Energy* **42** 101854
[Pütterich2011] Pütterich T, Dux R, Janzer M A and McDermott R M 2011 *J. Nucl. Mater.* **415** S334
[Polevoi2017] Polevoi A R, Loarte A, Kukushkin A S, Pacher H D, Pacher G W and Köchl F 2017 *Nucl. Fusion* **57** 022014
[Polevoi2018] Polevoi A R, Loarte A, Dux R, Eich T, Fable E, Coster D, Maruyama S, Medvedev S Y, Köchl F and Zhogolev V E 2018 *Nucl. Fusion* **58** 056020
[Polevoi2020] Polevoi A R, Ivanov A A, Medvedev S Y, Huijsmans G T A, Kim S H, Loarte A, Fable E and Kuyanov A Y 2020 *Nucl. Fusion* **60** 096024
[Polevoi2023] Polevoi A R *et al* 2023 *Nucl. Fusion* **63** 076003
[Poli2018] Poli F M, Fredrickson E D, Henderson M A, Kim S-H, Bertelli N, Poli E, Farina D and Figini L 2018 *Nucl. Fusion* **58** 016007
[Pusztai2023] Pusztai I *et al* 2024 *Proc. 49th EPS Conf. on Plasma Physics* (*Bordeaux, France*)
[Reynolds-Barredo2020] Reynolds-Barredo J M, Tribaldos V, Loarte A, Polevoi A R, Hosokawa M and Sanchez R 2020 *Nucl. Fusion* **60** 086017
[Rice2015] Rice J E *et al* 2015 *Nucl. Fusion* **55** 033014
[Righi1999] Righi E *et al* 1999 *Nucl. Fusion* **39** 309
[Rimini2024] Rimini F *et al* 2024 *Proc. 50th EPS Conf. on Plasma Physics* (*Salamanca, Spain*)
[Romazanov2022] Romazanov J *et al* 2022 *Nucl. Fusion* **62** 036011
[Rosenbluth1997] Rosenbluth M N and Putvinski S V 1997 *Nucl. Fusion* **37** 1355
[Ryter2013] Ryter F *et al* (the ASDEX Upgrade Team) 2013 *Nucl. Fusion* **53** 113003
[Schmid2015] Schmid K, Krieger K, Lisgo S W, Meisl G and Brezinsek S 2015 *J. Nucl. Mater.* **463** 66
[Schmid2024] Schmid K and Wauters T 2024 *Nucl. Mater. Energy* **41** 101789
[Schmidtmayr2018] Schmidtmayr M *et al* 2018 *Nucl. Fusion* **58** 056003
[Schweinzer2016] Schweinzer J *et al* 2016 *Nucl. Fusion* **56** 106007
[Singh2017] Singh M J, Boilson D, Polevoi A R, Oikawa T and Mitteau R 2017 *New J. Phys.* **19** 055004
[Snyder2011] Snyder P B, Groebner R J, Hughes J W, Osborne T H, Beurskens M, Leonard A W, Wilson H R and Xu X Q 2011 *Nucl. Fusion* **51** 103016
[Solano2023] Solano E R *et al* (JET Contributors) 2023 *Nucl. Fusion* **63** 112011
[Strachan1997] Strachan J D *et al* 1997 *Plasma Phys. Control. Fusion* **39** B103
[Tsitrone2024] Tsitrone E *et al* 2024 *Proc. 26th PSI Conf.* (*Marseille, France*) submitted to Nuclear Materials and Energy
[Turco2024] Turco F, Luce T C, Boyes W, Hanson J M and Hyatt A W 2024 *Nucl. Fusion* **64** 076048
[Vallhagen2024] Vallhagen O, Hanebring L, Artola F J, Lehnen M, Nardon E, Fülöp T, Hoppe M, Newton S L and Pusztai I 2024 *Nucl. Fusion* **64** 086033
[van Vugt2019] van Vugt D C, Huijsmans G T A, Hoelzl M and Loarte A 2019 *Phys. Plasmas* **26** 042508
[Vincenzi2024a] Vincenzi P *et al* 2024 *Proc. 50th EPS Conf. on Plasma Physics* (*Salamanca, Spain*) **67** 045013
[Vincenzi2024b] Vincenzi P *et al* 2024 *Nucl. Fusion* **65** 036009
[Wagner2010] Wagner F *et al* 2010 *Plasma Phys. Control. Fusion* **52** 124044
[Walsh2011] Walsh M *et al* 2011 *2011 IEEE/NPSS 24th Symp. on Fusion Engineering* (*Chicago, IL, USA*) pp 1–8
[Wang2024] Wang C *et al* 2024 *Nucl. Fusion* accepted
[Wauters2022] Wauters T *et al* 2022 *Phys. Scr.* **97** 044001
[Wauters2024] Wauters T *et al* 2024 *Proc. 26th PSI Conf.* (*Marseille, France*) submitted to Nuclear Materials and Energy
[Winter1989] Winter J *et al* 1989 *J. Nucl. Mater.* **162–164** 713
[Winter1990] Winter J *et al* 1990 *J. Nucl. Mater.* **176 & 177** 14
[Yang2020] Yang X *et al* 2020 *Nucl. Fusion* **60** 086012